



This is to certify that the

thesis entitled Part I) AN NMR ANALYSIS OF CRYPTAND 111. CONFORMATIONS AND RATES OF PROTON BINDING. Part II) AN NMR STUDY OF ALKALI METAL ANIONS IN SOLUTION

presented by Patrick Bernard Smith

has been accepted towards fulfillment of the requirements for

Ph.D. degree in Chemistry

Date November 10, 1978

O-7639



OVERDUE FINES ARE 25¢ PER DAY PER ITEM

Return to book drop to remove this checkout from your record.

PART I) AN NMR ANALYSIS OF CRYPTAND 111:
CONFORMATIONS AND RATES OF PROTON BINDING
PART II) AN NMR STUDY OF ALKALI METAL ANIONS
IN SOLUTION

Ву

Patrick Bernard Smith

A DISSERTATION

Submitted to
Michigan State University
in partial fulfillment of the requirements
for the degree of

DOCTOR OF PHILOSOPHY

Department of Chemistry

2101110

ABSTRACT

PART I) AN NMR ANALYSIS OF CRYPTAND 111: CONFORMATIONS AND RATES OF PROTON BINDING PART II) AN NMR STUDY OF ALKALI METAL ANIONS IN SOLUTION

By

Patrick Bernard Smith

The conformations and sites of proton binding by cryptand lll (Clll) have been characterized in great detail. The free ligand exists in a conformation which has both nitrogen lone pairs pointing inside its cavity (endo-endo), although external protonation studies indicate a degree of flexibility toward nitrogen inversion. The endo-endo form of the ligand in the absence of acid is preferred over the exo-endo form (one nitrogen lone pair pointing inside the cavity and the other outside) by a factor of about 50 in water at 298 K.

External proton binding by Clll occurs primarily at the lone pairs of the nitrogen atoms with no apparent participation in the binding by the oxygen atoms. Clll will protonate externally at a nitrogen lone pair (exo-endo form). The pK value for external protonation in water at 298 K is 7.1 ± 0.1 . The pK value for the second external protonation, which occurs at the other nitrogen atom (exo-exo form), is between 0.0 and 1.5 in water at 298 K.

The exo-endo form of Clll·H⁺ is preferred over the exo-exo form by a factor of 10⁷ or greater.

One or two protons may also be bound internally by Clll. The first internal protonation is irreversible since the complex cannot be deprotonated unless the cryptand is decomposed. Internal proton binding also occurs primarily at the nitrogen atoms. The internal proton rapidly exchanges between the nitrogen lone pairs, this motion being more rapid than the NMR time-scale even at 170 K. The internally monoprotonated complex exists predominantly in the endo-endo form, which is favored over the exo-endo configuration by a factor of about 10⁸. The internally monoprotonated complex will externally protonate at a nitrogen atom (exo-endo form). The pK value for this process in water at 298 K is roughly 0.4.

The internally diprotonated ligand, Clll·2H⁺,i-i exists in the endo-endo form. The internal protons of Clll·2H⁺,i-i either exchange very slowly or not at all.

The temperature dependence of the NMR spectra of Clll and its internally protonated complexes indicate that as the temperature is lowered, one or more molecular motions are slowed down considerably. One such motion, which has been assigned to a vicinal carbon wagging motion, possesses $\Delta H^{\frac{1}{7}} = 9.0 \pm 0.5$ kcal mol⁻¹ and $\Delta S^{\frac{1}{7}} = -6$ cal mol⁻¹ deg⁻¹ for the internally monoprotonated species. A second type of molecular motion, which is only observed in the case of the internally monoprotonated ligand, is also slowed down at

Patrick Bernard Smith temperatures below 190 K. This motion has $\Delta H^{\frac{1}{7}} = 16 \pm 2$ kcal mol⁻¹ and $\Delta S^{\frac{1}{7}} = +39$ cal mol⁻¹ deg⁻¹ and has been assigned to a concerted torsional motion of the ligand.

The rates of internal protonation and deprotonation processes of Clll are very slow, due to large activation barriers which are about 25 kcal mol⁻¹ for each of the processes. The rate of the first internal protonation exhibits a definite pH dependence which has been correlated with the pH dependence of the equilibria involving the externally protonated forms of Clll. It appears that two forms of the ligand are able to go to products with different rate constants, the first constant being $3.8 \pm 0.6 \times 10^{-3} \, \mathrm{sec}^{-1}$ and the second being $2.3 \pm 0.3 \times 10^{-4} \, \mathrm{sec}^{-1}$.

The rates for the second internal protonation and the removal of the second internal proton are also expected to exhibit a pH dependence although the rates of the second internal protonation have not been studied as a function of pH. The rate of deprotonation of Clll·2H⁺,i-i by base has been shown to depend on the base strength.

The rate data provide a means by which to estimate the thermodynamic stability of the various complexes. The pK_a value for the first internal protonation of Clll in water at 298 K is ≥ 17.8 and $\triangle G^{\circ} \le -5$ kcal mol⁻¹. For the second internal protonation, pK_a $\simeq 8.3$ and $\triangle G^{\circ} \simeq +8$ kcal mol⁻¹.

NMR provides an excellent way to identify and characterize alkali metal anion solutions. NMR data reveal that the trend in thermodynamic stability of the alkali metal anions, relative to the solid metals is Na-Cs->K-,Rb-.

to Karole

ACKNOWLEDGEMENTS

The author wishes to express special gratitude to Professor James L. Dye for his continual guidance and encouragement. Professors A. I. Popov, J. F. Harrison, D. G. Farnum, and L. R. Sousa are also acknowledged for their many helpful discussions and insights.

Appreciation is also extended to Mr. M. Yemen, Mr. M. DaGue, Dr. E. Kauffmann, Mr. B. Van Eck, and Dr. Harlan Lewis for their many hours of assistance. Mr. F. Bennis and Mr. W. Burkhardt must also be recognized for their assistance and support concerning the operation and maintenance of the NMR spectrometers.

Financial support from the Dow Chemical Company, the United States Energy Research and Development Association, and the General Electric Company is also acknowledged.

Finally, my sincere thanks to my wife, Karole, and our families for their unending love, confidence, and support.

TABLE OF CONTENTS

LIST	OF	TABLES	3.	•	•		•	•	•	•	•	•	•	•	•	•	•	•	•	•	•	vii
LIST	OF	FIGURE	ES	•	•			•	•	•	•	•	•	•	•	•	•	•	•	•	•	ix
LIST	OF	COMMO	NLY	US	ED	TE	ERM	S	•	•	•	•	•	•	•	•	•	•	•	•	•	xiii
		PART CONFOR	•																			
Chapt	er																					
1.	. I	HISTOR	ICAI	,	•	• •		•	•	•	•	•	•	•	•	•	•		•	•	•	1
		I)	INT	ron	DU	CTI	ON	•	•	•	•	•	•	•	•	•		•	•		•	1
		II)	GEN	IER	AL	FE	EAT	URI	ES	OF	7 1	IMF	₹	•	•	•		•		•	•	8
			E	A) 3) 2)	S	pir	Ch n-S Re	pir	n (οι	ıp]	lir	ng	•		•			•	•		9 17 19
2.	. I	EXPERI	MENT	CAL				•	•	•		•	•	•			•	•	•	•		29
		I)	GLA	SS	WA:	RE	CL	EAI	1IV	1G	•	•	•	•	•		•		•	•	•	29
		II)	SOI	LVE	ти	ΡĮ	JRI	FI	CAC	ric	И	•	•	•		•	•		•	•	•	29
		III)	LIC	AN	D :	PUF	RIF	IC	AT]	(01	1	•	•	•	•	•	•	•	•	•	•	30
		IV)	SAN	1PL	E :	PRE	EPA	RA?	ric	N		•	•	•			•	•		•	•	31
				A) B)		Sa lka	oar amp ali rep	les Me	s eta	i	Ar	•	•	•	•		•		•	•		31 33
		V)	Cli	11	SY	NTF	IES	IS	AN	1D	ΡŪ	JR]	F.	IC <i>I</i>	T	101	1	•	•	•	•	35
		VI)	MET	CAL	P	UR]	FI	CA!	ric	N	•		•	•	•		•	•	•	•	•	37
		VII)	VAC	טטכ	M :	PRO	CE	DUI	RES	3		•	•	•	•	•	•	•	•	•	•	40
	1	VIII)	NMF	R S	PE	СТР	ROM	ETI	ΞR	•	•	•	•		•	•		•	•	•	•	42
		IX)	SAF	тЕТ	Y			•						_								43

3.	CONFORM	MATIONAL ANALYSIS OF CRYPTAND 111	45
	I)	INTRODUCTION	45
		A) Clll Symmetry Considerations	53
	II)	NMR SPECTRA AT AMBIENT TEMPERATURES	56
		A) Clll in d-Acetone	59 60 62
		Shift	65 66 78
		Clll•H ⁺ ,i	82 83
	III)	TEMPERATURE DEPENDENCE OF THE NMR SPECTRA	84
		A) Clll in d ₆ -Acetone	85 89 105 108 117 121
4.	THE KIN	NETICS OF INTERNAL PROTONATION OF C111 .	125
	I)	INTRODUCTION	125
	II)	THE FIRST INTERNAL PROTONATION OF C111 .	126
	III)	THE KINETICS OF THE SECOND INTERNAL PROTONATION OF C111 IN WATER	138
	IV)	THE KINETICS OF DEPROTONATION OF Clll-2H+,i-i	142
	V)	METHOD OF ANALYSIS	145
	VI)	SUMMARY	147
	VII)	THE REACTION OF Clll.H, i WITH Na+C222.Na	152
	VIII)	THE REACTION BETWEEN C111.2H, 1-1 AND ES	153
5.	DISCUSS	SION	156

PART II) AN NMR STUDY OF ALKALI METAL ANIONS IN SOLUTION

I)	INTRODUCTION	164
II)	THERMODYNAMIC STABILITY OF THE ALKALI METAL ANIONS	172
III)	IDENTIFICATION OF NEW SPECIES	178

LIST OF TABLES

TABLE		Page
1.	Summary of relaxation mechanisms	27
2.	The solubility of Clll and its complexes in various solvents	38
3.	The chemical shifts of Clll and its complexes at ambient temperature	58
4.	The dependence of the chemical shifts of Clll in d6-acetone upon addition of trifluoro-acetic acid (TFAA)	72
5.	The dependence of the chemical shifts of Clll in d6-acetone upon addition of dichloro-acetic acid (DCAA)	75
6.	The pH dependence of the chemical shift of the CH ₂ N protons of Clll in water at 299°K.	80
7.	The pH dependence of the chemical shifts of Clll. H, i in water	83
8.	The temperature dependence of the NMR parameters for a 0.02 M solution of Clll in d ₆ -acetone	89
9.	The temperature dependence of the NMR spectra of a 0.04 M solution of Clll·H ⁺ ,i·Br ⁻ in d ₆ -acetone	91
10.	The temperature dependence of the NMR parameters for a 0.04 M solution of Clll·H ⁺ ,i·Br ⁻ in d ₄ -MeOH	104
11.	The temperature dependence of the NMR parameters for a 0.04 M solution of Clll•2H ⁺ ,i-i•2Cl ⁻ in d ₄ -MeOH	107
12.	The temperature dependence of the NMR parameters for a 0.04 M solution of Clll.H.i in du-MeOH. acidified with HCl	110

TABLE		Page
13.	The temperature dependence of the equilibrium constant for the conversion of Clll·H ⁺ ,i to Clll·2H ⁺ ,i-o in d ₄ -MeOH: K^N from the CH ₂ -N protons and K^1 from the internal proton	112
14.	The temperature dependence of the equilibrium constant for the formation of Clll·2H ⁺ ,o-o in d ₆ -acetone with the addition of TFAA	121
15.	The dependence of the equilibrium constant for the conversion of Clll·H ⁺ ,o to Clll·2H ⁺ ,o-o on the concentration of TFAA	122
16.	Buffer compositions and their ionic strengths in D ₂ O	127
17.	The dependence of the rate of internal monoprotonation of Clll upon pH and temperature .	128
18.	The dependence of the rate of the second internal protonation of Clll·H+,i upon temperature in 1 M HCl	142
19.	The dependence of the rate of deprotonation of Clll •2H+,i-i upon temperature in 5 M KOH .	145
20.	The activation and thermodynamic parameters for internal protonation processes at 298 K .	148
21.	A selected list of chemical shifts and line-widths in alkali metal NMR	171
22.	The products of some alkali metal solution preparations	173
23.	The products of the reaction of Na and Cs metals and C222 in THF	176
24.	The temperature dependence of the chemical shift of Cs [†] C222 in EA	179
25.	The temperature dependence of the EPR signal of a 0.08 M solution of Na ⁺ 18-C-6•Na ⁻ in MA .	187

LIST OF FIGURES

Page		FIGURE
3	ructures of cryptand 222, 18-crown-6 and ryptand 111	1.
4	ne dependence of the formation constant on ne ratio of the size of the ion to the ligand's cavity size	2.
6	ne protonation scheme of Clll	3.
14	lagram showing the components of the Musher neory of proton chemical shifts	4.
16	ne effect of unpaired electrons on the NMR pectrum	5.
20	ne effect of bond angle on scalar coupling, or A) vicinal protons and B) geminal pro-	6.
32	oparatus used in the preparation of anhy- rous samples for NMR analysis	7.
34	paratus used in the synthesis of alkali etal anion solutions	8.
36	ceps in the synthesis of Clll	9.
39	Prombone apparatus for the storage of kali metals	10.
41	acuum line arrangement used in sample preparation	11.
45	ne conformations of C222	12.
49	etry (large cavity) and B) compact cavity.	13.
	ne possible binding sites and conformations (Clll, A) unprotonated, B) external proposation, C) internal protonation, D) external protonation of the internally	14.

FIGURE		Page
	monoprotonated complex and E) internal diprotonation	50
15.	Model showing the torsional angle of C222 .	53
16.	Model showing the symmetry elements of C111 in the D_{3h} configuration	55
17.	The NMR spectra of Clll and its protonated complexes at ambient temperature	57
18.	The dependence of the NMR spectrum of Clll in d ₆ -acetone upon the addition of trifluoroacetic acid (TFAA)	69
19.	The dependence of the NMR spectrum of Clll in d ₆ -acetone upon the addition of dichloro-acetic acid (DCAA)	73
20.	The dependence of the chemical shift of the CH ₂ O protons of Clll in d ₆ -acetone upon addition of DCAA	74
21.	The NMR spectra of Clll in water at various pH values	77
22.	The pH dependence of the chemical shift of the CH_2N protons of Clll in D_2O	79
23.	The spectrum of Clll in CHF ₂ Cl at 163 K at 250 MHz	86
24.	The temperature dependence of the NMR spectra of Clll in d ₆ -acetone	88
25.	The temperature dependence of the NMR spectra of Clll. H, i in d6-acetone	90
26.	Computer-simulation of the temperature dependence of the spectra of the CH_2O protons of $Clll \cdot H^+$, i in d_6 -acetone	93
27.	The dependence of $ln(k)$ on l/T for the torsional motion from the spectra of the CH_2O protons of $Clll \cdot H^+, i \dots \dots \dots$.	95
28.	The temperature dependence of the internal proton resonance of Clll·H ⁺ ,i in d ₆ -acetone	97

FIGURE		Page
29.	Computer-simulation of the temperature dependence of the internal proton resonance of Clll·H ⁺ ,1 in d ₆ -acetone	98
30.	The dependence of $ln(k)$ on $1/T$ for the skeletal locking process from the spectra of the internal proton of $Clll \cdot H^+, 1 \cdot \dots \cdot$	99
31.	The temperature dependence of the NMR spectra of Clll+H+,i in d4-MeOH	103
32.	The temperature dependence of the NMR spectra of Clll·2H ⁺ ,i-i in d_{μ} -MeOH	106
33.	The temperature dependence of the NMR spectra of Clll+H ⁺ ,i in d _{μ} -MeOH, acidified with HCl .	109
34.	The dependence of $ln(K)$ on l/T for the equilibrium between $Clll \cdot H^+$, i and $Clll \cdot 2H^+$, i-o in d_{μ} -MeOH	113
35.	The variation in the NMR spectrum of the internal proton of Clll·H ⁺ ,i in d_{μ} -MeOH with the addition of HCl at 200 K	115
36.	The temperature dependence of the NMR spectrum of the internal proton of Clll·H ⁺ ,i in d ₄ -MeOH with about 50 mole % HCl added	116
37.	The temperature dependence of the NMR spectra of Clll·H ⁺ ,o in d ₆ -acetone, acidified with TFAA	118
38.	The variation of $ln(K_2)$ with $1/T$ for the formation of $Clll \cdot 2H^+$, o-o in d_6 -acetone upon the addition of TFAA	120
39.	The dependence of the equilibrium constant for the conversion of Clll·H ⁺ ,o to Clll·2H ⁺ ,o-o in d ₆ -acetone on TFAA concentration	123
40.	A typical rate analysis for internal protonation of Clll in water	129
41.	The dependence of ln(k) on 1/T for the internal protonation of Clll in water at two different pH values: squares; pH = 7.5 and cir-	120
	cles; pH = 4.9	130

Page		FIGURE
133	The pH titration of Clll with HCl in water (only external protonation occurs)	42.
135	The variation of the relative concentrations of the various forms of Clll in water with pH	43.
136	The dependence of the rate of internal monoprotonation of Clll on pH: dashed line; pK = 7.1 and solid line; pK = 7.5	44.
140	A typical rate analysis for the second internal protonation of $Clll \cdot H^{\dagger}$, i in 1 M HCl .	45.
141	The dependence of ln(k) on 1/T for the second internal protonation of Clll·H ⁺ ,i in 1 M HCl	46.
143	A typical rate analysis for the deprotonation of Clll • 2H+, i-i in 5 M KOH	47.
144	The dependence of $ln(k)$ on l/T for the deprotonation of $Clll \cdot 2H^{\dagger}$, $i-i$ in 5 M KOH (crosses) and 1 M KOH (circle)	48.
151	The potential energy diagram for the internal protonation processes	49.
159	The dependence of the total energy of the complex on the location of the H, proton along the C, axis for Clll·H+,i in D, symmetry	50.
165	The electronic spectra of the alkali metals in tetrahydrofuran (THF)	51.
180	The temperature dependence of the NMR spectrum of Cs [†] C222•Cs ⁻ in MA	52.
183	The temperature dependence of the NMR spectrum of Cs [†] C222•Cs ⁻ in THF	53.
186	The temperature dependence of the NMR spectrum of Na+18-C-6.Na-in MA	54.

LIST OF COMMONLY USED TERMS

C222 cryptand 2-2-2

Clll cryptand l-l-l

18-C-6 18-crown-6

Clll·H⁺,o externally complexed Clll

Clll·H⁺,i internally complexed Clll

Hi inclusively bound proton

μ magnetic moment

 H_{O} magnetic field strength

I nuclear spin or moment of inertia

γ magnetogyric ratio

H_{loc} local magnetic field at the nucleus

σ screening constant

 σ_{p} paramagnetic contribution to σ

 $\sigma_{
m d}$ diamagnetic contribution to σ

Δ average excitation energy

J coupling constant

 T_1 spin-lattice relaxation

T₂ spin-spin relaxation

R relaxation rate

 $\Delta v_{1/2}$ full linewidth at half height in Hz

τ correlation time or exchange time

 η viscosity

k Boltzmann's constant

A Planck's constant divided by 2π

T temperature in °K

S nuclear spin

Larmor frequency

 δ chemical shift

MA methylamine

EA ethylamine

IPA isopropylamine

DEE diethylether

Na-K sodium-potassium alloy

THF tetrahydrofuran

solvated electron

M alkali metal anion

M^T alkali metal cation

K equilibrium constant

k rate constant

PART I

AN NMR ANALYSIS OF CRYPTAND III:
CONFORMATIONS AND RATES OF PROTON BINDING

CHAPTER 1

HISTORICAL

I) INTRODUCTION

The complexation of metal cations in solution is of particular interest to chemists and biologists partly because of the mystery surrounding ion transport in biological systems (1). Most attention has been given to transition metal complexes with ligands such as ammonia, carbon monoxide, EDTA. etc. (2), since these elements tend to form rather stable and long-lived adducts. This is true because the transition metal ions, in general, have valence deficiencies, and thus coordinate to electron donating ligands in order to satisfy the valence condition. In sharp contrast to the transition metals is another group of biologically significant ions, the alkali and alkaline earth elements which do not have this valence deficiency. Instead, they tend to be rather inert and very labile in solution. These ions complex with conventional ligands so inefficiently that they have often been used to maintain constant ionic strength in solutions where the complexation of other metal ions was being studied.

Alkali metal complexation has been shown to be important in the phenomenon of active ion transport across membranes. Biologically significant molecules have been observed to facilitate this process (1,3). These molecules include porphyrin and corrin ring complexes, phthalocyanines and

valinomycin, each of which is a macrocycle that possesses a hydrophilic cavity and an organic backbone. The macrocycle is thought to bind the ion in the cavity, while maintaining its organic nature, thereby dissolving the ionic species in the membrane. This process allows the complexing agent to "carry" the ion across an otherwise inaccessible membrane barrier with the expenditure of little energy.

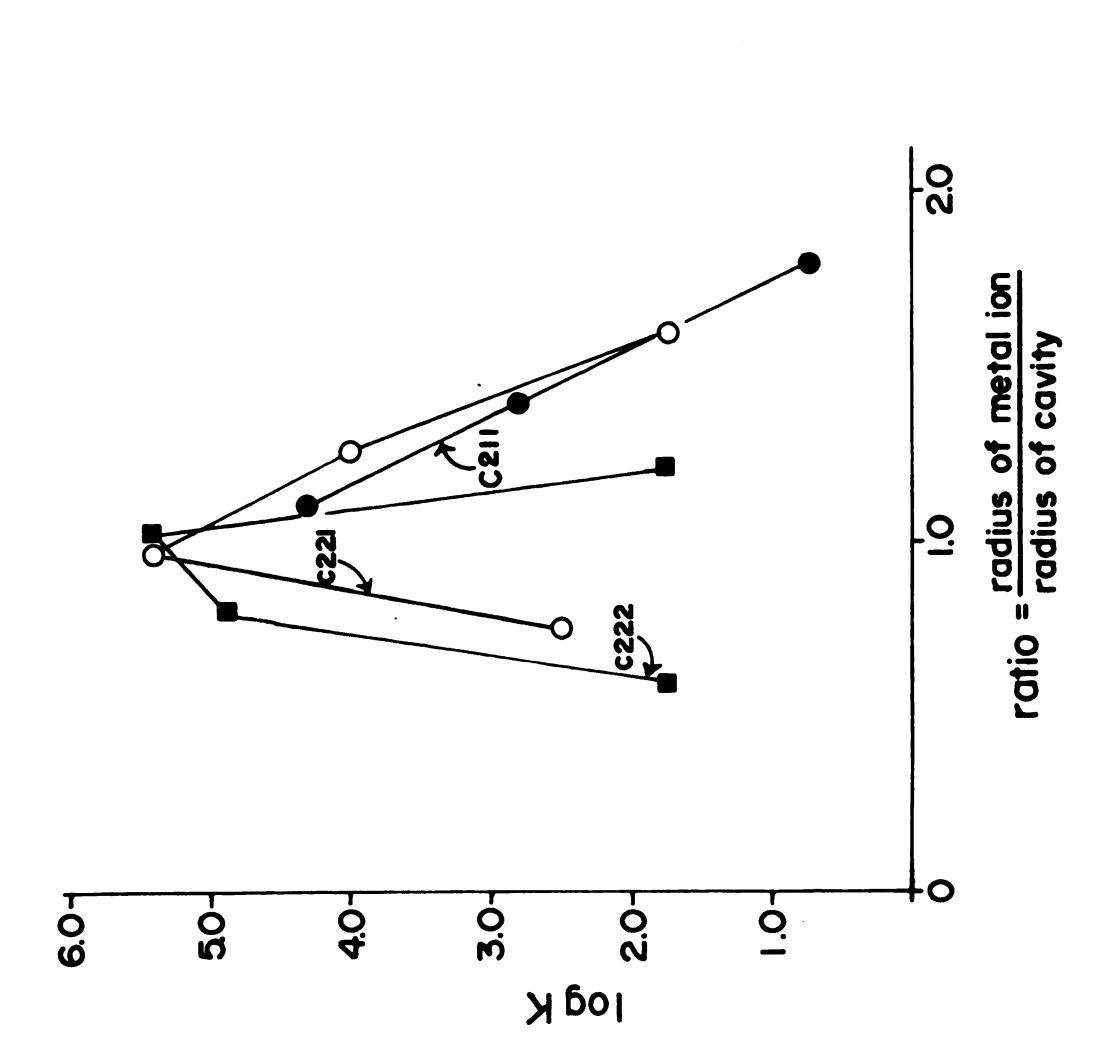
Synthetic macrocycles whose function mimics their naturally occurring analogues were introduced by Pedersen in 1967⁽⁴⁾. These monocyclic polyethers were named "crown ethers" because Pedersen envisioned them as sitting atop the complexed ion in a fashion resembling a crown. Since the introduction of crown ethers, many more macrocyclic complexing agents have been synthesized, the designers of which employed freedom of imagination and prowess in the field of synthesis to achieve very specific ends. Cryptands, bicyclic polyethers developed by J.-M. Lehn and co-workers, are the most famous of these, since they combine extremely strong binding characteristics with a well-defined, three dimensional cavity. Thus, they possess selectivity in their binding characteristics with various ions, based on the ratio of cavity to ionic size (5). Typical crown ethers and cryptands are shown in Figure 1. The demonstrated ability to synthesize these macrocycles, coupled with the unlimited freedom of their design has provided for great utility of these ligands in the aforementioned biological applications as well as in several other significant applications (6-12).



Figure 1. Structures of cryptand 222, 18-crown-6 and cryptand 111.

It is not within the scope of this work to present a detailed review of their applications. Instead, let it suffice to say that macrocyclic polyethers hold potential in all areas of ionic separations and have, indeed, proven useful in many (13-24).

As mentioned previously, cryptands differentiate between ionic species by binding most strongly those ions which are compatible with their cavity dimensions. This is portrayed in Figure 2 for several cryptands in which the binding constant of a particular ligand is plotted versus the ratio of the sizes of ion and ligand cavity. These plots peak as the ionic size equals that of the cavity of the ligand, and fall off considerably on either side of this value. The smallest cryptand, Clll, is not shown because its cavity is too small to bind alkali metal ions efficiently (24). Cryptand lll does bind Li⁺ slightly with a pK of approximately 2.2 in water, but comparison with C211, which has a pK of 5.5, demonstrates that Clll is too small for



The dependence of the formation constant on the ratio of the size of the ion to the ligand's cavity size. Figure 2.

efficient binding to occur. (From molecular models, the cavity radius of Clll has been estimated to be about 1.0 A.) This size dilemma would render Clll rather mundane in the realm of ionic complexation except that it binds protons and does so with such efficiency that it is the strongest proton complexing agent yet reported. Clll binds one or two protons in a number of binding sites and conformations, thus qualifying it as a model of the binding characteristics of the larger cryptands as well as biological systems (25).

Lehn and co-workers published two preliminary papers about $Clll^{(26-27)}$, in which they described the synthesis and unusual proton binding ability of Clll. They also discussed the possibility of several different protonated complexes which might be formed as illustrated in Figure 3. In protic solvents or acidic media, Clll was shown to complex a proton externally, presumably at the nitrogen with its lone pair pointing outside the cavity. This complex behaved as a typical protonated amine, the proton being readily exchangeable with protons in solution. Evidence for such complex formation came from a rise in pH upon addition to aqueous solutions and from line broadening in the NMR spectra. Lehn estimated that the pK for external protonation would be about 7.5-8.0 based on triethanolamine or N-ethylmorpholine if the ligand were present with one nitrogen lone pair pointing outside the cavity and available for binding (exo-endo configuration). The actual pK was found to be somewhat lower (6.3) based on the pH of a $2x10^{-4}$ M solution of Clll

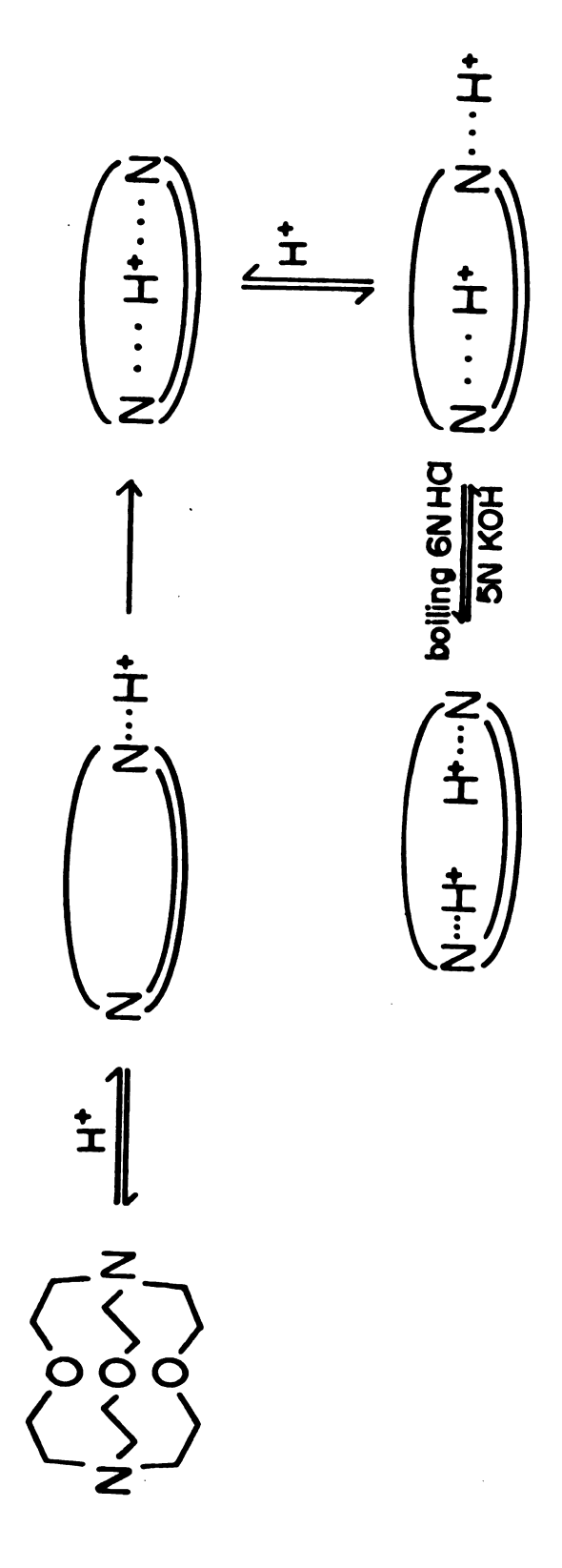


Figure 3. The protonation scheme of Clll.

and therefore, an equilibrium between exo-endo and endoendo forms was suspected. A second external protonation
(at the other nitrogen) was thought to induce too severe a
strain to be possible because both nitrogens would be
forced into the exo conformation. This conclusion was based
on molecular models and the fact that the reduction of the
dilactam of Clll by diborane results in the monoborane adduct rather than the diborane adduct obtained in the case
of larger cryptands (see Experimental section for details).

Simultaneous with the rapid external protonation, a second, much slower process was observed by which a proton was very tightly bound. This process proceeded with a half-life of several days at room temperature and presumably corresponded to inside protonation. The resulting complex was so stable that heating it to 60°C in 5 M KOH for days did not significantly deprotonate it! Even with excess sodium in liquid ammonia, the proton could not be removed without destroying the ligand.

The internally monoprotonated ligand, Clll·H⁺,i, could be protonated a second time externally. The degree of external protonation was pH dependent, leading to the conclusion that there was again an equilibrium between the endo-endo and exo-endo configurations, the former being more favorable. As the pH was decreased, the ligand was forced into the exo-endo form but the exchange was always very rapid.

A second proton could also be taken inside the cavity (endo-endo), but only under rigorous conditions (1 M HCl at

100°C for one hour). Again, this inclusive proton was found to be bound tightly and was very difficult to remove from the cavity, the complex being stable for days in 5 M KOH at room temperature. Above 60°C, however, one of the two protons could be removed slowly. Treatment with sodium in liquid ammonia caused reduction to the free amine in about 10% yield with about 90% decomposition. No monoprotonated ligand was ever obtained and thus an intermediate of the sort, Clll·H₂⁺, i-i was postulated, the reaction proceeding via reduction rather than proton abstraction by base.

In general it was thought that proton binding occurred mainly at the nitrogens and that external protonation was weak and rapidly exchangeable whereas internal protonation was difficult to achieve but very strong. Subsequent sections of this discussion will deal with binding characteristics and rates of encapsulation of protons by Clll.

II) GENERAL FEATURES OF NMR

Nuclear magnetic resonance provides a direct probe of the electronic environment of the nucleus since the resonance frequency, or Larmor frequency, of that nucleus is greatly dependent on electronic shielding. The symmetry of the electron cloud and the electron density in the vicinity of a nucleus contribute to local magnetic fields which influence its chemical shift. These contributions will be discussed qualitatively in order to give significance to the Clll

spectra in the latter portions of this work. For a more detailed discussion, see references 28-33.

A) The Chemical Shift

When a nucleus is placed in a magnetic field, Ho, its nuclear spin states are no longer degenerate but are separated by an energy difference given by:

$$\Delta E = \frac{\mu H_O}{I} = \gamma H_O \hbar \qquad (Hz)$$
 (1)

where:

 μ - Magnetic moment of the nucleus H_{o} - Magnetic field (gauss) I - Nuclear spin

γ - Magnetogyric ratio

h - Plank's constant divided by 2

Transitions are induced between the levels by irradiation at the Larmor frequency, equal to the energy separation of the nuclear spin states (in the radio frequency region). The electronic distribution becomes important when determining the true magnetic field at the nucleus, H_{loc}, because the electrons produce magnetic fields of their own as they interact with H and may therefore cause considerable shifting in the resonant frequency from that given by equation (1). The electrons perturb the field at the nucleus in a number of ways. First, as was mentioned before, when an atom is placed in a magnetic field the nuclear spin states separate but the field also induces a precession of the electron cloud about the field, Ho. The electronic precession in turn generates a magnetic field, which opposes Ho so that

the nucleus is "screened" by these electrons according to the equation:

$$H_{loc} = H_o(1-\sigma) \tag{2}$$

where:

H_{loc} - the field at the nucleus - the screening constant

This type of screening, which results in an upfield shift, is called diamagnetic screening and may be a sum of several contributions. Other effects, which cause downfield shifts due to the mixing of excited state molecular wave functions, are referred to as paramagnetic terms after the development of Ramsey (28), and hence:

$$\sigma = \sigma_{d} + \sigma_{p} \tag{3}$$

Ramsey expressed these terms theoretically from perturbation theory as follows:

$$\sigma = \frac{e^{2}}{2MC^{2}} < \chi_{O} | \sum_{k} \frac{\mathbf{r}_{k}^{2} \hat{\mathbf{1}} - \hat{\mathbf{r}}_{k} \hat{\mathbf{r}}_{k}}{\mathbf{r}_{k}^{3}} | \chi_{O} > +$$

$$\sum_{M} (E_{O} - E_{M})^{-1} \left[< \chi_{O} | \sum_{k} \hat{\mathbf{1}}_{k} | \chi_{M} > < \chi_{M} | \sum_{k} \frac{\hat{\mathbf{1}}_{k}}{\mathbf{r}_{k}^{3}} | \chi_{O} > \right]$$
(4)

where:

e - electronic charge

M - mass of the electron
C - velocity of light

1_k - angular momentum of the kth electron
r_k - radial distance of the kth electron from the origin

The first term depends only on ground state electronic wave functions and is a function of the symmetry of the electronic distribution and the density of electrons in the

vicinity of the nucleus. The second term is much more difficult to determine because it involves mixing of ground and excited state wave functions, the latter, in general, not being known. Simplistically, σ_d may be thought of in terms of s-type (spherically symmetrical) orbitals and the screening they produce as a result of precession about H_o . Paramagnetic screening, on the other hand, results from excitation of electrons to p, d, and higher states which in turn hinders the precession of the s-type electrons about H_o by introducing directionally dependent electric fields. It follows that the magnitude of σ_p is greatly influenced by the accessibility of the excited states. Since the calculation of σ_p is impossible due to the lack of proper wave functions, an average excitation energy approximation has been made in order to simplify it so that:

$$\sigma_{\rm p} = \left(\frac{-e^2}{\Delta M^2 C^2}\right) < \chi_{\rm o} \mid_{\rm kk} \sim \left(\frac{\hat{1}_{\rm k} \hat{1}_{\rm k}}{r_{\rm k}^3}\right) \mid_{\rm \chi_{\rm o}} >$$
 (5)

where:

Δ - average excitation energy

When Δ is large, as in proton NMR, σ_p contributes little to the chemical shift. When Δ is small, excitation occurs readily and σ_p , which potentially can be very large, usually dominates. More specifically, σ_d dominates in proton NMR even though it is only about 18 ppm, since σ_p is negligible. In carbon and fluorine NMR, σ_d is much larger, (about 260 and 338 ppm respectively), but σ_p may get as large as 1,000 ppm and is therefore the more dominant of the two. In some

heavy metal systems, the value of σ_p may get as large as 10,000 ppm because of a high density of excited states and their ease of accessibility. The σ_d term is also relatively constant for a particular nucleus even though it may be large and its range of shifts is usually only about 20 ppm at most. The magnitude of σ_p , on the other hand, varies greatly from nucleus to nucleus, but more importantly, may change by several hundred ppm for the same nucleus in different environments. For example, Cs⁺ in the gas phase and Cs⁺ inclusively complexed by the cryptand, C222, are shifted about 500 ppm from one another (34).

Ramsey's equations provide a good theoretical starting point, but in practice are of little value in the prediction of chemical shifts due to the unavailability of molecular wave functions. More empirical approaches have found greater utility in this area and will be discussed. In order to be consistant with the literature, downfield shifts will be referred to as paramagnetic and upfield shifts as diamagnetic, but this terminology should not be confused with the two terms in the Ramsey equation. There are contributions to $\sigma_{\rm d}$ which lead to paramagnetic shifts, as we shall see, but which do not involve the mixing of excited and ground electronic states. For example, the paramagnetic term in the Ramsey equation is extremely small for proton NMR and yet large downfield shifts from TMS are observed. These shifts are due to reduction of $\sigma_{\rm d}$ by the

decrease in electron density, etc., rather than to contributions from the $\sigma_{\rm d}$ term.

In general, the contributions to the chemical shift may be classified as either diamagnetic or paramagnetic, but there are several factors which may influence these terms. Four of the more important contributions in proton NMR include:

- a) anisotropic screening
- b) electric field effects
- c) unpaired electrons
- d) solvent effects
- a) through d) contribute to σ_d whereas only d) may significantly contribute to σ_p for nuclei with available excited state orbitals.

a) Anisotropic Screening

Anisotropic effects are caused by an asymetrical electronic distribution of neighboring substituents which does not average to zero with molecular tumbling. This asymmetry causes time-independent local fields at the nucleus which result in the shift. Perhaps the most familiar example of these effects is in relation to ring currents produced by aromatic systems, but all π electron systems have the potential to produce anisotropic screening. These shifts are normally only about 1-4 ppm, significant in proton NMR, but much less so in carbon NMR.

b) Electric Field Effects

A charged species or highly polar group may induce polarization of a bond and alter the electronic distribution

about a nucleus. This causes a two-fold change in the local field at the nucleus by altering the electron density around the nucleus and by initiating an anisotropic electronic environment. The shift produced may be represented in the following way⁽³⁰⁾:

$$\sigma_{e} = -13.3 \left(\sum_{i} \frac{q_{i} \cos \theta_{i}}{r_{i}^{2}} \right) -17.0 \left(\sum_{i} \frac{q_{i}}{r_{i}^{2}} \right) \quad (ppm)$$
 (6)

where:

 q_1 - the total charge of the polar group in units of one electron $\cos \theta_1$ - defined in Figure 4

This equation reduces to:

$$\sigma = -11.2q - 12.0q^2 \tag{7}$$

for axial symmetry assuming r = 1.09A, the typical hydrogencarbon bond length. The former equation, called the Musher equation, provides the means by which to predict the shift expected from a change in the charge distribution at or near a nucleus. It should therefore prove amenable to the study of the protonation of Clll, since the dominant cause of change in the chemical shift of the backbone protons upon protonation is a result of this electric field effect.

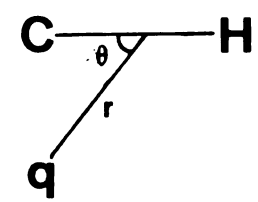


Figure 4. Diagram showing the components of the Musher theory of proton chemical shifts.

c) Unpaired Electrons

The magnetic moment of an electron is 860 times as large as that of a proton and therefore, scalar coupling of nuclei with unpaired spins produces enormous local fields, as large as hundreds of thousands of ppm. Dipole - dipole relaxation via electrons is also very efficient and in many cases broadens lines to obscurity. This phenomenon is represented in Figure 5 in which a) shows a line in the absence of scalar coupling. The normal chemical shift range in proton NMR is about 18 ppm, so that scalar coupling to electrons with a magnitude of 100,000 ppm may put the resonance well out of the tunable range of the spectrometer. Figure 5b) shows the spectrum when electron relaxation is slow, and 5c) when the relaxation is comparable to the hyperfine coupling, A. In the latter case the line is broadened over several kilohertz and in most instances it is not observable. When the relaxation is very fast compared to A, a narrow line occurs as shown in 5d) whose shift is the population average of the two lines as shown in 5b), when electron relaxation is slow. This average position does not lie at the frequency average of those in 5b) because there is a large population difference between the levels as a result of the Boltzmann distribution and in fact, the line is usually shifted many kilohertz from the average frequency. (This shift also occurs in proton NMR with the collapse of multiplets resulting from J coupling, but is not seen because the energy separation between spin states is three orders of

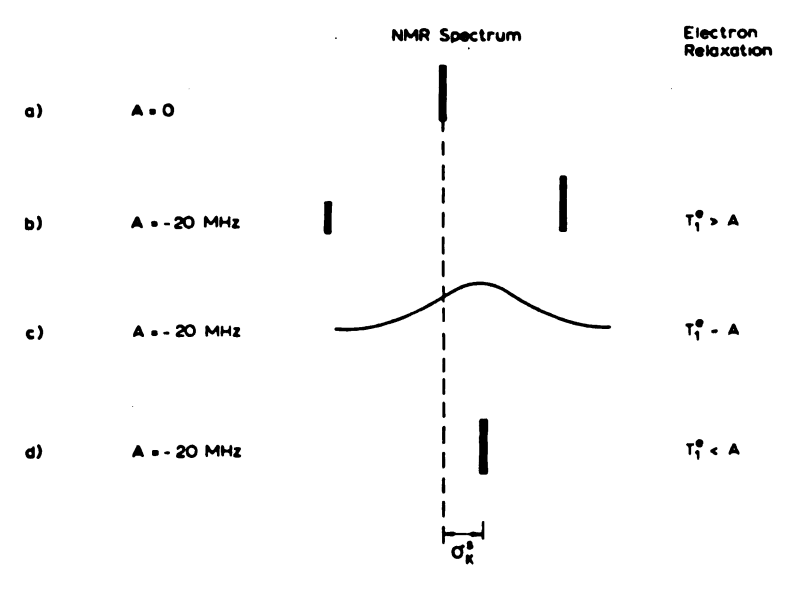


Figure 5. The effect of unpaired electrons on the NMR spectrum.

magnitude less than with electrons and the population difference is therefore negligible.)

d) Solvent Effects

The solvent may have a very great influence on the chemical shift of solute particles by means of the following effects:

- 1) the magnetic susceptibility of the solvent which is due to time-independent magnetic anisotropics. This is usually less than 1 ppm and easily measured;
- 2) orientation of a polar solvent about a polar solute in such a way as to enhance its electronic shielding;
- 3) interaction of a solvent with the solute. The characteristics of the solvent such as polarity, dielectric constant and donating ability greatly determine the extent

of ion-pairing, solvation, hydrogen bonding, etc., in solution. For many alkali ion systems, the major contribution to the chemical shift is the donation of electrons from the solvent into their p and d orbitals. The role of solvent is often overlooked, but may produce large and subtle shifts.

e) Summary

Electric field and anisotropic shieldings are most important in proton NMR and other nuclei of small chemical shift range (σ_p small) because their magnitude is usually less than 10 ppm. For nuclei in which σ_p dominates, however, the chemical shift range is much larger and these two sources of shielding are often not as important. The role of solvent is subtle, but must be considered, because it may have large effects on the chemical shift.

B) Spin-Spin Coupling

Nuclei which have magnetic moments couple with one another in a magnetic field and perturb the energy of the nuclear states involved. This scalar or spin-spin coupling is observed in splitting of the NMR signal into 2 n I + 1 lines, where n is the number of equivalent nuclei causing the splitting and I is the spin of those nuclei. This coupling will average to zero unless the effect is anisotropic, and it is therefore observed only for bonded partners in solution, since the lifetime of the coupling interaction must be longer than the reciprocal of the coupling in Hz to be observed. Spin-spin coupling may arise from three sources:

the interaction of nuclear and electron magnetic currents

arising from 'their motion in the magnetic field, dipoledipole interaction of the nuclei and electrons, and the socalled Fermi contact term, which is a function of the electron density at the nucleus. The contact term is always dominant, being about 100 times larger than the others. This interaction is transmitted through the chemical bond as electrons and nuclei spin pair via the contact term, the bonding electrons also spin pair and thereby transmit the spin characteristics of the first nucleus to the other as it spin pairs with its bonding electron. The contact interaction depends on s-electrons, since only they have a finite probability density at the nucleus, but the interaction is transmitted in some cases by excited state electrons. magnitude of the contact term depends only on the accessibility of excited states, bond angle and distance, and is therefore Ho independent. The theory also predicts that the size of the contact term is proportional to the product of the magnetogyric ratios of the nuclei involved:

$$J_{AB} = \frac{\hbar \Upsilon_A \Upsilon_B}{\Lambda} \left(\frac{32\pi}{9} \right) \beta^2 (Sn | \delta(\mathbf{r}_N) | S_N) (S_N - | \delta(\mathbf{r}_N) | S_N) P \qquad (8)$$

where:

 γ_1 - magnetogyric ratio of nucleus i Δ - average excitation energy $(S_N | \delta(r_N) | S_N)$ - magnitude of valence at nucleus N P - charge density matrix

This equation predicts, for example, that the coupling between two protons is (γ_H/γ_D) or 7 times as large as the coupling

between a proton and a deuteron, all other factors being constant.

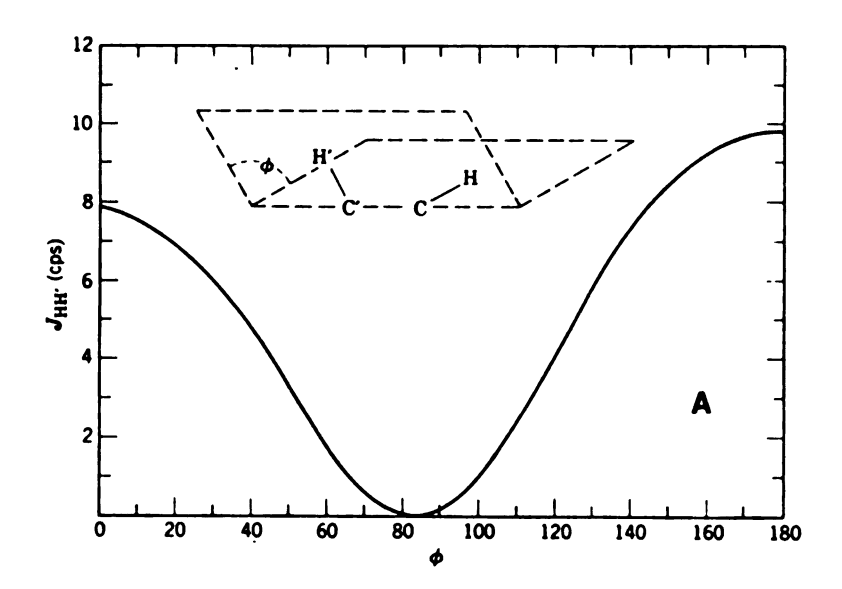
Scalar coupling depends greatly on bond angle as shown in Figures 6a) and b) for vicinal (three bond) and geminal (two bond) coupling. Vicinal coupling reaches a maximum of 8 to 10 Hz at 0 and 180° bond angle with a minimum at about 85°, but geminal coupling may be much greater.

C) NMR Relaxation

Relaxation in the broad sense of the term concerns itself with the exchange of energy from one system to another. Three conditions must be satisfied in order to achieve successful relaxation:

- 1) there must be a system in an excited state with energy to donate;
- 2) there must be another system which can accept this energy;
- 3) there must be a pathway by which the two systems may couple in order to transfer this energy.

In NMR, the energy to be transferred is always at the Larmor frequency, since it involves the relaxation of a nucleus from a high energy spin state to a lower energy state. Thus, the acceptor system must be able to accept energy at the Larmor frequency. There are at least five mechanisms by which relaxation may occur and they depend, in part, on the characteristics of the nucleus, but some general statements may be made about relaxation phenomena.



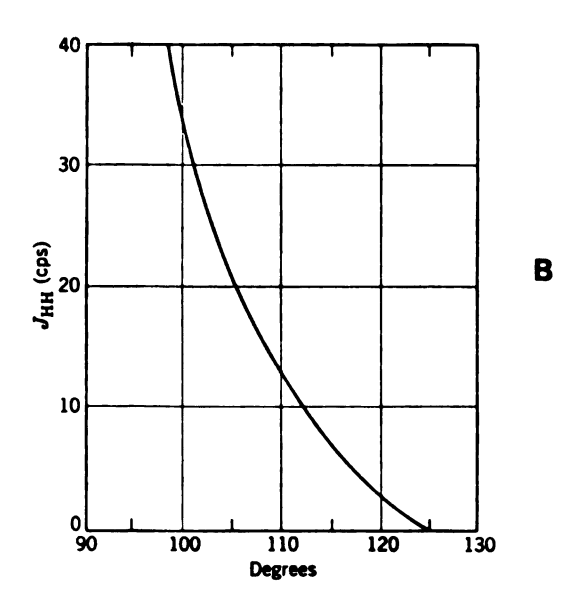


Figure 6. The effect of bond angle on scalar coupling, for A) vicinal protons and B) geminal protons.

The dissipation of energy from a nucleus in an excited nuclear spin state to its surroundings (lattice) is referred to as spin-lattice or T₁ relaxation. The relaxation pathway is generated by alternating local fields due to random rotations and translations (Brownian motion) of neighboring molecules and anisotropics of bonded substituents, which occur at the Larmor frequency. Another type of relaxation called spin-spin or T₂ relaxation, is produced by the interaction of the magnetic moments of like nuclei which induces the relaxation of the one nucleus, while at the same time promoting the other to the excited state. Energy is transferred between the nuclei, but no net change in the energy of the system results.

These two relaxation times may be described in terms of the magnetic moment of the system, $M_{\rm O}$, which precesses about $H_{\rm O}$. $T_{\rm l}$ is related to the component along $H_{\rm O}$, which determines the magnitude of $M_{\rm O}$, whereas $T_{\rm l}$ is related to those components perpendicular to $H_{\rm O}$, or the phase characteristics of $M_{\rm O}$. This can be shown mathematically by expressing the relaxation rate, $R = \frac{1}{T_{\rm l},2}$, in terms of the local field, b, and the magnetic moment, $M_{\rm O}$ for $H_{\rm O}$ along the z-axis:

$$R = (\hat{b}x\hat{M}) = i(b_yM_z - b_zM_y)$$

$$+ j(b_zM_x - b_xM_z) + k(b_xM_y - b_yM_x)$$
(9)

 T_1 processes are, by definition, dependent on the k terms whereas T_2 processes depend on the i and j terms. T_1 processes are not dependent on local fields in the z-direction, but T_2 processes are, and since b_z is identical in both laboratory

and rotating frame, a static local field may induce T_2 but not T_1 relaxation. This is especially important when field inhomogeneity is on the order of $\frac{1}{T_2}$. The spin-spin relaxation time, T_2 , is always larger than or equal to T_1 and is related to the line width by:

$$T_2 = \frac{1}{\pi \Delta v_1}$$
 (10) where:

 $\Delta v_{\frac{1}{2}}$ is the full linewidth at half height in Hz.

a) Dipole-Dipole Relaxation

The dominant source of relaxation for spin = $\frac{1}{2}$ nuclei is dipole-dipole relaxation, which results from the interaction of the magnetic dipoles of two nuclei and produces local fields at the nucleus which may be represented by:

$$H_{loc}^{D-D} = \pm \mu_s (3\cos^2\theta - 1) r_{lS}^{-3}$$
 (11)

 $\mu_{\rm S}$ is the magnetic moment of S, θ is the angle between H_O and the axis joining nuclei S and I and r_{IS} is the distance between I and S. These fields can be very large, but as a rule, molecular motions average them to zero. In the case of solids or liquid crystals, this is not true, and dipolar splitting may often be observed. For most liquids, however, molecular reorientation is rapid and in the "extreme narrowing" limit for nuclei of spin $\frac{1}{2}$, dipolar relaxation may be represented by:

$$\frac{1}{T_1} = \frac{1}{T_2} = (\hbar \gamma_I \gamma_S)^2 \Sigma r_{IS}^{-6} \tau_c$$
 (12)

The correlation time, τ_a , can be defined as the average time between collisions for translational motion, or the average time for a molecule to rotate by one radian for reorientation motions and may be represented as follows for a sphere in a viscous fluid (35):

$$\tau_{c} = \frac{4\pi\eta a^{3}}{3kT} \tag{13}$$

where:

 η - the solution viscosity a - the radius of the sphere

The correlation time is dependent on the shape of the molecule because a branched molecule will tend to be more highly restrictive to reorientation than a molecule with spherical shape as assumed in the derivation of equation (13). For solutions of normal viscosity, τ_c lies between 10^{-10} and 10^{-13} seconds and T_1 is equal to T_2 . As the correlation time increases due to large molecular size, increased solution viscosity, etc., equation (12) is no longer valid and T_1 may be greater than T₂.

b) Spin-Rotation Relaxation

The motion of electrons in a molecule also produces local magnetic fields, which when modulated by molecular collisions, provide another pathway for relaxation, called spin-rotation relaxation. For molecules with moment of inertia, I, undergoing isotropic reorientation in a liquid medium, the relaxation time may be given by:

$$\frac{1}{T_{1,2}} = (2IkT/3\hbar^2)(2C_{\perp}^2 + C_{//}^2)_{\tau_J}$$
 (14)

where C is the appropriate spin-rotation coupling constant, τ_J is the angular momentum correlation time defined below the normal boiling point of the liquid by:

$$\tau_{J} \cdot \tau_{c} = \frac{1}{6kT} \tag{15}$$

 τ_{J} is inversely proportional to temperature and therefore spin-rotation relaxation becomes less efficient as the temperature increases in contrast to other relaxation pathways.

c) Scalar Relaxation

When a nucleus is spin coupled to another nucleus, time dependent local magnetic fields may be produced as a result of fluctuations in the coupling constant by either chemical exchange or by rapid relaxation of the spin state of one of the nuclei. As an example of the second mechanism, consider a spin $\frac{1}{2}$ nucleus (a proton) coupled to a quadrupolar nucleus (a nitrogen). Fast quadrupolar relaxation of the nitrogen modulates the coupling constant and produces the relaxation mechanism. This relaxation rate may be represented as follows:

$$(T_1^{SC})^{-1} = \frac{8}{3} \pi^2 J^2 S(S+1) \left[\frac{\tau_e}{1 + 4\pi^2 (\nu_I - \nu_S)^2 \tau_e^2} \right]$$
 (16)

$$(T_2^{SC})^{-1} = 4/3\pi^2 J^2 S(S+1) \left[\tau_e + \frac{\tau_e}{1+4\pi^2 (\nu_I - \nu_S)^2 \tau_e^2} \right]$$
 (17)

where:

J - the coupling constant
S - the spin of the coupled nucleus, S

 $\nu_{_{\boldsymbol{T}}}$ and $\nu_{_{\boldsymbol{S}}}$ - the Larmor frequencies of the nuclei

 τ_{e} - the exchange time or the lifetime of the spin state of S, depending on the mechanism

The local fields produced by scalar coupling are much smaller than those produced by dipole-dipole interactions, but this mechanism may be dominant under the proper conditions, namely when $(v_T - v_S) \sqrt{\tau}_e$, or when $\tau_e \sqrt{1/A}$. In the latter case, T_2 may be very different from T₁ SC, since it contains a frequency independent term. In the case of very rapid exchange times or relaxation of the coupled nucleus, (heteronuclear decoupling), $T_1^{SC} = T_2^{SC}$ and dipole-dipole relaxation is dominant.

Chemical Shift Anisotropy

Anisotropies in the shielding constant, o, may produce alternating local fields, as they are modulated with respect to H by molecular tumbling. Bound substituents with π electrons are the most common, but in most of these molecules, dipolar relaxation is still dominant. For the case of axial symmetry, the relaxation times may be represented:

$$(T_1^{CA})^{-1} = \frac{2}{15} \gamma^2 H_0^2 (\sigma_{//} - \sigma_{\perp}) \left[\frac{\tau_c}{1 + (2\pi \nu_0)^2 \tau_c^2} \right]$$
 (18)

$$(T_2^{CA})^{-1} = \frac{1}{45} \gamma^2 H_0^2 (\sigma_{///} - \sigma_{\perp}) \left[4\tau_c + \frac{^3\tau_c}{1 + (2\pi\nu_0)^2 \tau_c^2} \right]$$
 (19)

e) Quadrupolar Relaxation

A quadrupole moment is associated with nuclei of spin greater than $\frac{1}{2}$, and therefore the charge distribution of the nucleus is not spherical as with spin $\frac{1}{2}$ nuclei. A fluctuating electric field may be produced as the quadrupolar nucleus tumbles in solution, which in turn gives rise to a relaxation pathway. In the "extreme narrowing" limit, $2\pi v_0 \tau_c <<1$ this relaxation is given by:

$$(T_1^Q)^{-1} = (T_2^Q)^{-1} = \frac{3}{40} \left[\frac{2I+3}{I^2(2I-1)} \right] x$$

$$(1+n^2/3) \left(\frac{e^2 qQ}{h} \right)^2 \tau_c$$
(20)

where:

Q - the quadrupole moment

q - the electric field gradient at the nucleus

η - the asymmetry of the electronic environment of the nucleus

For quadrupolar nuclei, this relaxation pathway dominates unless the nucleus possesses high symmetry or the quadrupole moment is very small.

f) Summary of Relaxation Mechanisms

The observed relaxation rate is a sum of the contributions:

$$(T_1^{Obs})^{-1} = (T_1^{D-D})^{-1} + (T_1^{SC})^{-1} + (T_1^{CA})^{-1} + (T_1^{Q})^{-1} + (T_1^{SR})^{-1} + \dots$$
 (21)

Table 1 illustrates the time ranges and coupling modes of the previously mentioned mechanisms (32).

Table 1. Summary of relaxation mechanisms.

Interaction	T _l range#	н Ф	Typical systems
Dipole-Dipole	1 < T ₁ < 100 sec	γΙγs ^h /r³	13CHCl ₃ , H ₂ O, PFO ₃ ² -, NHμ ⁺ , HCo(CO) ₄
Quadrupole	10-7 < T ₁ < 10 ² sec	(e²qQ/h)	NH3, HBF2, CHCl3, D ₂ 0
Chemical shift anisotropy	10 < T ₁ < 100 sec	$^{(T_{\mathfrak{o}^{-}} \mathscr{H}_{\mathfrak{o}})^{o_{H} \lambda}}$	сн ³ соон
Scalar coupling	0.1 < T < 100 sec	$(2A^2/3)[S(S+1)]^{1/2}$	13CHBr3, PBr3
Spin-rotation	10 ⁻² < T ₁ < 100 sec	ч/(//ɔ-Tɔ)	$^{{ m ClO}_3{ m F}}$, $^{{ m 1}^3{ m CS}_2}$, $^{{ m PFO}_3}$ -, $^{{ m CH}_4}$

*For $\tau_c \sim 10^{-11} \text{ sec.}$ $t_1/T_1 = R_1 = E_e^2$

Because T_1 may not necessarily be equal to T_2 , a quantitative analysis using the pulsed-fourier transform (P-FT) method of data acquisition may be jeopardized. Care must be taken in order to insure complete relaxation before pulse repetition or else standardization may be necessary. A detailed discussion of these problems will be presented in subsequent sections of this work.

CHAPTER 2

EXPERIMENTAL

I) GLASSWARE CLEANING

All glassware used in alkali metal anion synthesis, solvent purification, or alkali metal storage was cleaned by first rinsing with an HF cleaner composed of 33% HNO3, 5% HF, 2% acid soluble detergent, and 60% water by volume. This rinsing was followed by several washings with distilled water and a 12 hour minimum soaking period in aqua regia. The vessels were then rinsed a minimum of five times with distilled water and five times with conductance water and dried at 110°C for at least eight hours. This procedure insured a fresh glass surface free of reactive species.

II) SOLVENT PURIFICATION

Tetrahydrofuran (THF) was dried over calcium hydride for at least 24 hours and then vacuum distilled over a sodium-potassium (Na-K) alloy. The resulting light blue color served as an indicator of solvent dryness. If this color faded, the solvent was transferred over a new metal alloy, but in most cases the solution was stable for several weeks. The Na-K alloy slowly attacked the THF to give a polymer, so the THF was transferred away from it for storage.

Methylamine (MA), ethylamine (EA), and isopropylamine (IPA) were also initially dried over calcium hydride and then vacuum distilled over the Na-K alloy. If a blue

solution did not result, the amine was redistilled over a fresh metal film until the blue color was stable for two days. The solvent was then distilled into Pyrex storage bottles since the Na-K alloy also slowly decomposed the amines to yield ammonia and other decomposition products.

Diethyl ether (DEE) was dried over calcium hydride and then vacuum distilled into a vessel containing benzophenone and excess Na-K alloy. A purple color developed with the formation of the benzophenone ketyl radical. If the purple color faded, the ether was redistilled onto a new mixture until the color became permanent. This solvent was stored over the metal since decomposition was negligible.

Deuterated solvents were refluxed at least eight hours with barium oxide and then vacuum distilled onto freshly dried type 4A molecular sieves (Linde, Union Carbide). The sieves were dried by passing dry nitrogen over them while baking at approximately 250°C. Final drying was accomplished by heating under vacuum. The solvent was stored over molecular sieves to insure dryness and samples were made up by vacuum distilling into an NMR tube with dry solute already in place. This procedure provided samples with less than 100 ppm water (usually about 50 ppm) with no noticeable contamination or decomposition.

III) LIGAND PURIFICATION

C222 (E.M. Laboratories, Inc.) was recrystallized twice from hexanes and vacuum sublimed at approximately

110°C in the dark using a cold finger filled with a dry ice-isopropanol mixture. Clll was purified by filtering through a type F-20 basic alumina column with anhydrous ether.

The liquid cryptands, C211 and C221 (both obtained from E.M. Laboratories) and C322 (synthesized in our laboratory at Michigan State University), were vacuum distilled.

The purification of 18-C-6 (PCR, Inc.) was accomplished by following the procedure established by E. Mei⁽³⁶⁾. All ligands were stored under vacuum and in the dark.

IV) SAMPLE PREPARATION

A) Preparation of Anhydrous NMR Samples

Figure 7 shows the apparatus used in the preparation of anhydrous samples for NMR analysis. The solvents were dried by using the previously mentioned methods and stored via vacuum distillation in Pyrex bottles equipped with high vacuum valves and Fischer-Porter joints. The solvent was introduced into the NMR tube by distilling through a tee, the bottle being attached to one end and a valve, fitted with a ground glass joint attached to the other end. An NMR tube, also equipped with a compatible ground glass joint was affixed to the valve (using a minimum of high vacuum grease) and the entire system evacuated. Thus, any volatiles could be pumped from salts, ligands, etc. before distilling in the solvent. The solvent could then be distilled, the sample removed from the tee, and capped by a layer of argon using a

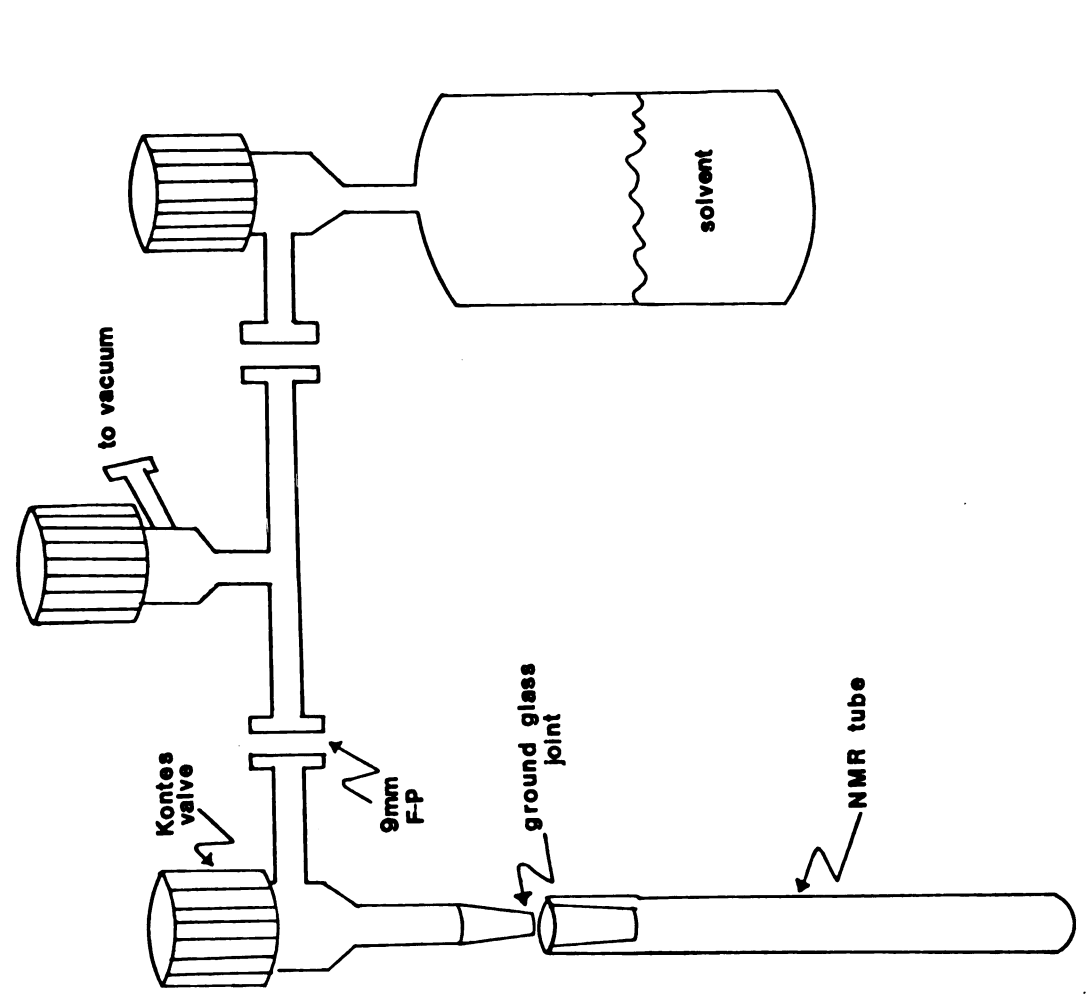


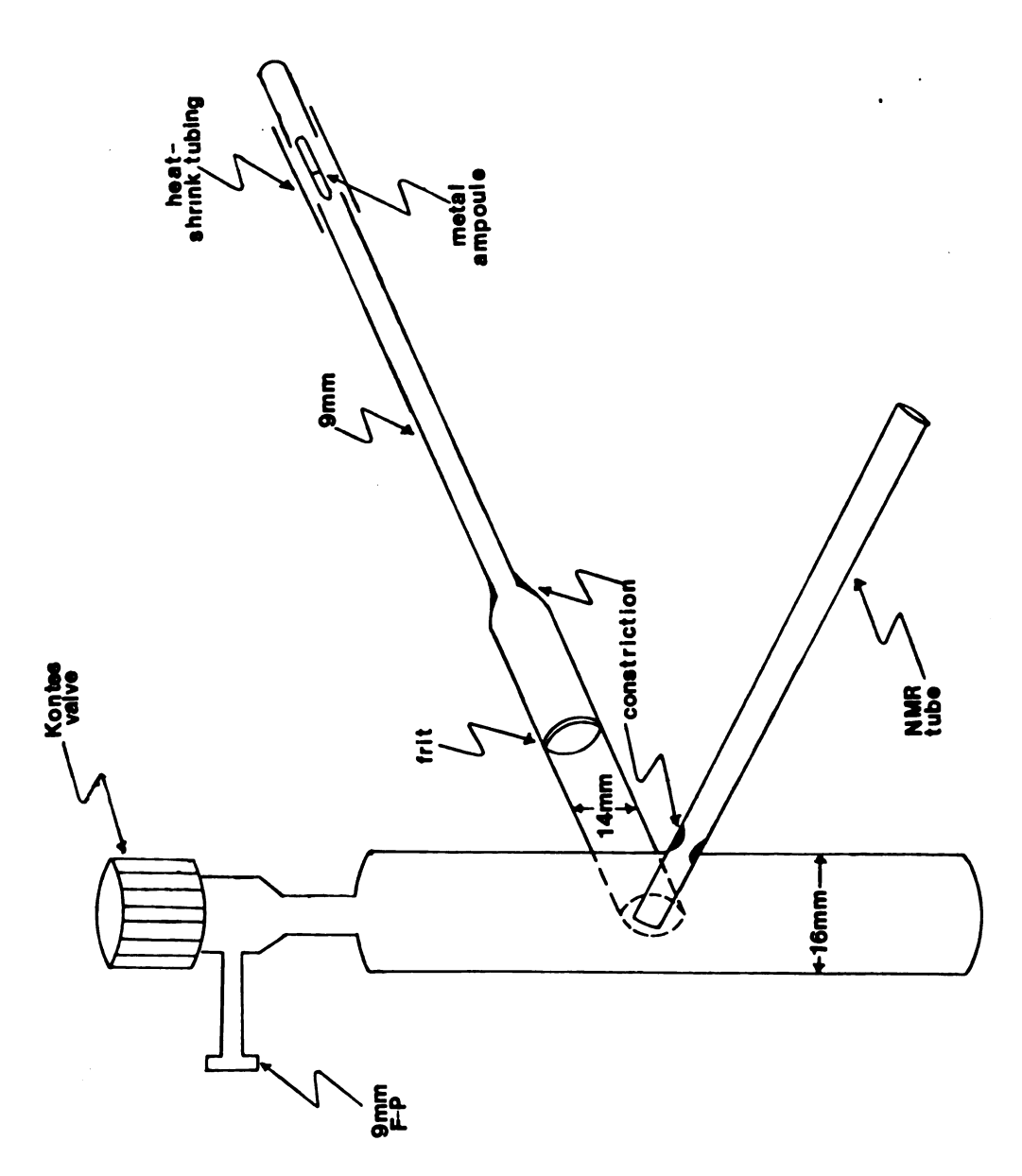
Figure 7. Apparatus used in the preparation of anhydrous samples for NMR analysis.

"Schlenk" line procedure (87) and the valve quickly replaced by a sealed ground glass top. This procedure allowed water content in the final sample to be kept well below 100 ppm (usually about 50ppm) with no contamination.

B) Alkali Metal Anion Solution Preparation

The apparatus used in alkali metal anion synthesis for observation via NMR or EPR is depicted in Figure 8. ligand was introduced from the top and evacuated to about 1×10^{-5} torr. Metal was introduced through a side-arm and distilled several times so as to obtain a pure metal mirror in the compartment before the frit. The side-arm was then removed by a flame seal-off at the constriction and discarded. The solvent was introduced as described earlier, by vacuum distillation through a tee and the apparatus transferred to a dry ice-isopropanol bath. The solution of ligand was transferred over the metal as many times and at as high a temperature as could be withstood without decomposition. When an equilibrium was achieved, the dark blue solution was poured into the NMR tube and flame sealed at the constriction. prepared sample was stored at dry ice temperature until NMR analysis was conducted, usually within an hour after sample preparation was complete.

The apparatus employed in the synthesis of solid powders and crystals of alkali metal anion salts was very similar to that previously described, except that the NMR tube was not incorporated in this process. The sample was initially made in an identical fashion by distilling metal and solvent,



Apparatus used in the synthesis of alkali metal anion solutions. Figure 8.

then washing over the metal several times. The deep blue solution was next poured away from the metal and cooled in a dry ice-isopropanol bath for about an hour and observed periodically for signs of precipitate formation. The cold solution was then decanted back over the metal and warmed as much as possible without inducing decomposition. This procedure was continued until either all the ligand was complexed or decomposition had begun. At this point, the cold solution was decanted back over the metal, leaving the powder behind, and the solvent distilled out of the vessel. The precipitate was either sealed under vacuum and stored in dry ice or washed with a nonpolar solvent, such as diethyl ether (if stable), and stored in a similar manner.

V) C111 SYNTHESIS AND PURIFICATION

The synthesis of Clll follows the scheme depicted in Figure 9 and involves the condensation of the acid chloride, I, with the monocyclic diamine, II, to give the bicyclic diamide, III⁽²⁶⁾. This is reduced with diborane to give the unusual monoborane adduct, IV, rather than a diborane adduct, presumably because the ligand cannot extend both nitrogen lone pairs outside the ligand (exo) except with much difficulty. The borane adduct is then reduced with KOH in methanol to give the free diamine.

Approximately 200 mg of Clll was received from Professor J.-M. Lehn and was purified by passing through an alumina column with anhydrous ether.

Figure 9. Steps in the synthesis of Clll.

Residues (8-10 grams) containing the bicyclic diamide of C111 and polymer by-products were also obtained from Lehn's laboratory. The residues were dissolved in CHCl3 and precipitated with diethyl ether. The polymer precipitated first and the diamide was left behind (about 1.4 grams of the impure diamide was obtained). The diamide was reduced by suspending it in dry tetrahydrofuran (140 ml) and about 35 ml of diborane solution (1 M in THF, Alfa Division, Ventron Corporation) was added dropwise with cooling. The mixture was refluxed for two hours and cooled to room temperature upon which 7 ml of conductance water was added. This addition caused much effervescence as the diborane was decomposed. The solution was evaporated to dryness and extracted with ether using a soxlet procedure. This procedure gave no monoborane product, but instead, about 0.7 grams of the monoprotonated, Clll HX, i was obtained. The means by

which the borane adduct was reduced and the monoprotonated ligand formed is not known.

The internally monoprotonated ligand with its unidentified anion was converted to the bromide by an ion exchange procedure using a Dowex 1 x 2 column. The resin was converted from the chloride to the bromide form by using an aqueous NaBr solution and testing the effluent with $AgNO_3$.

Clll·HBr,i was converted to the NO $_3^-$ form by using AgNO $_3$ precipitation followed by filtration through a small alumina column.

Table 2 gives an indication of the solubility of several Clll complexes in many solvents.

VI) METAL PURIFICATION

Alkali metals were purchased as follows:

Na: Alpha Division, Ventron Corporation (99.95%)

K: Alpha Division, Ventron Corporation (99.95%)

Rb: Fairmont Chemical Company

Cs: Donated by The Dow Chemical Company

All metals were stored under vacuum in pre-measured tubes using the "trombone" apparatus shown in Figure 10. The trombone consists of three Pyrex chambers separated by constrictions for sealing off, which allow the metal to be divided into three portions. These chambers also contain long glass tubes of premeasured inner dimensions into which the metals can be distributed. The volume of these tubes

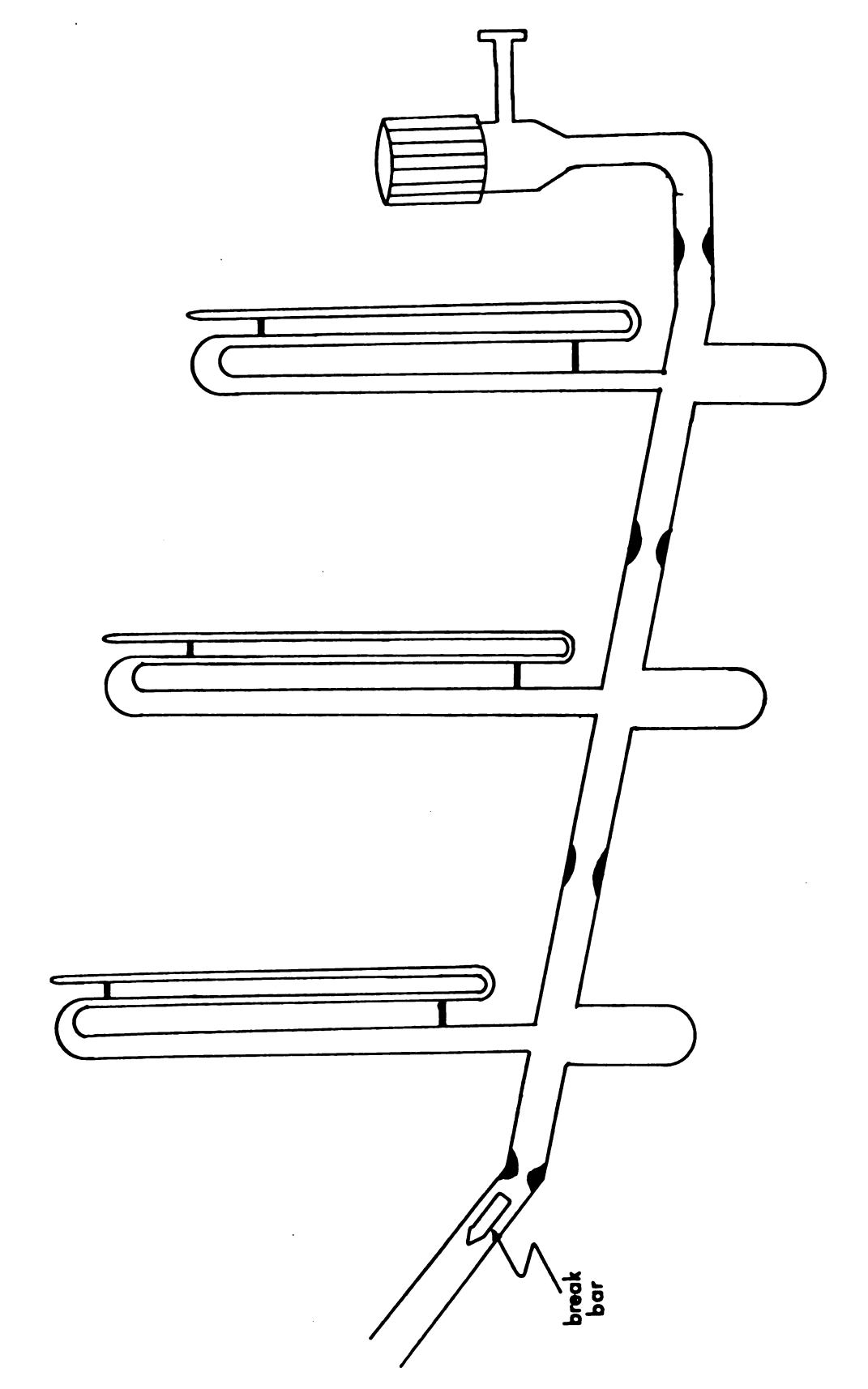
Table 2. The solubility of Clll and its complexes in various solvents.

Species	Solvent	Solubility
Clll Water,	MeOH, Acetone, Ether, Benzen	e v
Clll.HCl,o	Water	Ÿ
Clll.HCl,o	Acetone	i
Clll•HBr,i	Water, Acetone, MeOH	v
Clll•HBr,i	Ether	i
clll•HNO ₃ ,i	MeOH, EtOH	s
clll•HNO ₃ ,i	Acetone	i
C111.2HCl,i-o	Water, MeOH	v
C111•2HC1,i-o	Ether, Acetone	i
C111.2HC1,i-i	Water, MeOH	v
C111 • 2HCl,i-i	Ether, Acetone	i

v - very soluble s - soluble i - insoluble

is two to three times greater than that of the metal to be distributed.

The metals were received in three to five gram ampoules under argon with a break seal for access. The ampoule was first flame sealed to the trombone into which a break bar had previously been placed. The entire system was then pumped to less than 1×10^{-5} torr, the break seal broken and the argon pumped out of the system. The metal was then distributed equally among the chambers which could be flamed sealed from each other to yield three separate systems. The metal was forced down the tubes by heating



"Trombone" apparatus for the storage of alkal1 metals. Figure 10.

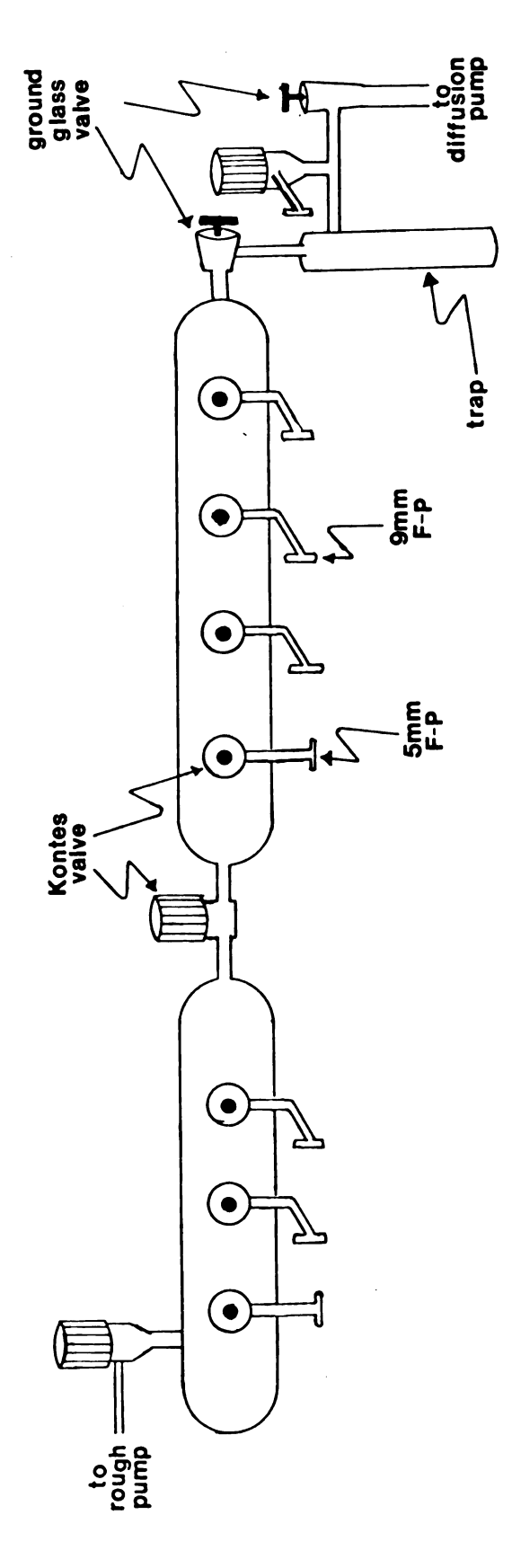
and gently shaking, then each tube was sealed off. In order to facilitate distribution of the metal into the tubes, it was imperative that the system had been pumped to high vacuum since any residual gas pressure would have blocked this transfer.

Known volumes of metals were easily obtained from these tubes since their inside diameters had been measured. The proper amount of metal could then be isolated and sealed from the rest of the tube and introduced into the sample preparation vessel using heat-shrink tubing as shown in Figure 8. The tube was scratched with a glass knife and placed into a side-arm of the apparatus. The side-arm was then capped with a glass end made vacuum tight with flexible heat-shrink tubing. The system could then be pumped to high vacuum (10⁻⁵ torr) and the metal tube broken by bending the heat-shrink tubing. The metal was then distilled into the vessel and the side-arm flame-sealed away.

VII) VACUUM PROCEDURES

Vacuum distillation provides a convenient method by which to purify and transfer air sensitive materials.

Standard high vacuum procedures were employed throughout this work. Figure 11 shows the type of vacuum line arrangement used. It was composed of two Pyrex chambers, one for high vacuum work and the other used exclusively for work which did not require high vacuum. These compartments were separated by a valve which permitted two preparations to be



Vacuum line arrangement used in sample preparation. Figure 11.

done simultaneously. Greaseless Teflon valves of the Kontes and Fischer-Porter type were utilized to eliminate the possibility of contamination by vacuum grease. Pressures of 10^{-6} torr were easily attained. The diffusion pump was separated from the manifold by a liquid nitrogen trap to prevent its contamination. All distillations were done through tees and not through the manifold in order to insure a clean and efficient system.

VIII) NMR SPECTROMETER

Two NMR spectrometers were utilized for the majority of the analyses presented in this dissertation. Proton and carbon-13 NMR studies have been performed using a Bruker WH-180 super-conducting NMR spectrometer operating at a field strength of 4.228 Tesla. The WH-180 operates only in the pulse-fourier transform (P-FT) mode and is equipped with quadrature detection which provides a 40% signal to noise enhancement. The spectrometer is completely computer controlled via a Nicolet 1180 computer package which provides versatile pulse and decoupling options. Homo and hetero nuclear and gated proton decoupling, internal deuterium lock, temperature control and multinuclear options are also capable with the instrument. The large field strength provides exceptional resolution and sensitivity such that samples of less than 1 mg may be utilized for analysis.

The temperature meter of the WH-180 was calibrated on several occasions by placing an NMR tube of methanol with a thermocouple in the probe and allowing it to equilibrate. The temperature in the probe was measured by a calibrated Doric digital thermocouple and compared with the setting of the temperature meter on the spectrometer. A calibration chart was thus developed and periodically monitered for accuracy. The temperatures could be reliably measured to ±3K with this procedure.

Nuclei other than ¹³C and ¹H have been analyzed on a greatly modified Varian DA-60 spectrometer which also operates in the P-FT mode. It is equipped with external lock, a Nicolet 1080 computer system, a versatile multinuclear package patterned after the development of Traficante (37), and operates at a field strength of 1.409 Tesla. The temperature of the sample in the probe may be monitored to ±2K by using a calibrated Doric digital thermocouple with the thermocouple affixed less than 20 mm from the sample tube. For further details of the design and operation of the DA-60 spectrometer see the Ph.D. dissertation of Joseph M. Ceraso (38).

IX) SAFETY

Many of the crown ethers have been reported to be highly toxic (39). 12-crown-4 is absorbed through the skin and its vapors may be inhaled in sufficient quantity to cause severe injury and death. Testicular atrophy.

sterility, lack of coordination, convulsions and death have been observed in rats exposed to 1 to 64 ppm in a 6 hour day for one week. The toxicological studies of some higher crown ethers indicate that this entire class of molecules should be treated with care. Caution should also be utilized when handling the cryptands although their toxicity has not been reported.

The Chemistry Department safety guidelines should be consulted and understood before attempting laboratory work. These guidelines may be obtained from the Chemistry Business office. It should also be emphasized that safety glasses are a mandatory protection for work involving vacuum techniques.

CHAPTER 3

CONFORMATIONAL ANALYSIS OF CRYPTAND 111

I) INTRODUCTION

The fact that cryptands bind ionic species is easy to demonstrate, but distinguishing how and where the interaction occurs is a much more subtle problem. Cryptands, for instance, may exist in a number of conformations and possess several potential binding sites. As shown in Figure 12, the free ligands are thought to exist as a mixture of rapidly interconverting isomers in solution (40-41). The nitrogen atoms are free to invert their lone pairs from inside the cavity (endo) to the outside (exo) with relative ease.



Figure 12. The conformations of C222.

It has not been established that these conformations contribute to ion binding or that they exist at all, except that the following model compounds seem to support the likelihood. These model compounds, synthesized by Park and Simmons (42-44), are macrobicyclic diamines similar to the cryptands, except that the strands consist of hydrocarbons rather than polyethers. Upon acidification, these protonated diamines undertake a new conformation which has been shown to be an

interconversion of the bridge-head nitrogens from the exoexo form to the endo-endo form, with the protons bound internally. The interconversions are very slow and proceed with equilibrium constants which are greatly dependent on the sizes of the hydrocarbon strands.

It has been demonstrated from their crystal structures that the cryptands exist in the endo-endo conformation when binding ions in the solid state and this form would be expected to be most thermodynamically stable, because the nitrogens could also participate in binding (45). In solution, one may only speculate as to the conformations of the ligand, because if the interconversion is taking place, it is too rapid to be observed.

Several experiments support the idea that the structure of the ligand is at least somewhat flexible in solution. Protonation studies of C222, C221, and C211 and its metal ion complexes reveal that the free diamines can protonate at both nitrogen atoms $^{(46-48)}$. The pK values for C222 are 1.53 x 10^{-10} and 6.3 x 10^{-8} (25). The pH titration of sodium-cryptate complexes indicates that protons and sodium are not compatible in the same cavity, the metal ion being forced out of the ligand at pH values where the cryptand is significantly protonated. This process is acid catalized in many instances (25). A mechanism has been suggested by which the proton would bind to the exo-endo conformation of the ligand (although it is thought to be unfavorable) and thereby initiate the removal of the metal ion. Many other mechanisms could also be

envisioned which would show acid catalysis and, therefore, these data do not substantiate the exo-endo conversion process.

In order for the cryptands to bind cations, the ligands must greatly distort one face so as to expose the cavity. This is evident in the slow rates of formation and dissociation of cryptate complexes in comparison with crown ether complexes, and other monocyclic ligands (49-52). Once the ion is located inside the cavity, the cryptand has the ability to conform to the size of the ion so as to provide the most stable binding (53). As previously mentioned, X-ray studies indicate that the nitrogen atoms and the oxygen atoms participate in ion binding. These studies substantiate the fact that the cavity size of the ligand may contract or expand to accommodate ions of various size.

Another illustrative example of this flexibility may be drawn from the complexation of Cs⁺ ion by C222. Cesium ion is too large to easily fit inside the ligand, as the ion's radius is 1.84 Å while the cavity radius is about 1.4 Å. Depending on the conditions, cesium seems to bind either in an exclusive fashion, sitting on one face of the ligand in a crown type complex, or it will go inside, even though the nominal cavity size is much too small to accommodate it. Indeed, crystal structures of cesium complexes with C222 reveal an inclusive complex, but cesium NMR data provide strong evidence for the presence of both inclusive and exclusive complexes in solution which rapidly interconvert at room

temperature and favor the inclusive form at lower temperatures (54-55). Recent crystallographic studies show that the KSCN·C221 complex has the exclusive configuration in the solid state (56).

Proton binding to Clll is similar to the metal ion binding in the larger cryptands, because Clll may also be envisioned as undertaking several topologies which could contribute to the binding. The major difference rests in the fact that a bare proton has negligible size and should be free to bind at any of the nitrogen atoms and oxygen atoms individually rather than interacting concurrently with all the donors, as is the case with metal ions. Another important distinction is that Clll is a very "tight" molecule, in that movement of the strands or nitrogen inversion seems to be much more difficult than in the larger cryptands, as shown in Figure 13. Synthetically, Clll also reflects this strain by the difficulty of ring closure, producing low yields, the bulk of the product being the dimer and polymers. Also, as mentioned earlier, the exo-exo diborane adduct is not obtained in the diborane reduction of the dilactam as with larger cryptands, instead the exo-endo monoborane adduct is produced. Since with Clll there appears to be a large activation barrier to nitrogen inversion as well as other molecular interconversions, it may serve as a good candidate for the observation of individual conformations.

In view of the previous discussion, it would be of value to define the sites which might be expected to





Space filling models of Clll, A) D_{3h} symmetry (large cavity) and B) compact cavity. Figure 13.

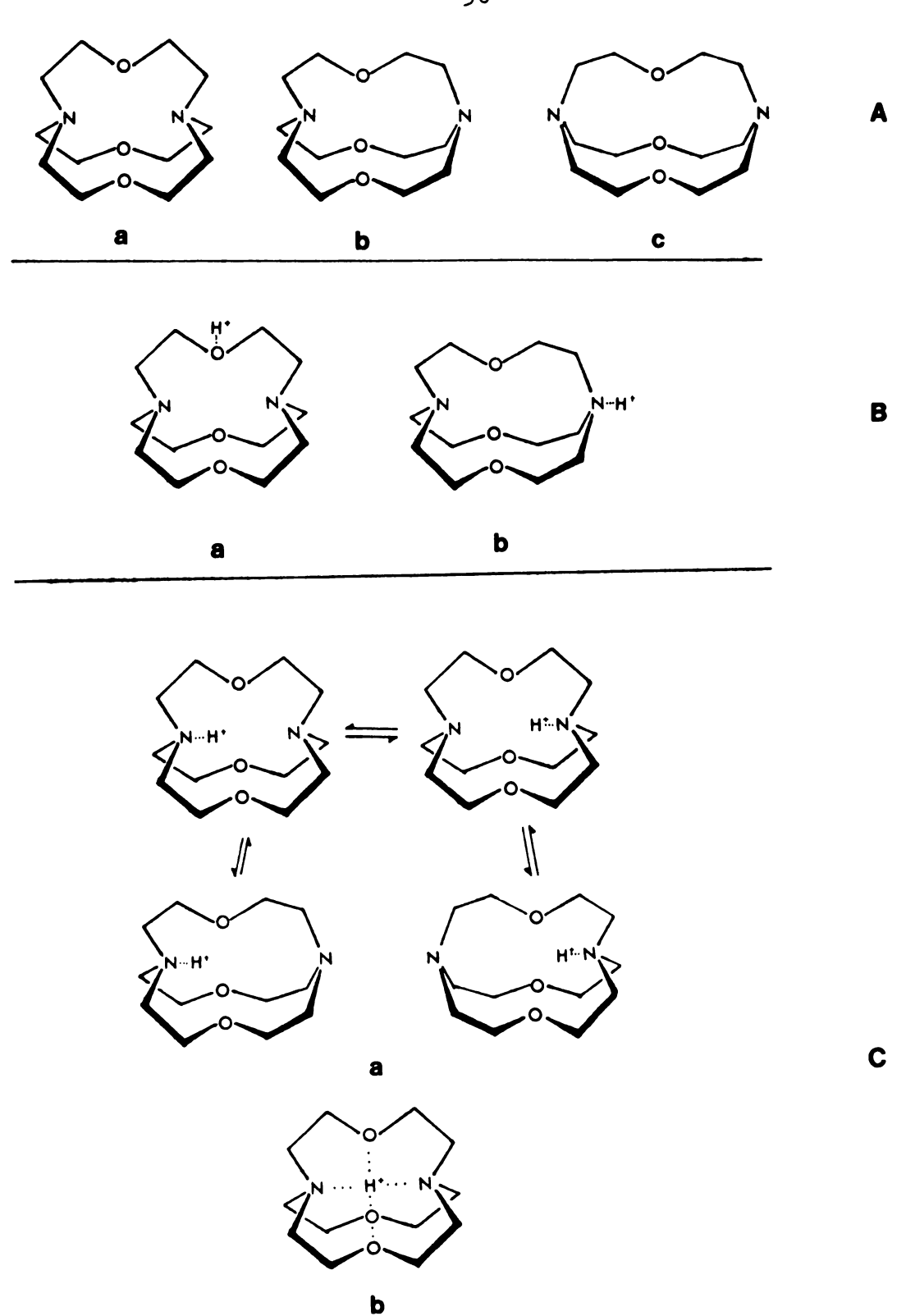
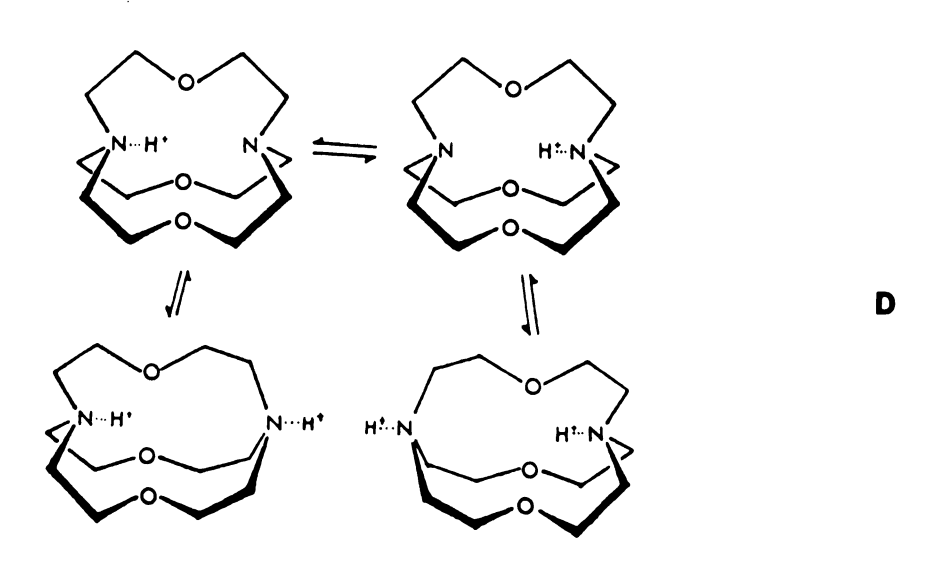


Figure 14. The possible binding sites and conformations of Clll, A) unprotonated, B) external protonation, C) internal protonation, D) external protonation of the internally monoprotonated complex and E) internal diprotonation.



participate in proton binding. Figure 14 shows the more logical structures, although the exo-exo conformations may be too strained to exist. Protons probably bind externally at the nitrogens, since in solution the latter are much stronger bases than are the ether oxygens. The latter, however, should not be rejected as viable sites, especially after one nitrogen has been externally protonated. Inside the cavity, the situation changes very drastically, because the ligand shields the inclusively bound proton from the solvent and the donicities of the polar groups would be expected to be very similar to those in the gas phase. Taft and coworders have tabulated gas phase bacisities of several amines and ethers (57-58), which demonstrate the similarity in base strength of these groups in the gas phase. Therefore, both the nitrogen atoms and the oxygen atoms might be expected to contribute to the binding inside the cavity of Clll.

Finally, torsional motions may also contribute to the strength of proton binding. The larger cryptands, for instance, conform to small ions bound inside, in order to optimize the interaction with the donor atoms. This optimization involves a concerted rotation of the nitrogens so that the angle, α , shown in Figure 15, can be large for small ions or small for the larger ions to provide conditions more conducive to binding. Figure 13 depicts models of Clll in both configurations. The one in which α is large, B), might be expected to be most stable because in this conformation, the nitrogens are closer

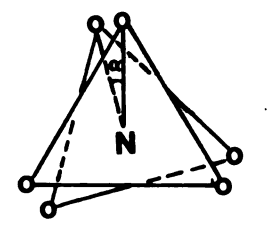


Figure 15. Model showing the torsional angle of C222.

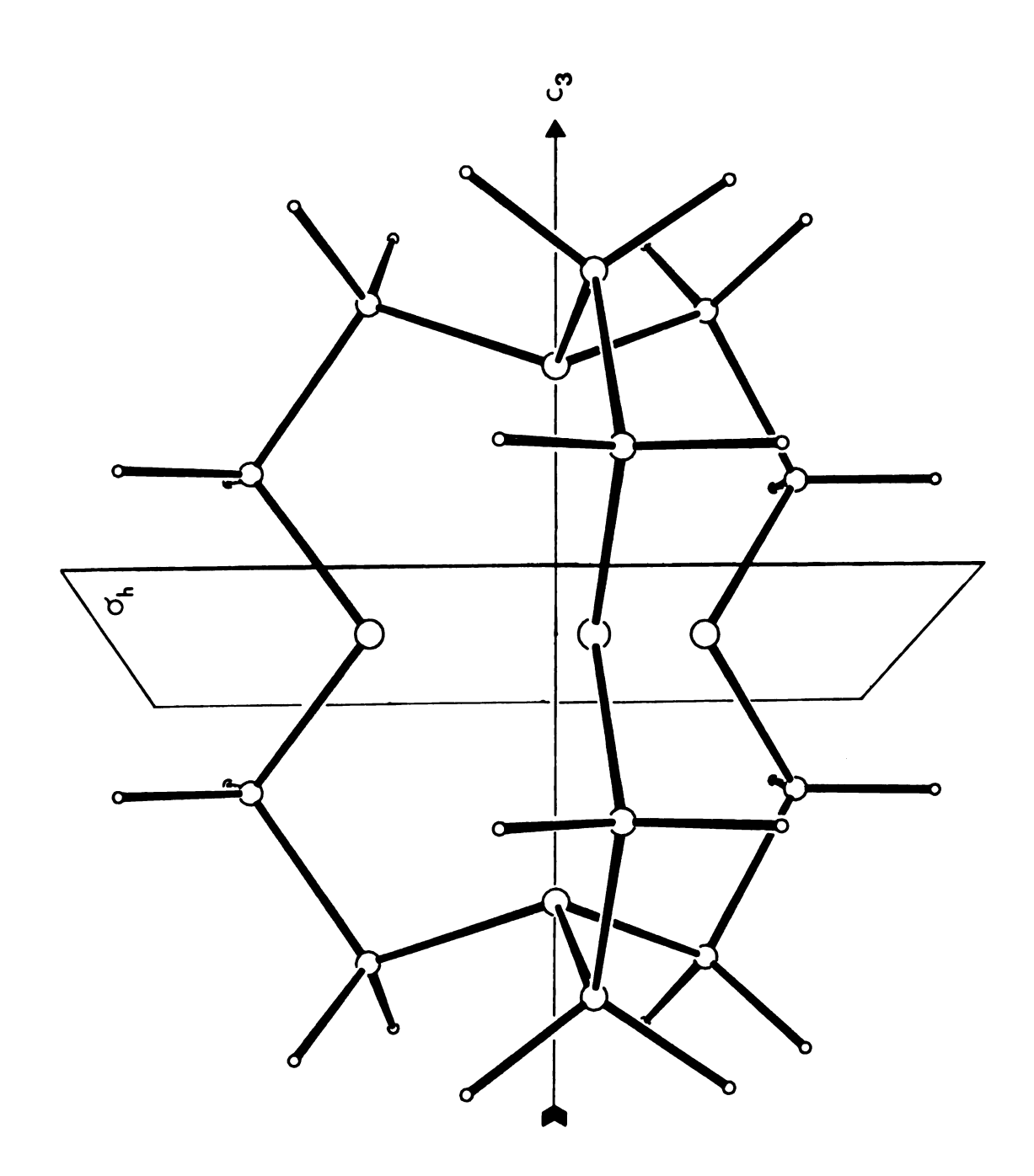
to the H₁. This conformation would also be expected to greatly shield the inclusive proton from the solvent.

A) Clll Symmetry Considerations

Nuclear magnetic resonance spectroscopy is admirably suited for the identification of the nonequivalence of nuclei which develops due to the asymmetric configurations. This nonequivalence is observed in both the proton chemical shift and in spin-spin coupling constant. For example, geminal protons (those on the same carbon) have identical chemical shifts and do not couple with one another if they are chemically equivalent, but if for some reason they become nonequivalent, they do couple to one another and their chemical shifts are no longer identical. A very frequent cause of geminal nonequivalence, and one which occurs often with the cryptands, is the slowing of molecular vibrations at low temperatures, which "locks" the geminal protons into slightly different chemical environments (on the NMR time-scale).

Nuclear magnetic resonance also provides characteristic information about the electronic environment of the binding site from the chemical shift and thereby facilitates the identification of the functionality of that site. The relative stabilities of various sites may be obtained from the populations in those sites and the dynamics of exchange between sites may be obtained from line broadening. The theory of line broadening in NMR has been thoroughly developed by Bloch⁽⁵⁹⁻⁶⁰⁾, so that the NMR spectra may be mathematically simulated in order to define the exchange rates associated with spectra at various temperatures (see the Appendix for a complete derivation). The temperature dependence of the exchange rates which, in principle, should adhere to the Arrhenius theory, provides activation parameters for exchange.

The interpretation of the NMR spectra of Clll and its complexes is greatly simplified if the symmetry of the molecule is understood. As can be seen in Figure 16, Clll is a highly symmetric molecule and belongs to the $\mathrm{D_{3h}}$ point group. The most useful symmetry elements for interpretation purposes are the $\mathrm{C_3}$ rotational axis through the nitrogens, the σ_{h} plane through the oxygens, and the three σ_{v} planes which include the $\mathrm{C_3}$ axis, a polyether strand, and bisect the other two strands. It is simplistic to assume that the σ_{v} symmetry exists, because gauch conformations are more energetically favored than are the eclipsed conformations which are necessary for σ_{v} symmetry. When rapid methylene wagging motions occur, so that the interconversion between the two gauche forms is rapid, the σ_{v} symmetry will be presented if the "average" conformation preserves this symmetry. This



Model showing the symmetry elements of Clll in the $\mathbf{D}_{\mathbf{3h}}$ configuration. Figure 16.

interconversion must proceed in milliseconds or faster in order to present an exchange averaged picture in the NMR spectrum, since the maximum exchange rate observable is on the order of the chemical shift difference of the two sites. This difference rarely exceeds 1,000 Hz. Therefore, if an exchange occurs, whether it be a proton jump or interconversion of two conformations of the ligand, and is more rapid than milliseconds, the NMR spectrum will present a single line (or a multiplet if scalar coupling is present) which is the population average of those sites involved. The chemical shift of this exchange averaged line is defined by:

$$\delta_{\text{obs}} = \sum_{i} x_{i} \delta_{i}$$
 (22)

where:

 δ_{obs} - the observed chemical shift δ_{i} - the shift in site i x_{i} - the mole fraction (the population) in site i

The room temperature spectra of the Clll complexes show that the $\boldsymbol{\sigma}_{_{\boldsymbol{\boldsymbol{v}}}}$ symmetry element is preserved because interconversion rates are faster than the NMR time-scale and the exchange averaged conformation preserves this symmetry.

II) NMR SPECTRA AT AMBIENT TEMPERATURES

At room temperature, molecular motions are rapid and the NMR spectrum of a given species usually reflects an exchange average of several different conformations. true of the spectra of Clll and its complexes shown in Figure 17 and the chemical shifts which are given in Table 3. The

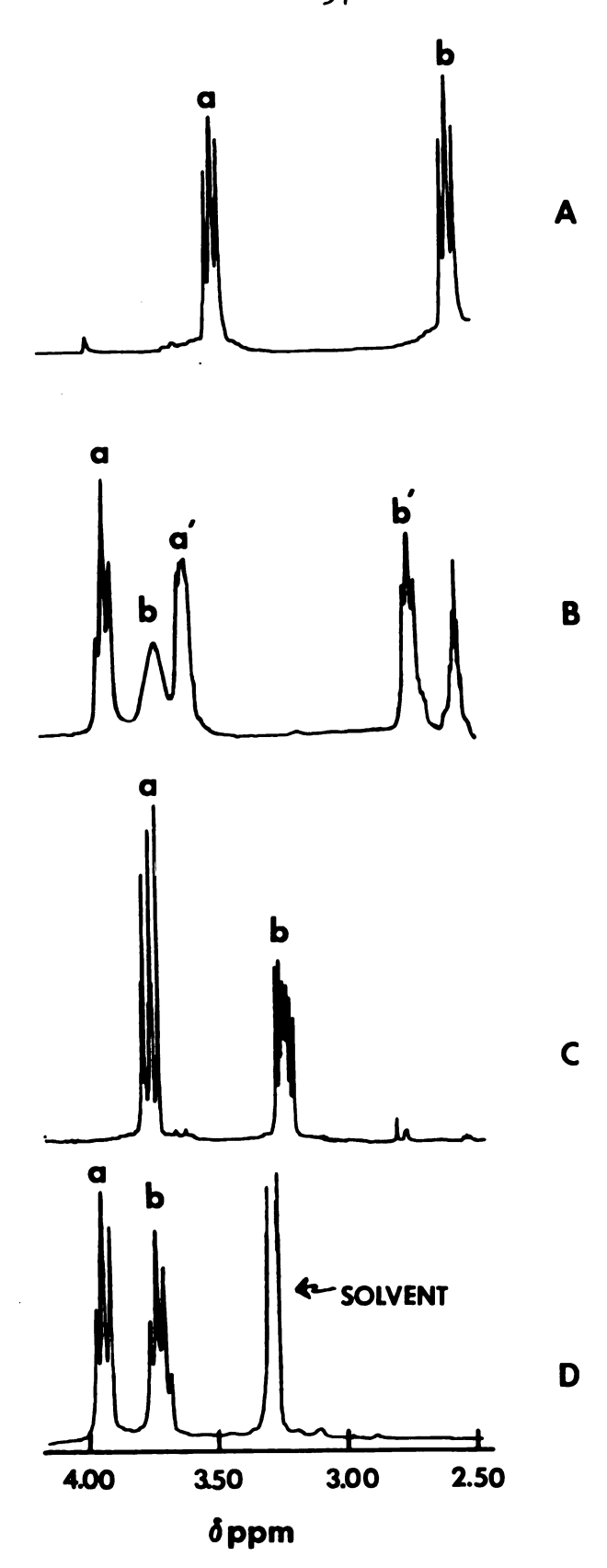


Figure 17. The NMR spectra of Clll and its protonated complexes at ambient temperature.

The chemical shifts of Cill and its complexes at ambient temperature Table 3.

rapre 3. The C	table 3. The chemical shilts of this and its complexes at ambient temperature.	cill and lts	complexes at amo.	lent temperature.	
Species	Solvent	Temp.	mdď CH ² O	mdd N CH ² N	H ₁ ppm
נווט	d ₆ -Acetone	295°K	3.44	2.52	
CIII	cdCl3	295°K	3.60	2.63	
C111.TFAA,o	d-Acetone	270°K	3.99, 3.65	3.76, 2.63	
C111.HBr,1	d ₆ -Acetone	295°K	3.76	3.24	6.07
C111.HBr,1	d ₄ -MeOH	295°K	3.67	3.10	8.98
C111.2HC1,1-1	ф-меон	295°K	3.96	3.74	7.33

most striking feature of these spectra is the dependence of the chemical shift of the backbone protons on protonation. The CH₂O proton lines shift downfield by about 0.3 ppm per proton added and the CH₂N proton lines shift by about 0.7 ppm per proton, more than double the CH₂O proton shift. This downfield shift is caused by the delocalization of the positive charge of the bound proton throughout the backbone of the molecule, which is an electric field contribution to the chemical shift. The fact that the CH₂N protons show a greater shift is indicative of greater interaction of the internal proton with the nitrogens than with the oxygens.

Assignment of the binding interactions should be done with care because these spectra represent the average of many rapidly interchanging molecular conformations. Nevertheless, some qualitative assignments may be made from them. Three of the four structures, Clll, Clll·H⁺,i and Clll·2H⁺,i-i, preserve the D_{3h} symmetry since the spectra show equivalence of the CH₂O protons as well as of the CH₂N protons. The fourth structure, Clll·H⁺,o, has lost at least some molecular symmetry, because these two sets of protons are no longer equivalent. A discussion of the three symmetric complexes will be presented first, focusing on each structure individually, and the externally protonated ligand will be discussed thereafter.

A) Clll in d₆-Acetone

The NMR spectrum of Clll contains two sets of triplets, one set at 3.44 ppm ($\rm CH_2O$ protons) and the other at 2.52 ppm ($\rm CH_2N$ protons). The two sets of protons split each other

with a coupling of 5 Hz. Figure 14A shows three possible conformations of the ligand. From the room temperature spectrum, one is not able to conclusively establish their presence except that, if exo-endo nitrogen inversion or any other conformational change is occurring, it is doing so rapidly on the NMR time-scale, and its average preserves D_{3h} symmetry. Based on an examination of molecular models, the exo-exo form is not expected to exist, but a rapid exchange between the endo-endo and exo-endo forms would preserve the D_{3h} symmetry. Rapid vicinal carbon wagging vibrations must also be occurring in order to retain the σ_{v} plane through the polyether strand, which is necessary for the geminal CH_{2} proton equivalence. This vibration entails exchange of the vicinal carbons between the gauche conformations whose average is the eclipsed conformation.

B) Clll·H⁺,i·Br⁻ in d₆-Acetone

The internally monoprotonated ligand shows D_{3h} symmetry at room temperature for the same reason as does Clll; namely, rapid interconversion between the conformers. The CH_2O protons are equivalent at 3.76 ppm as are the CH_2N protons at 3.24 ppm. These two sets of protons again split each other into triplets of 5 Hz, and the inclusive proton, H_1 , also couples to the CH_2N protons with a coupling constant of 2.5 Hz, resulting in a six line pattern. The H_1 resonance is located at 9.07 ppm with a linewidth of about 15 Hz. No coupling is observed to the nitrogens or oxygens by any of

the protons or carbons, presumably because of very fast quadrupolar relaxation, but the breadth of the H_1 signal (approximately 15 Hz) and the backbone proton lines (approximately 1.5 Hz) probably originates from efficient scalar relaxation by the nitrogens⁽⁶²⁾. No coupling of the H_1 to the carbons is observed in the C^{13} NMR spectrum, but it would be expected to be about one fifth that of the CH_2O proton splitting and would not be observable⁽⁶¹⁾.

The fact that coupling of the H_{\uparrow} proton is observed to the CH2N protons and not the CH2O protons is good evidence that the H_{i} proton interacts most strongly with the nitrogens and not the oxygens. Coupling is transmitted through a chemical bond via Fermi contact interactions (62), and the magnitude of the coupling interaction is similar through the protonated ether oxygens and the protonated amines. Three bond coupling constants of about 5 Hz have been documented for ethers protonated with super acids and for protonated amines (63-64). Therefore, if the ether oxygens did interact appreciably with the H_1 , we would expect to observe coupling to the CH_2O protons, although attenuated slightly since there are three oxygens, rather than only two nitrogens. The 2.5 Hz coupling of the H₁ to the CH₂N protons agrees with literature values for protonated amines. The observed coupling is half the literature value since the $\mathbf{H}_{\mathbf{i}}$ is shared equally between the nitrogens.

A structure which would be consistant with the nitrogen protonation as well as the preservation of D_{3h} symmetry is

shown in "a" of Figure 14C. The proton jump between the nitrogen atoms is always rapid. The exo-endo inversion is probably hindered by coulombic interactions between the H, and the nitrogen lone pair, and therefore occurs very infrequently. The internal proton exchange phenomenon is very unusual, since it occurs much more rapidly than the NMR time-scale (since it preserves symmetry), and yet coupling to the CH_2N protons by the H_1 is not lost. Normally, when proton exchange is more rapid than the NMR time-scale, coupling between the exchanging protons and those attached near the binding site is lost. This loss occurs because protons of either spin state have an equal probability of binding at the site and the NMR spectrum presents a single line which is an exchange average of the two. With Clll.H, i, the spin character of the exchanging proton is preserved between jumps (ignoring T_1 relaxation which is slow by comparison), because the same proton exchanges back and forth between the two nitrogens. The H, is not able to exchange with protons in solution, but is restricted to move only within the confines of the cavity of Clll.

c) Clll.2H, i-i.2Cl in d4 MeOH

The internally diprotonated ligand must exist in the endo-endo form as a prerequisite for D_{3h} symmetry, due to the size restrictions of the cavity. The H_1 protons must be located on the C_3 axis, each equidistant from the center of the cavity. Their distance from the nitrogens is probably

less than in the monoprotonated ligand, because of the coulombic repulsion of the two protons. As a result of the symmetry, the spectrum, as seen in Figure 17D, presents the equivalence of all $\mathrm{CH_{2}O}$ protons at 3.96 ppm and $\mathrm{CH_{2}N}$ protons at 3.74 ppm, the two sets splitting each other into triplets with a coupling constant of 5 Hz. The H, protons, whose resonance is located at 7.33 ppm, couple to the CH_2N protons (but not to the CH20 protons) with a coupling of 5 Hz, producing two sets of overlapping triplets which result in a four line multiplet. Coupling, which originates from the Fermi contact interaction, is a function of the ability of the nitrogens to donate electron density to the $\mathbf{H}_{\mathbf{1}}$. The introduction of a second proton into the cavity of Clll •H +, i would be expected to double the coupling through the nitrogen, because each nitrogen binds to one full proton rather than sharing one between them. Thus, the contribution of electron density from each nitrogen doubles. This is exactly what is observed, since the coupling to the CH2N protons increases from 2.5 Hz to 5.0 Hz with the addition of the second internal proton.

When one of the two internal protons is replaced by a deuteron which has a coupling constant one sixth of that of a proton (less than 1 Hz for three bond coupling), the NMR spectrum of the CH₂N protons indicates two overlapping patterns which may be distinguished by decoupling experiments. One pattern shows coupling of 5 Hz to the H₁, whereas the other does not, a result of negligible exchange of the proton

and deuteron between the nitrogens inside the cavity. This complex probably exists in the configuration displayed in Figure 13A with the cavity as large as possible in order to allow maximum separation for the $\rm H_{i}$ protons.

The upfield shift of the H₁ protons in going from the mono to the di internally protonated ligand is a consequence of two opposite contributions. The size limitations of the cavity of Clll tend to restrict the donation of electrons from the nitrogens to the internal protons because, as they gain electron density, they also increase in size. This contribution induces a downfield shift. The increase in charge density inside the cavity greatly overshadows the former contribution, and induces a large electronic shielding, which in turn produces the observed upfield shift.

The linewidth of the H₁ is dominated by scalar relaxation to the nitrogen, and on the basis of a twofold increase in coupling constant from the mono to the di internally protonated ligand, the linewidth of the H₁ would be predicted to increase by a factor of four between the two complexes on the basis of the Fermi contact term. The observed linewidth of the H₁ in Clll·2H⁺,1-1 is about 50 Hz, which is in the range of the predicted values (48 to 60 Hz). The linewidth decreases with decreasing temperature because the relaxation rate of the nitrogen increases and thereby causes the scalar interaction to be less efficient (62). All assignments have been verified by decoupling experiments wherever possible.

The room temperature spectra indicate that the H_i protons interact at the nitrogens, and that the shifts produced for both the skeletal protons and the inclusive protons upon protonation are a result of the electric field contribution to the chemical shift. For this reason, Musher's equations, which predict the shifts resulting from changes in charge distribution, should prove valuable in understanding the observed shifts.

D) Musher's Theory of the Chemical Shift (30)

Musher's equations describe the chemical shift induced by the electric fields associated with charged or polar groups. The magnitude of the field is proportional to the charge density and the distance of the bond from the charge, as described in the Historical section. In order to calculate the shift expected upon protonation of Clll, a geometry for the ligand must be assumed. The nuclear coordinates have been calculated utilizing \mathbf{D}_{Qh} symmetry, and the assumption was made that the center of positive charge was at the nitro-The theory predicts a downfield chemical shift of 4.1 ppm and 1.0 ppm respectively for the CH₂N and CH₂O protons upon the introduction of two protons into the cavity of Clll. The observed downfield shifts are 1.4 and 0.6 ppm, which are in the right direction and relative magnitude, but much smaller than the theory predicts. The theory predicts an upfield shift of about 2.6 ppm for the H_i in going from Clll ·H⁺,i to Clll •2H, i-i, and again it is in the correct direction but too large (the real shift is 1.4 ppm). The theory applies

to gas phase interactions, so that solvent interactions with the ligand may cause the discrepency between the theory and the observed shifts, but it lends credence to the belief that protonation occurs at the nitrogens, and is also able to account for the entire shift.

E) Clll·H⁺,o in d₆-Acetone

The NMR spectrum of Clll·H⁺,o in d₆-acetone acidified with trifluoracetic acid (TFAA) (Figure 17B), reflects the loss of molecular symmetry, because four lines of equal area are present rather than two. (The multiplet at about 2.5 ppm is a ${\rm C}^{13}$ satellite of acetone.) There are two plausible sites for external protonation, shown in Figure 14B, one at an exo nitrogen and the other at an oxygen. Only nitrogen protonation, with the loss of ${}^{\sigma}_{\rm h}$ symmetry, could give rise to four lines of equal intensity. Protonation of the oxygen atoms would not give lines of equal intensity. Therefore, the resonances a and b correspond to ${\rm CH}_2{\rm O}$ and ${\rm CH}_2{\rm N}$ protons on the protonated side of the molecule and a' and b' to the unprotonated side.

Assuming these assignments are correct, the chemical shifts of the skeletal protons are informative in determining the contribution of exo-endo conformational changes to the chemical shifts of the Clll complexes. The Clll·2H, i-i complex and Clll probably exist in the endo-endo form. Those resonances from the protonated side of Clll·H, o, namely a and b, are very similar in their chemical shift to those of Clll·2H, i-i, whereas those on the unprotonated side, a' and

b', are very similar to those of Clll. Therefore, even in the presence of a greatly different conformation, the chemical shift of the backbone protons is dominated by nitrogen protonation and the contribution from the conformational change is less than 0.2 ppm.

Perhaps the most striking feature in relation to external protonation of Clll by TFAA is the lifetime of the complex, being greater than milliseconds. The spectrum of this complex demonstrates that the exo-endo form of Clll exists in solution.

The theory of Eigen concerning general proton-transfer processes predicts that when the strength of an acid is much different than that of the conjugate acid of the base used in proton-transfer reactions, the rate of transfer is fast. The transfer also is complete, favoring the formation of the species with greater $pK_a^{(65)}$ and the reverse reaction is slow. If the relative strengths are similar, however, the proton is rapidly exchanged between the two, but the transfer is incomplete. Eigen has shown that a proton-transfer reaction may be written as follows:

$$AH + B \xrightarrow{K_1} AH \cdots B \xrightarrow{K_2} A \cdots HB \xrightarrow{K_3} A + HB$$
 (23)

where AH···B and A···HB are encounter complexes. When the reaction favors one set of products, say A + BH, as is the case involving protonation of Clll with TFAA, the proton is rapidly transferred and the resulting complex is long-lived. This can give a long enough value of the exchange time, τ , to

permit observation of both HB and B when less than a stoichiometric amount of HA has been used. However, if the values of pK and pK are similar, fast proton exchange and an incomplete transfer occurs.

The external protonation of Clll has been studied by NMR as a function of acid strength in d_6 -acetone and d_{μ} methanol. Three acids were utilized; namely, HCl, trifluoroacetic acid (TFAA), and dichloroacetic acid (DCAA), each of which appeared to interact differently with Clll. HCl was generated by addition of about 0.1 ml acetyl chloride to about 10 ml of d_h -methanol and allowing time enough for the reaction to proceed to methyl acetate and HCl. This method provided an internal standard for a quantitative determination of acid content. When one drop of this solution was added to a solution of Clll in d_h -methanol, a white powder immediately precipitated, and the NMR signal of Clll was no longer observed. Presumably the acid formed the monohydrochloride salt of Clll, the proton being bound externally and the resulting complex was insoluble in $\ensuremath{\mathrm{d}_4}\text{-methanol.}$ This sample was immediately cooled to -70°C, after which some yellowing of the solution was noted. Addition of KOH cleared the solution and caused the precipitate to quickly redissolve.

Addition of TFAA to a solution of Clll in d₆-acetone at 270 K caused no precipitation, but a dramatic change in the NMR spectrum was observed compared to that of the free amine, as shown in Figure 18. Addition of less than one equivalent of acid caused immediate production of a

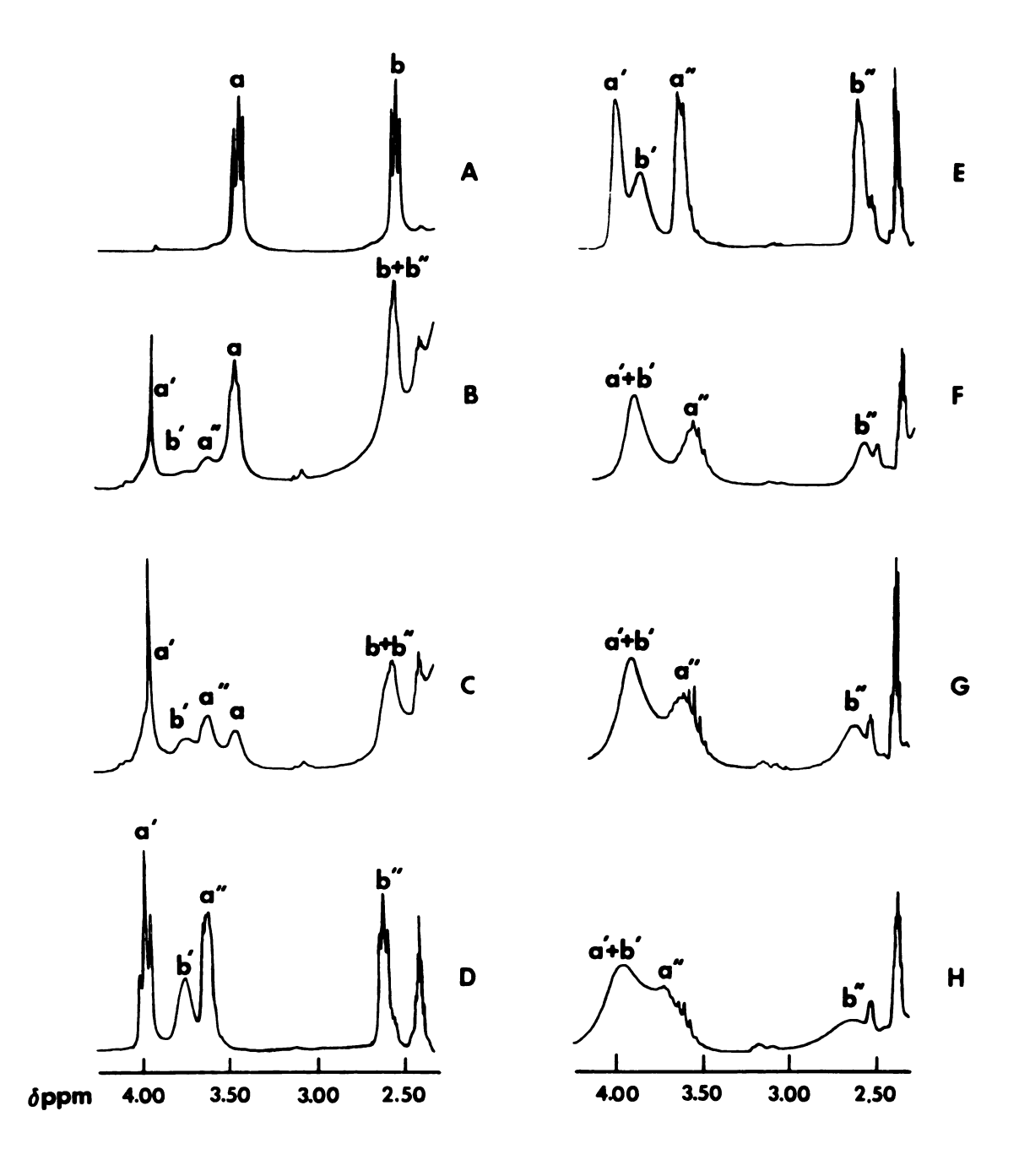


Figure 18. The dependence of the NMR spectrum of Clll in d₆-acetone upon the addition of trifluoroacetic acid (TFAA).

monoprotonated form of the ligand. This externally protonated form exchanges only slowly with the free amine (as evidenced by slight line broadening) via the following scheme:

$$C111 + HTFAA \Longrightarrow C111 \cdot H^{+}, o + TFAA^{-}$$
 (24)

but the proton transfer greatly favors the Clll. As TFAA is added, lines a', b', a", and b" grow as a and b (those of the free ligand), disappear (an impurity peak overlaps the signal, a'). The new lines are consistant with the structure "b" of Figure 14B. As mentioned previously, the σ_h symmetry is removed, thus the exchange scheme (24) must be slower than the NMR time-scale and highly favor the monoprotonated form.

As more than one equivalent of acid is added, the downfield CH₂N line shifts farther downfield and eventually coalesces with the CH₂O line at 4.00 ppm. Continued addition of acid causes the upfield resonances to disappear and that at 4.00 ppm to grow. At a mole ratio of about 50/l acid to Clll, the sample is almost completely converted to this new form, since the resonance at 4.00 ppm accounts for nearly the entire area of the resonances. This new form is probably a diprotonated species, which has protons bound externally at both nitrogens, the ligand being in the exo-exo form. A logical reaction scheme is shown below:

$$C111 + H^{+} \longrightarrow C111 \cdot H^{+}, o \tag{25}$$

$$C111 \cdot H^{+}, o + H^{+} \longrightarrow C111 \cdot 2H^{+}, o-o$$
 (26)

Reaction (25) goes to products quickly and completely as mentioned earlier, but with excess acid, reaction (26) becomes important. The first external protonation is stable and the transfer is fast and complete, whereas the second exo protonation is much more difficult to achieve. Therefore, the proton is exchanged rapidly and the equilibrium needs to be forced to the right by a large excess of acid. External oxygen protonation is ruled out as a major contributor to the second external protonation, because the CH₂O protons would show a much larger downfield shift than the CH2N protons. The fact that the CH20 and CH2N proton lines coalesce at 4.0 ppm with excess acid indicates that the interaction involves exo-exo nitrogen protonation. External nitrogen protonation is also necessary to account for the very large shift in the CH₂N proton resonances as acid is added. identical chemical shifts of the CH₂O and CH₂N protons in this externally diprotonated species seems to be accidental.

The acid concentration was determined by the comparison of the exchangeable proton line of TFAA (the -OH signal) with those of the ligand. Considerable error is inherent in this method, since at least two acid proton signals are present, that bound to the ligand and that bound to the TFAA anion. The latter line is very broad and the bound proton line often overlaps the ligand signals. Water also interferes. This makes the measurement of the acid concentration very difficult, but general trends have been established. Table 4 lists the chemical shifts of the resonances as a function of TFAA present.

Table 4. The dependence of the chemical shifts of Clll in d6-acetone upon addition of trifluoroacetic acid (TFAA).

MR	acid (±40%)	6 ^{CH} 2 ^O ppm	6 CH ₂ N
A	0.0	3.47	2.56
В	0.7	3.99, 3.65	3.76, 2.63
D	1.4	4.01, 3.65	3.88, 2.63
E	1.7	4.03, 3.66	3.96, 2.64
F	7.6	4.02, 3.66	4.02, 2.64
G	8.4	4.01, 3.70	4.01, 2.67
H	29	3.98, 3.73	3.98, 2.77
I	50	3.91	3.91, 2.78

Dichloroacetic acid, DCAA, has been utilized to better determine the amount of acid added, since it has one non-exchangeable proton. As shown in Figure 19, the addition of DCAA gives very different NMR spectra than does the addition of TFAA. Proton exchange between the free and the monoprotonated amine at 270 K is much more rapid. As DCAA is added, the lines broaden and shift downfield, the CH₂N protons showing a more dramatic effect than the CH₂O protons. A plot of the chemical shift of the CH₂O protons as a function of total acid added, as shown in Figure 20 and Table 5, gives a break in the slope at a mole ratio of 1:1 acid to Clll indicating efficient formation of the monoprotonated form (as with TFAA) and a difficult second protonation. The break occurs at a chemical shift of 3.79 ppm, which is midway between the values

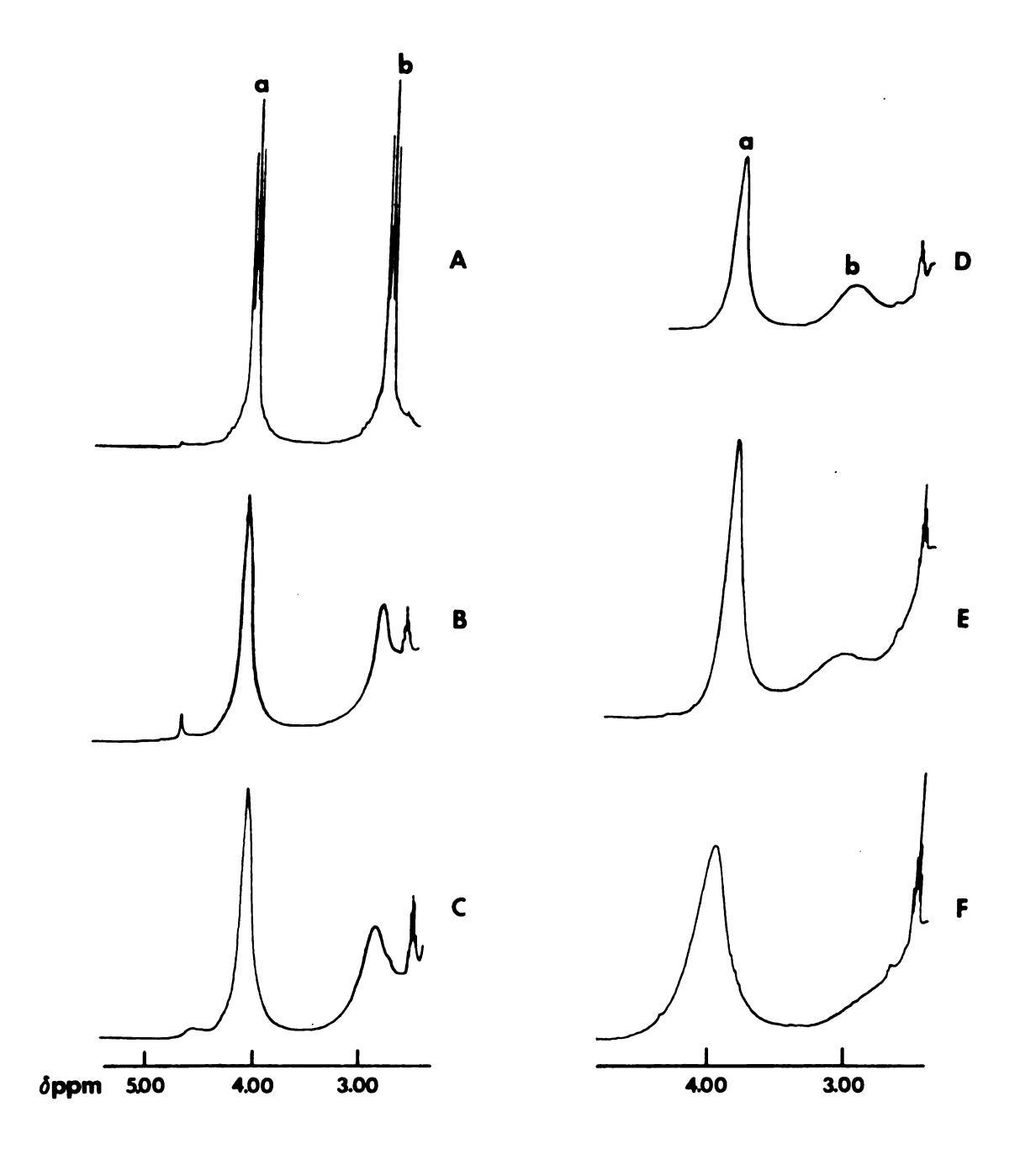
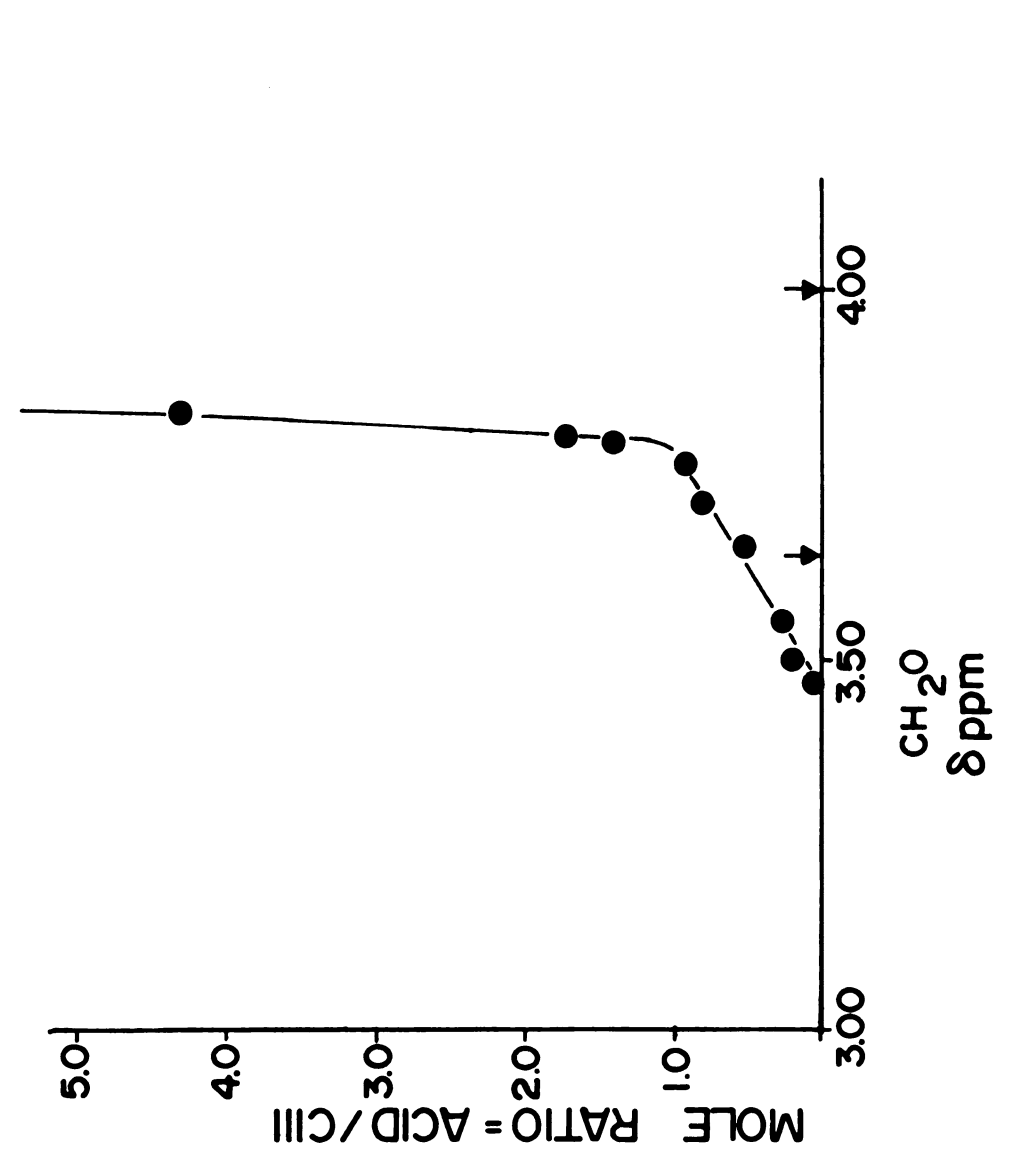


Figure 19. The dependence of the NMR spectrum of Clll in d_6 -acetone upon the addition of dichloroacetic acid (DCAA).



The dependence of the chemical shift of the ${\rm CH}_2{\rm O}$ protons of Clll in d₆-acetone upon addition of DCAA. Figure 20.

Table 5. The dependence of the chemical shifts of Clll in d6-acetone upon addition of dichloroacetic acid (DCAA).

Mole	ratio DCAA (±20%)	¢ ^{CH2O}	6 ^{CH} 2N
A	0.0	3.47	2.56
В	0.18	3.50	2.58
C	0.25	3.55	2.67
D	0.52	3.65	2.85
E	0.8	3.71	2.96
	0.9	3.76	2.97
	1.4	3.79	too broad
	1.7	3.80	to define
F	4.3	3.83	

of 4.00 and 3.64 ppm observed for the $\mathrm{CH_2O}$ proton lines of $\mathrm{Clll}\cdot \mathrm{H}^+$, o with TFAA. This implies that the same two conformations of the ligand are present upon protonation with either DCAA or TFAA, but with DCAA, they are rapidly interconverting and an exchange averaged signal is observed. Thus proton exchange is rapid with DCAA so that the time-average σ_h symmetry element is retained. As with TFAA, the reaction (25) goes to completion, since the $\mathrm{CH_2O}$ chemical shift at the break point is midway between those observed with TFAA. Reaction (26) is fast and incomplete as before. (The same correlation could probably be made utilizing the $\mathrm{CH_2N}$ proton lines, except that they are too broad to locate accurately.)

Eigen's formulation concerning proton exchange processes indicates that in order to achieve proton exchange times of 10^{-3} seconds or longer between an acid and a base, the difference in their pK_a values must be at least 6.5 to $7.0^{(65)}$. The pK_a values of TFAA, DCAA and Cll1 are known in water but they are not known in acetone. Therefore, we must assume that their relative strengths in acetone are similar to those in water. The pK_a values of TFAA, DCAA and Cll1 in water are 0.23, 1.25 and 7.08 respectively $^{(66)}$. The difference between the pK_a values of Cll1 and TFAA (6.85) is large enough to yield proton exchange times in the millisecond region, whereas the difference between the pK_a values of Cll1 and DCAA (5.83) would be predicted to give rates of about 10^{-4} seconds according to Eigen's theory. These findings are consistent with external protonation.

The mole ratio of DCAA present was measured by comparing the resonances of the acid (both the backbone proton and the exchangeable proton of DCAA being coincidentally located at 6.6 to 6.0 ppm) to the CH₂O proton lines of the ligand. A delay of 20 seconds between pulses was utilized to insure complete relaxation. Delays of 10 seconds and longer caused no measurable change in the values obtained. The temperature of the samples was kept below 275 K to preclude inside protonation. The acidified samples were stored in a freezer at about -30°C for months with no apparent inside protonation.

F) Clll.H, o in Water

The NMR spectra of Clll have been determined for a number of pH values utilizing buffers in D20. These data were obtained in conjunction with the rate studies of inside protonation presented in the following section. The chemical shift and lineshape of each spectrum shows a pH dependence in D₂O, which is similar to that observed in acetone. The spectra at several pH values are shown in Figure 21. These spectra reveal that external protonation in water is fast, since neither the CH₂N lines nor the CH₂O lines give evidence of nonequivalence. The variation of the chemical shift of these lines with pH is given in Table 6, and plotted for the CH_2N protons in Figure 22. The plot shows a break at a pH of about 6, above which the lines are very narrow due to rapid proton exchange between Clll and Clll.H, o. Using the values of 2.53 ppm and 3.10 ppm for the chemical shifts of the CH2N protons of Clll and Clll.H, o in the absence of exchange, and equation (22) from the Introduction, a value for the pK_a of the first protonation of about 8 \pm 2 is obtained from the break in the curve.

Below a pH value of 6, the lines begin to broaden greatly and continue to shift downfield, indicating conversion to the externally diprotonated species. At a pH value of about 2.6 they begin to sharpen again. This behavior indicates that the rate of formation of the externally diprotonated species from the externally monoprotonated species is not extremely fast. The plot in Figure 22 indicates that the conversion to

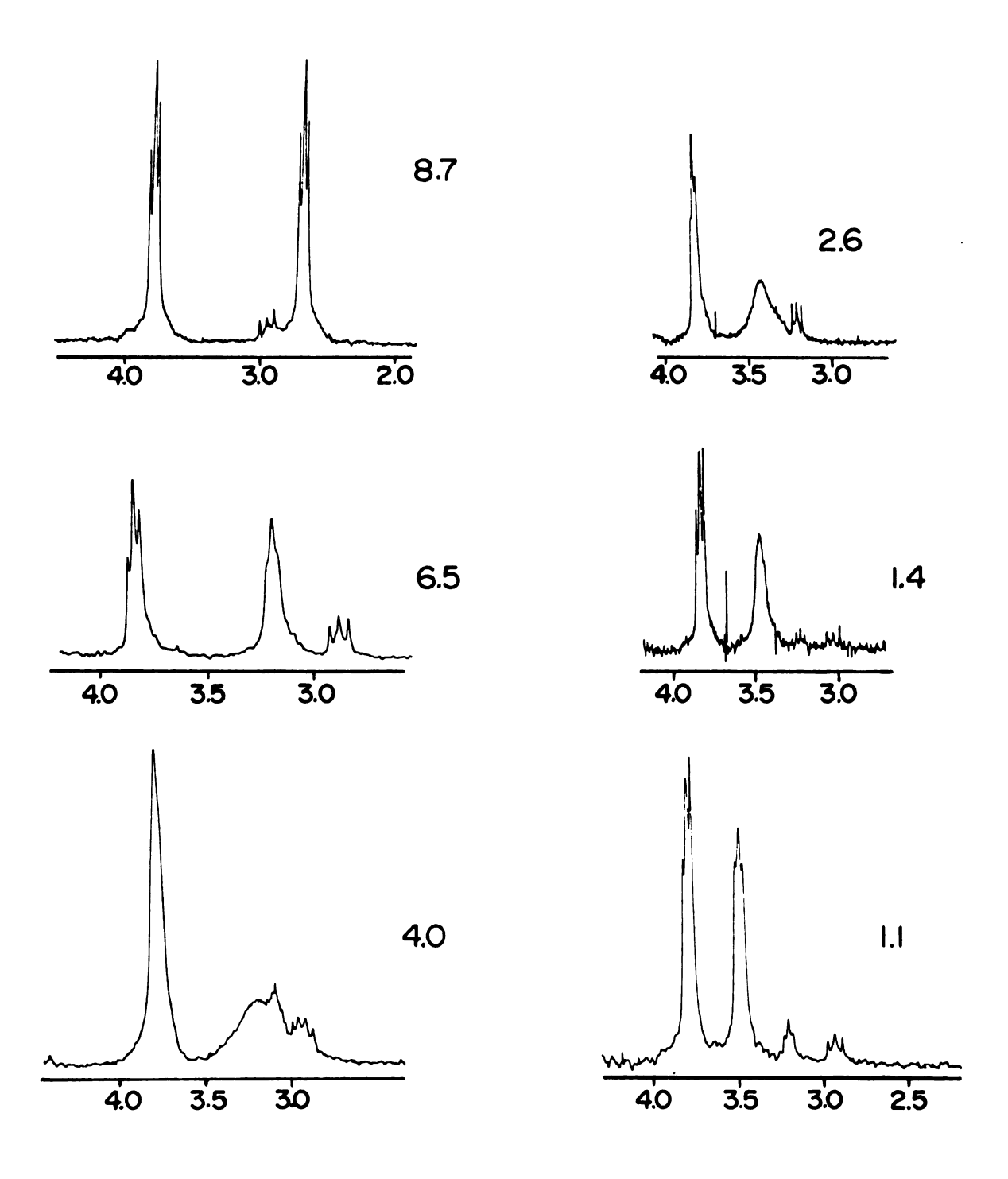


Figure 21. The NMR spectra of Clll in water at various pH values.

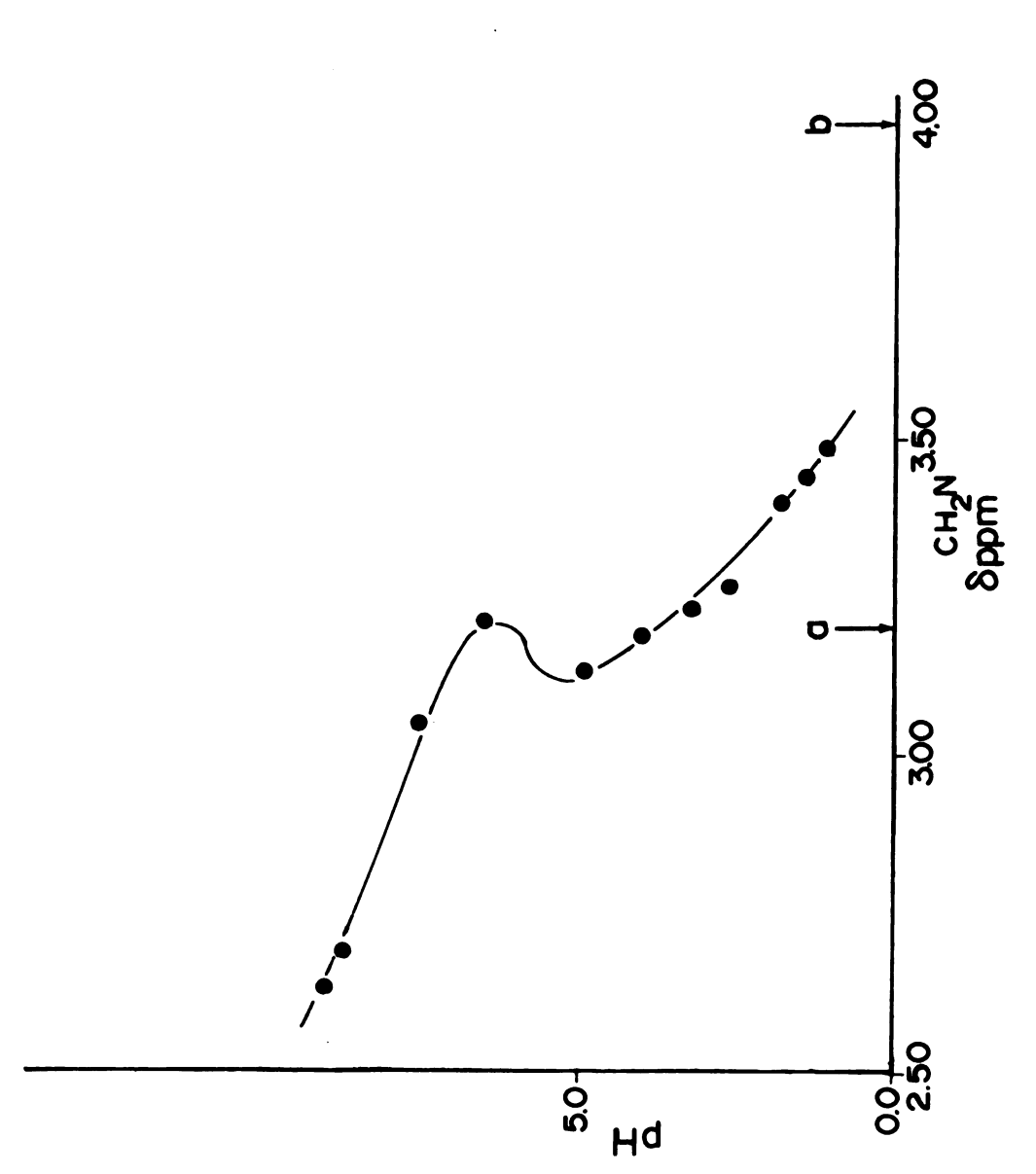


Figure 22. The pH dependence of the chemical shift of the ${
m CH}_2{
m N}$ protons of CIII in ${
m D}_2{
m O}$.

Table 6. The pH dependence of the chemical shift of the CH₂N protons of Clll in water at 299°K.*

pH [†]	CH ₂ O ppm	CH ₂ N
9.0		2.53
8.7		2.69
7.5	3.78	3.05
6.5	3.85	3.21
4.9	3.82	3.13
4.0	3.81	3.19
3.2		3.23
2.6		3.27
1.8		3.40
1.4	3.79	3.44
1.1	3.81	3.49

^{*} Reference to DSS., those absent in the CH₂O column are due to overlap.

the diprotonated species is not complete, even at a pH value of 1.0. Comparison with the shift in acetone indicates only about 50% conversion. The average shift of the CH₂N protons of Clll·H⁺,o in acetone is very similar (±0.1 ppm) to that in water (arrow "a" of Figure 22). Thus a chemical shift for the CH₂N protons of Clll·2H⁺,o-o of 3.9 ppm (arrow "b") may be assumed, from which a pK_a value lower than 2 is obtained for the second external protonation. The pH values of all buffers were measured (and

[†] Corrected for deuterium effects.

corrected for deuterium influence) (67) with a calibrated radiometer and microelectrode.

A pH titration of Clll was also performed in water. Only one break was observed, yielding $pK_a = 7.1 \pm 0.1$ for the first external protonation. The titration went only to a pH value of 1.0, which was probably still too high to permit observation of the second break. From the pH dependence of the NMR chemical shift, the second pK_a is estimated to be between 0 and 1.5 in water.

The pK_a values of Clll and its complexes reflect the presence of the exo conformation, since only this form may be externally protonated. 1,4 diazabicyclo (2-2-2) octane, or Dabco, is a carbon analogue of the cryptands, whose small size requires both nitrogens to be in the exo conformation. The pK_a values of the cryptands would be expected to be very similar to that of Dabco, 8.8 ± 0.2 at 25°C, if the molecule had no endo conformation present. Proton transfer reactions of the cryptands actually involve a two step process:

Clll (endo-endo)

$$K_1$$

Clll (endo-endo)

(27)

and the apparent K_{a} of Clll is equal to the following:

$$K_a^{app} = (K_a)(K_1) \tag{28}$$

Assuming that the value of K_a for external protonation of Clll in the exo form is equal to that of Dabco, 1.6 x 10^{-9} , the observed value of K_a^{app} , 7.9 x 10^8 M, gives $K_1 = 50$.

Therefore, the endo-endo form is favored over the endo-exo form by about 2 kcal mol^{-1} in the absence of acid and the endo-endo form accounts for about 98% of the ligand at room temperature in the absence of acid. For the second external protonation, if we assume that K_a^{app} is 10^{-2} or less, we obtain $K_1 > 10^{+7}$, establishing a difference of at least 6 kcal mol^{-1} between the two forms. The value of K_1 represents the analog of K_1 in equation (27) for the monoprotonated ligand.

G) The External Protonation of Clll •H+,i

In water and in methanol, the chemical shifts of the ${\rm CH_2O}$ and ${\rm CH_2N}$ protons are strongly dependent on the strength of the added acid and on the temperature, indicating that the exo-endo diprotonated complex is present in equilibrium with the internally monoprotonated form. The spectra in ${\rm d_4}\text{-MeOH}$ will be discussed in detail in the next section, but the results of this analysis show that the exo-endo inversion and the proton exchange rates are very rapid. A pK_a value of 3 is obtained for external protonation in methanol.

The pH dependence of the NMR spectra of Clll·H⁺,i in water indicates that an exchange similar to the one observed in methanol is occurring. A compilation of the pH dependence of the chemical shifts of the CH_2O and CH_2N proton lines of Clll·H⁺,i in water is shown in Table 7. It we assume that the chemical shift for the CH_2N protons of Clll·H⁺,i is 3.0 ppm and the shift of the same protons of Clll·H⁺,i-o is 3.45 ppm (from Table 7), a value of 0.4 ± 0.5 is obtained for

the pK_a of the process. This pK_a value indicates that the preference for the endo-endo form is higher in water than in methanol by two orders of magnitude. Using the K_a of Dabco, an equilibrium constant, K_1'' , of about 10^8 in water and about 10^6 in methanol is obtained for the ratio of the endo-endo form to the endo-exo form. Thus the endo-endo form is the only significant species in solution in the absence of added acid. The endo-exo form of Clll·H⁺, i seems to be as difficult to attain as the exo-exo form of Clll.

Table 7. The pH dependence of the chemical shifts of Clll •H+, i in water (26).

Acid Strength	CH ₂ N ppm	CH ₂ O ppm
3N	3.45	3.82
lN	3.34	3.76
0.4N	3.20	3.72
0.1N	3.10	3.70
0.01N	3.03	3.66
0.0	3.02	3.66

H) General Conclusions

- 1) External protonation occurs at the nitrogens in both Clll and Clll.++.i.
- 2) Internal protonation would be expected to also involve oxygen interaction, but the NMR evidence suggests otherwise.

- 3) The chemical shifts of the CH₂O and CH₂N protons upon protonation are determined mainly by electric field effects caused by the protonation at the nitrogen and not by conformational changes.
- 4) Exo-endo inversion is rapid at room temperature, but favors the endo-endo form especially in Clll·H⁺,1.
- 5) Exo-endo inversion does not take place in Clll-2H⁺,i-i.
- 6) The solvent and acid used, greatly influence the extent of external proton binding and the exchange rate but have no observable effect on inclusively bound protons.

III) TEMPERATURE DEPENDENCE OF THE NMR SPECTRA

The time-scale of proton NMR is relatively slow since it is only able to distinguish between processes which occur more slowly than milliseconds and, in fact, is limited in the Clll systems to exchange times longer than about 0.01 seconds. Exchange phenomena which occur more rapidly than this yield only a population average signal, and the character of the individual site is lost. One of two things may be done in order to identify individual sites when exchange times are more rapid than 10⁻³ seconds. First, an analysis method which employs a faster time-scale may be utilized, such as IR, UV or EPR spectroscopy if applicable. The other alternative is to continue using NMR methods, but at lower temperatures. A change in temperature affects more factors than just the rates of exchange processes, however. It also

alters the populations of the sites involved in the exchange in accord with Boltzmann statistics, and changes such physical properties of the medium as the viscosity and the dielectric constant. The enthalpy and entropy of a binding site are temperature invariant if external influences of the medium remain constant. Therefore, going to lower temperatures does not cause stronger binding (unless the site is perturbed externally) although the lifetimes at sites do become longer, as governed by the Arrhenius or Eyring equations (68).

The equations which describe chemical exchange are well characterized for NMR. McConnell modified the Bloch equations to describe chemical exchange processes and obtained equations which are applicable to phenomena involving single lines and first order multiplets (59-60). These equations are developed in a simplified form in the Appendix, and may be easily utilized in processes which involve fewer than four or five sites. For systems of more sites, or second order spectra, a density matrix approach would be more suitable (69).

A) Clll in d_6 -Acetone

The temperature dependence of the proton and carbon-13 NMR spectra of Cll1 in CHF_2Cl has been reported by Lehn and co-workers (26) at 250 MHz. The C^{13} NMR spectra were temperature-independent down to 178 K except for slight line shifts, but the proton spectra at 163 K show a well resolved ABXY pattern for the backbone CH_2N and CH_2O protons with chemical

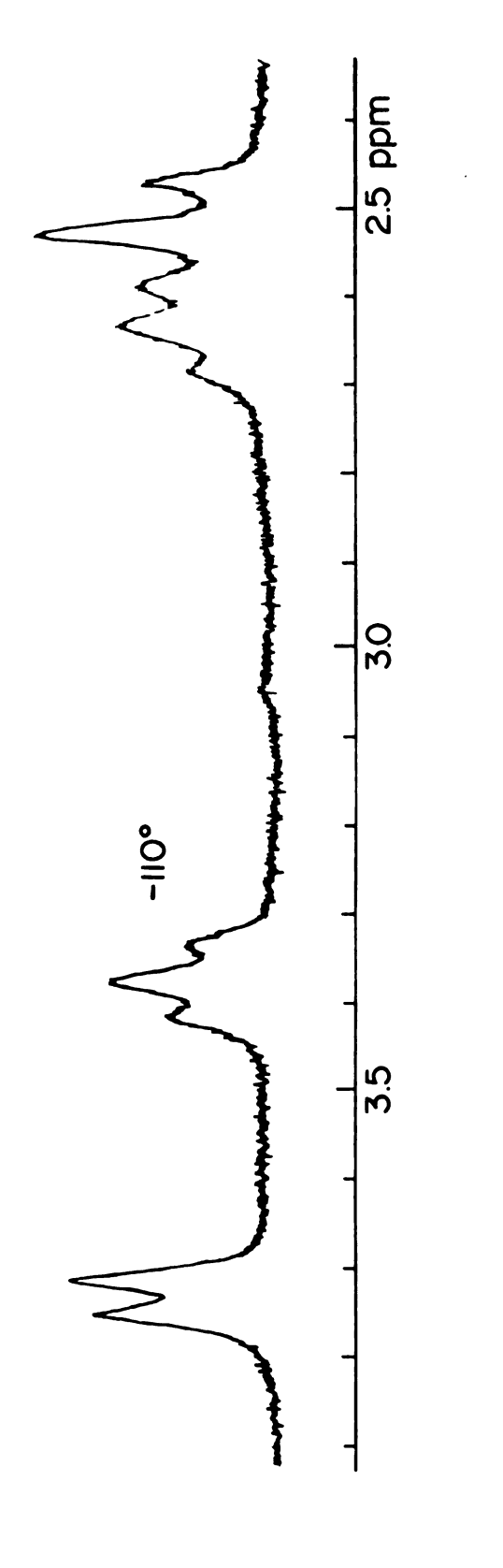
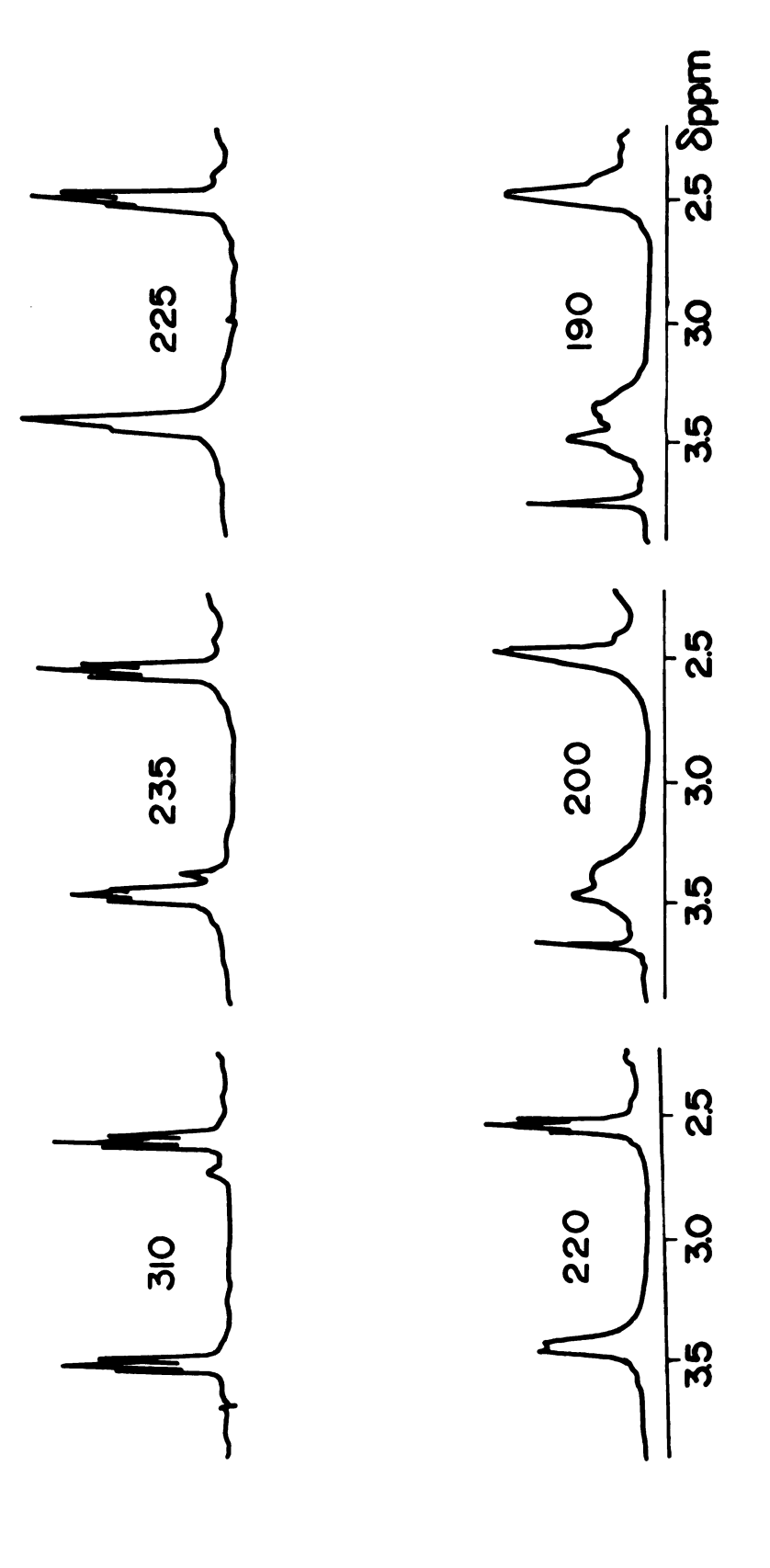


Figure 23. The spectrum of Cill in CHF₂Cl at 163 K at 250 $\mathrm{MHz}^{(26)}$

shifts and coupling constants of 3.67 (A), 3.32 (B), 2.58 (X), and 2.47 (Y); $J_{AB} \simeq 10$, $J_{XY} \simeq 14$, $J_{BX} \simeq 10$, $J_{AX} \simeq J_{BY} \simeq J_{AY} \leq$ 2 Hz as depicted in Figure 23. Since the pattern was of the ABXY form, the conformation at low temperatures did not involve exo-endo isomers, because the σ_h symmetry element was still intact. Instead, the process was described as the slowing of a torsional motion, such as vicinal carbon wagging motions, concerted twists of the strands, etc. The rate of this torsional motion was obtained at the coalexcence temperature of -65° C, which yielded a ΔG^{\ddagger} of 9.8 ± 0.1 kcal mol⁻¹ (from the Eyring equation). The torsional motion was assigned to a possible concerted process, such as the passage of a strand through the intramolecular cavity, since the activation barrier for the process was relatively large. Typical vicinal carbon wagging motions possess activation enthalpies of 3 to 6 kcal mol⁻¹, depending on substituents, whereas concerted processes normally yield an activation barrier which is roughly the sum of the individual components. Therefore, a concerted twist would be expected to have an activation barrier of 10 to 18 kcal mol -1, and the value reported by Lehn of 9.8 kcal mol⁻¹ would put it in the range of concerted processes. (The free energy of activation has no direct physical meaning, since it is the sum of ΔH^{T} and $-T\Delta S^{\frac{1}{4}}$, both of which can be given physical meaning. Therefore, in order to equate the ΔG^{\ddagger} obtained form coalescence data with the activation enthalpy, ΔS^{\ddagger} must be assumed to be zero.)



The temperature dependence of the NMR spectra of Clll in d_6 -acetone. Figure 24.

Figure 24 shows spectra for the same process in d₆-acetone at 180 MHz which have very similar features, except that they are more poorly resolved, due to a lower field strength, higher temperature and a more polar solvent. The assignments are the same as those at 250 MHz (see Table 8), but the separations due to nonequivalence are not as pronounced in acetone as they are in CHF₂Cl. From the coalescence temperature of -58°C for the process in acetone, ΔG^{\ddagger} = 10.7 ± 0.3 kcal mol⁻¹, in agreement with Lehn's results.

Table 8. The temperature dependence of the NMR parameters for a 0.02 M solution of Clll in d₆-acetone.

Temp (°K)	δ ^{CH} 2O ppm	6CH2N	
290°K	3.44	2.52	
190°K	3.49, 3.39	2.52	

B) Clll·H⁺,i·Br⁻ in d₆-Acetone

The temperature characteristics of Clll·H⁺,1 (Figure 25 and Table 9) are more striking than for the free amine. As the temperature is lowered, both CH₂O and CH₂N proton lines broaden, the CH₂O proton lines broaden more extensively because their chemical shifts in the two conformers are farther apart than are the CH₂N proton shifts. The CH₂O lines split at about 215 K, and the CH₂N lines at about 207 K. A very similar coupling pattern emerges with the spectrum at 195 K, compared to that of Clll at 163 K from Lehn's publication. This pattern is also an ABXY spectrum with lines and coupling

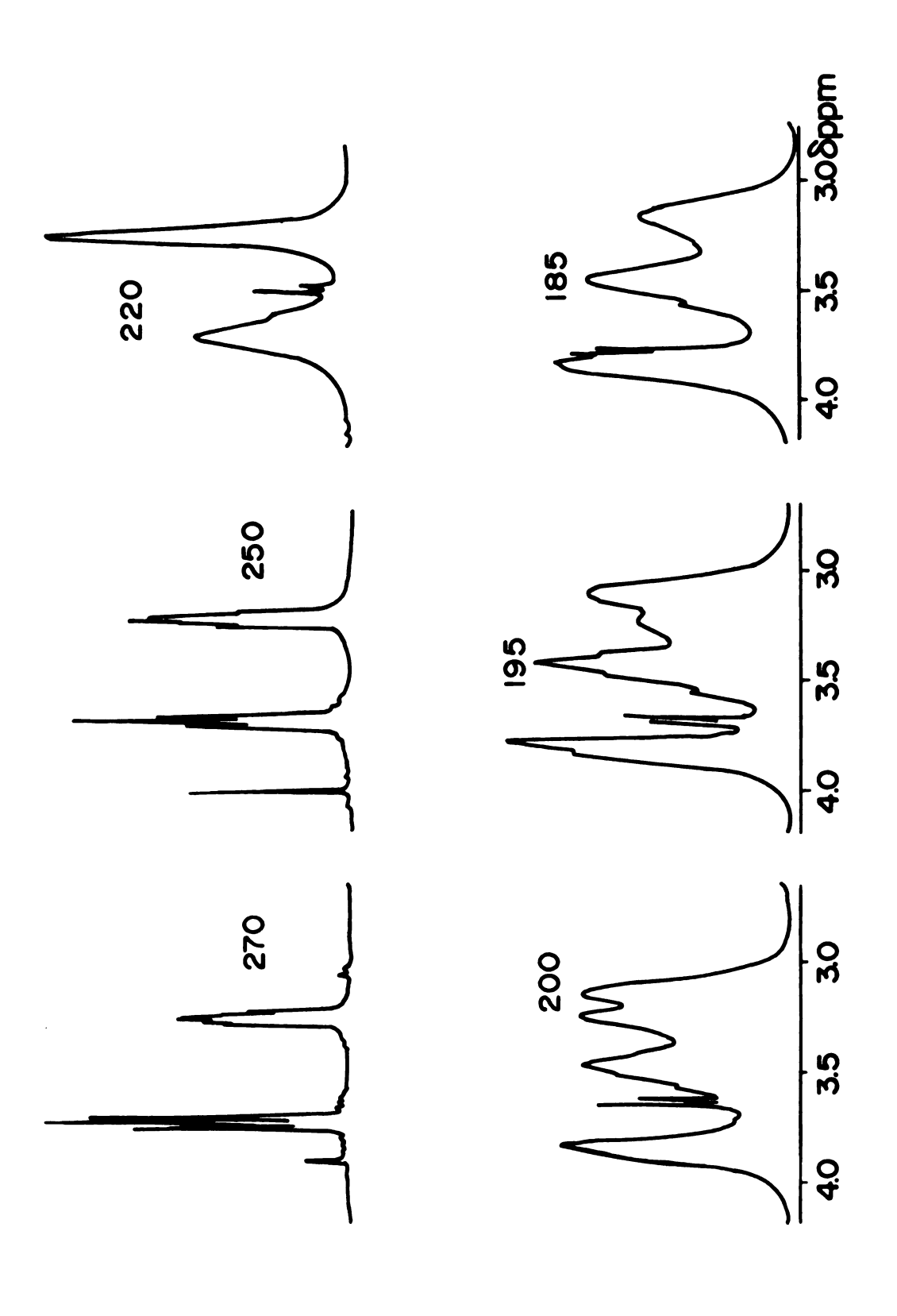


Figure 25. The temperature dependence of the NMR spectra of Clll.H $^+$, i in d $_6$ -acetone.

Table 9. The temperature dependence of the NMR spectra of a 0.04 M solution of Clll.H, i.Br in d6-acetone.

† (hz)
ı
)

Dashes indicate disappearence of a signal, blanks indicate no data available.

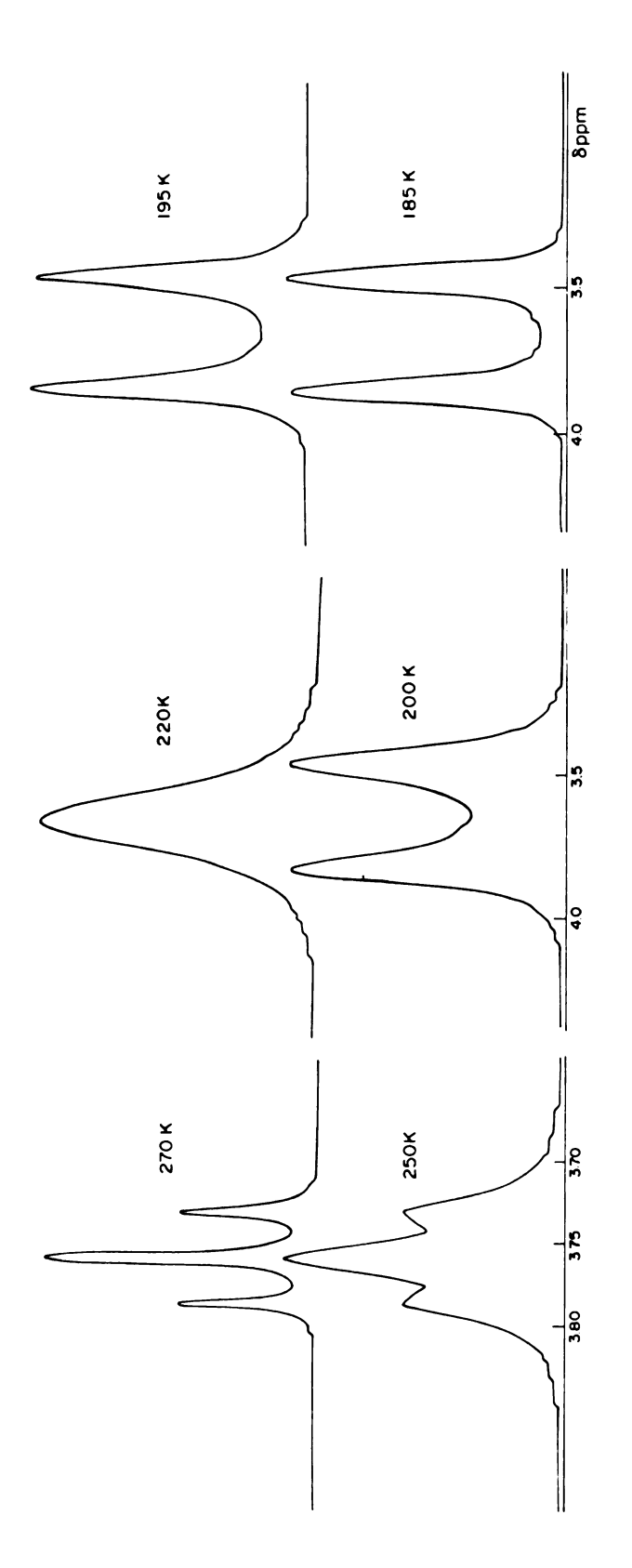
^{*} Chemical shifts are reported ± 0.3 ppm.

Tuncertainty in the linewidths is ± 10%.

constants of 3.85 (A), 3.46 (B), 3.24 (X), and 3.08 (Y); $J_{AB} = 10 \text{ Hz}, J_{XY} = 10-14 \text{ Hz}, J_{BX} = 10 \text{ Hz}, J_{AX} = J_{BY} = J_{AY} \\ \leq 2\text{Hz}. \text{ The preferential vicinal coupling, } (J_{BX} >> J_{AX}, \\ J_{AY}, J_{BY}), \text{ explains the unusual breadth of X. These assignments demonstrate again that exo-endo isomerism does not contribute to the observed spectra and that the nonequivalence is caused by the slowing of torsional motions as the temperature is decreased. The fact that the <math>\text{CH}_2\text{O}$ protons broaden and split to a larger extent than do the CH_2N protons signals indicates that the CH_2O protons are more nonequivalent in the gauche conformation.

The carbon-13 NMR (CMR) spectra of the same sample are temperature invariant, except for line broadening below 200 K. Carbon-13 NMR would be expected to be very sensitive to exoendo nitrogen processes. Since the carbons retain their equivalence even at very low temperatures, the CMR spectra provide evidence that this inversion process either does not occur or remains very rapid.

The lineshapes of the ${\rm CH_2O}$ protons and the ${\rm CH_2N}$ protons have been simulated using the modified Bloch equations. The simulation of the ${\rm CH_2O}$ proton signals was done using linewidth values of 0.3 Hz for both sites and 5.0 Hz for both sites in the absence of exchange. Either choice produced nearly the same calculated lineshape. A chemical shift difference of 76 Hz between the two sites was utilized. The lineshapes were simulated for several values of τ , the exchange time, which in this case, is the rate of the torsional



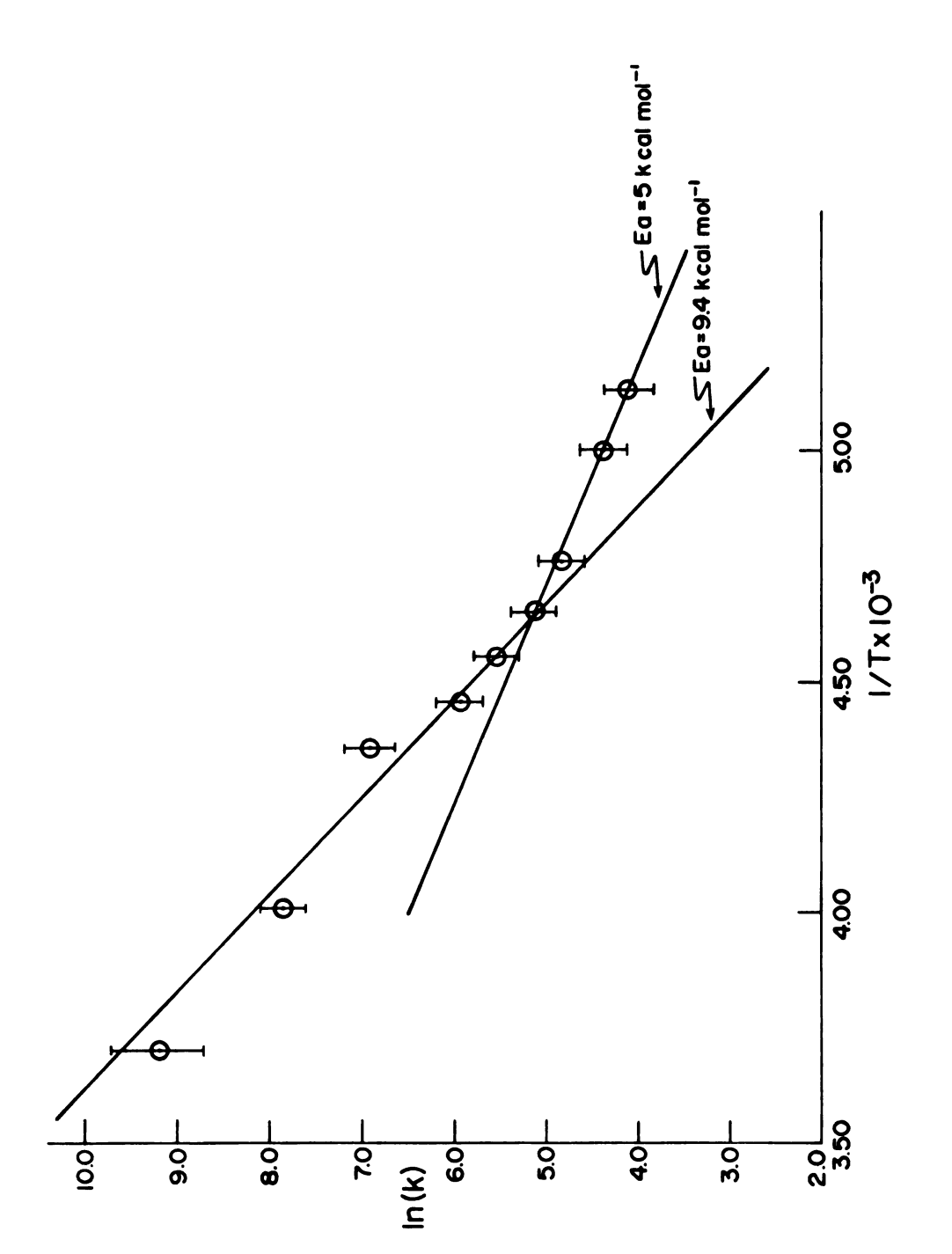
Computer-simulation of the temperature dependence of the spectra of the CH $_2^{\rm O}$ protons of Clll+H $_1^{\rm +}$ in d $_6-$ acetone. Figure 26.

motion. The simulated lineshapes are shown in Figure 26.

As this motion is slowed down, the lines go from a very sharp triplet to a broad singlet, and then split again when the exchange time is greater than 3 msec.

The linewidths and general appearance of the experimental and calculated spectra were closely analysized in order to best match the simulated spectra with the real spectra shown in Figure 25. The rate of exchange, k, was then obtained at various temperatures and an Arrhenius plot made by graphing ln (k) versus 1/T (Figure 27). This plot gives a straight line which yields $E_a = 9.4 \pm 0.5$ kcal mol⁻¹ down to about 210 K. Then the slope deviates as another process begins to interfere. This latter process causes line broadening in excess of that predicted for the slowing of a single exchange process.

The exchange process which causes the line broadening above 210 K is probably due to the slowing of a torsional motion. From the coalescence temperature (215 K and 207 K for the $\rm CH_2O$ and $\rm CH_2N$ proton signals), rate constants of 169 $\rm sec^{-1}$ and 60 $\rm sec^{-1}$ are obtained, with $\rm \Delta G^{\dagger}=10.3\pm0.3$ kcal $\rm mol^{-1}$, $\rm \Delta H^{\dagger}=9.0\pm0.5$ kcal $\rm mol^{-1}$, and $\rm \Delta S^{\dagger}=-6$ cal $\rm mol^{-1}$ deg⁻¹. These values are somewhat large for typical vicinal carbon wagging motions, but the bicyclic nature of Clll probably causes these vibrations to be coupled throughout the rest of the molecule. The concerted exchange process which Lehn suggested for the free Clll, namely, the passage of a strand through the intramolecular cavity of Clll, could not



The dependence of ln(k) on 1/T for the torsional motion from the spectra of the $\rm CH_2O$ protons of Clll.H⁺,1. Figure 27.

take place with the internally monoprotonated species.

Thus, vicinal carbon wagging motions probably give rise to this phenomenon.

Below 200 K, another process begins to slow to the millisecond time-scale as suggested by the temperature dependence of the resonance of the internal proton. The motion of the internal proton is very rapid at room temperature, giving rise to a single narrow line at 9.0 ppm. As the temperature is reduced, this line broadens greatly and splits within a very narrow temperature range, as shown in Figure 28. The two resulting peaks are located at 10.8 and 8.0 ppm with areas of roughly 1 to 3. The value of ΔG^{\dagger} at coalescence (187 K) is 8.4 \pm 0.3 kcal mol⁻¹.

These lineshapes were also simulated using linewidths of 30 Hz for both sites as well as 10 Hz for both sites in the absence of exchange, the choice of which did not appreciably change the calculated lineshape. The chemical shift difference of the two sites in the absence of exchange was taken as 504 Hz (2.3 ppm). The simulated lineshapes are given in Figure 29, and the plot of ln(k) versus 1/T is given in Figure 30. The Arrhenius plot (shown in Figure 30) has two distinct slopes, a behavior similar to that of Figure 27 for the vicinal carbon wagging motion. Again, two processes seem to be involved, one which is operative at high temperatures, and one which is important below 190 K. Close comparison of the two plots reveals that in the intermediate region, where the two plots overlap, the slope of the lines deviate

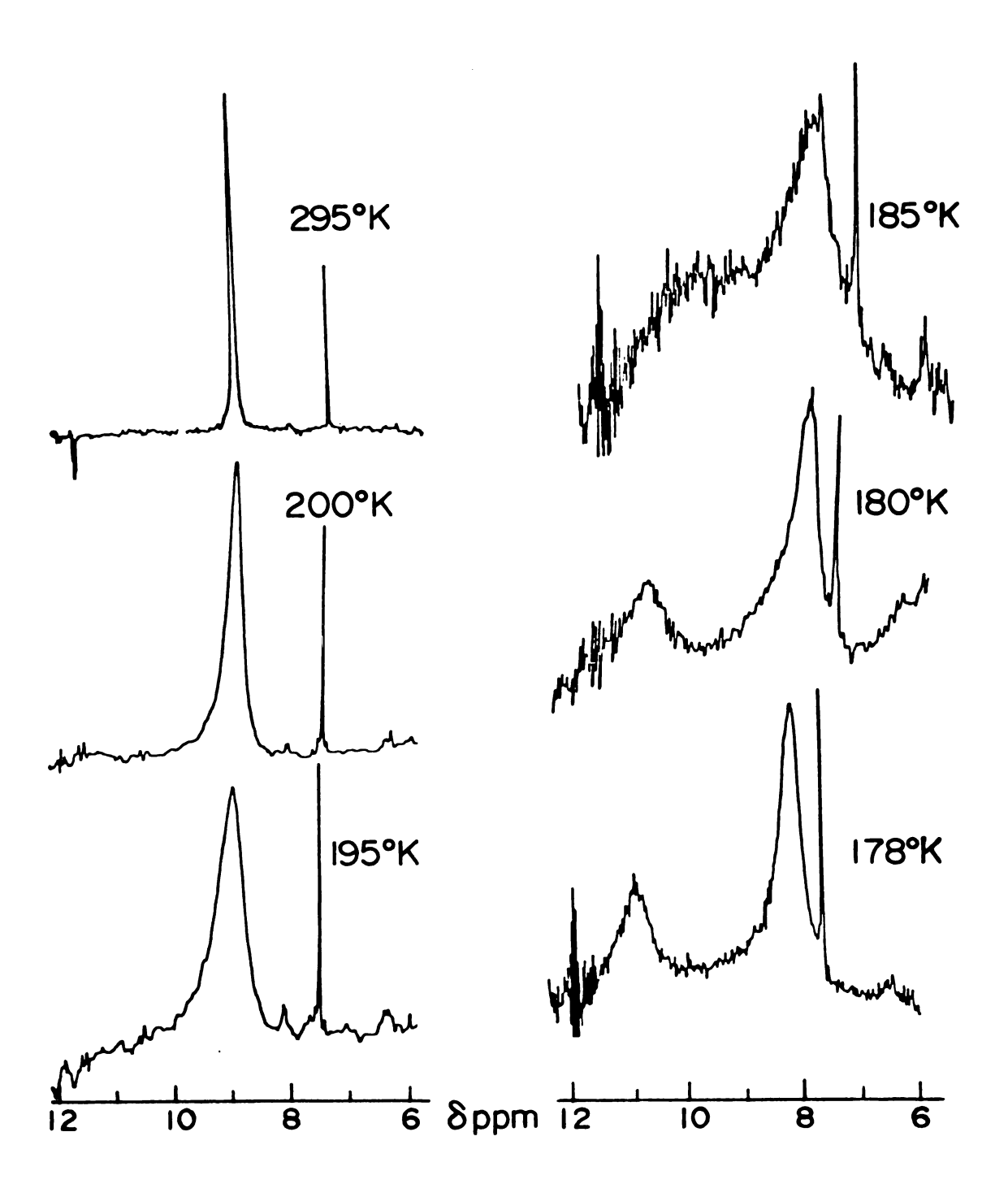
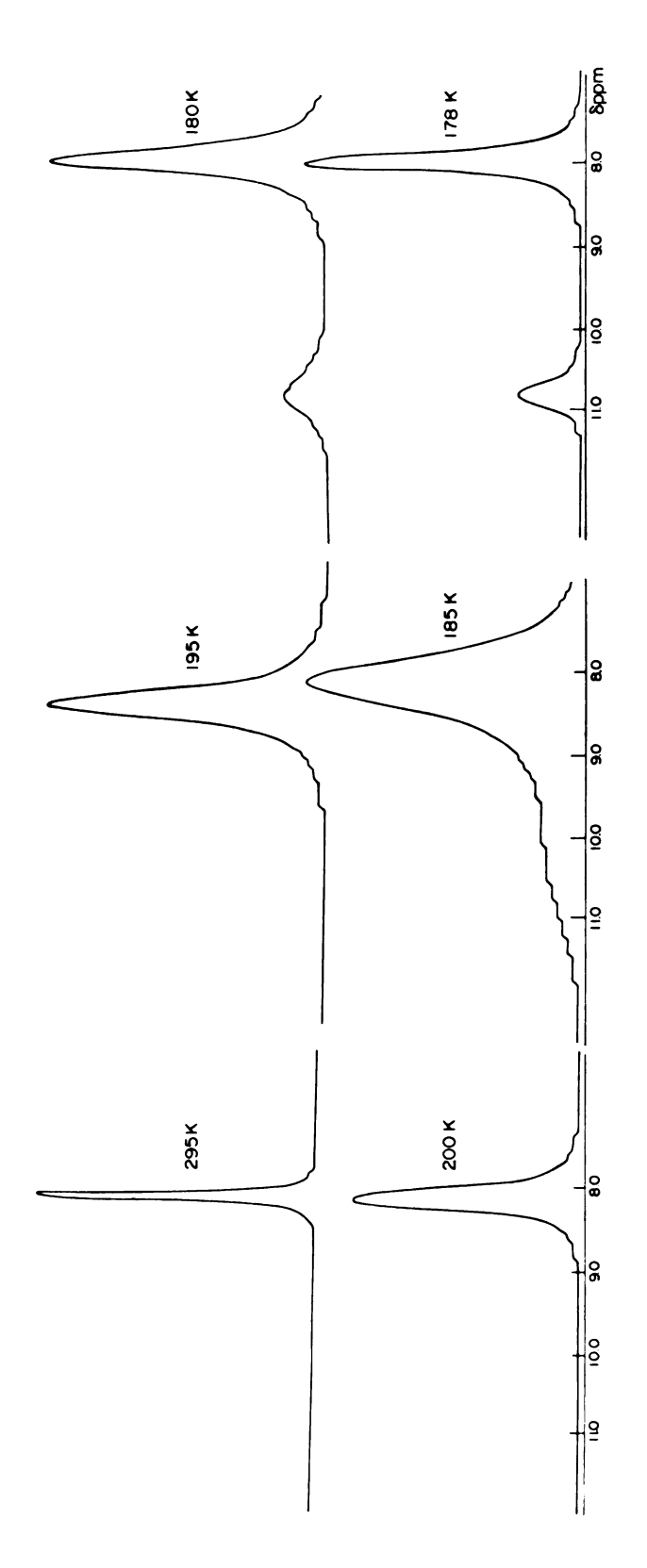
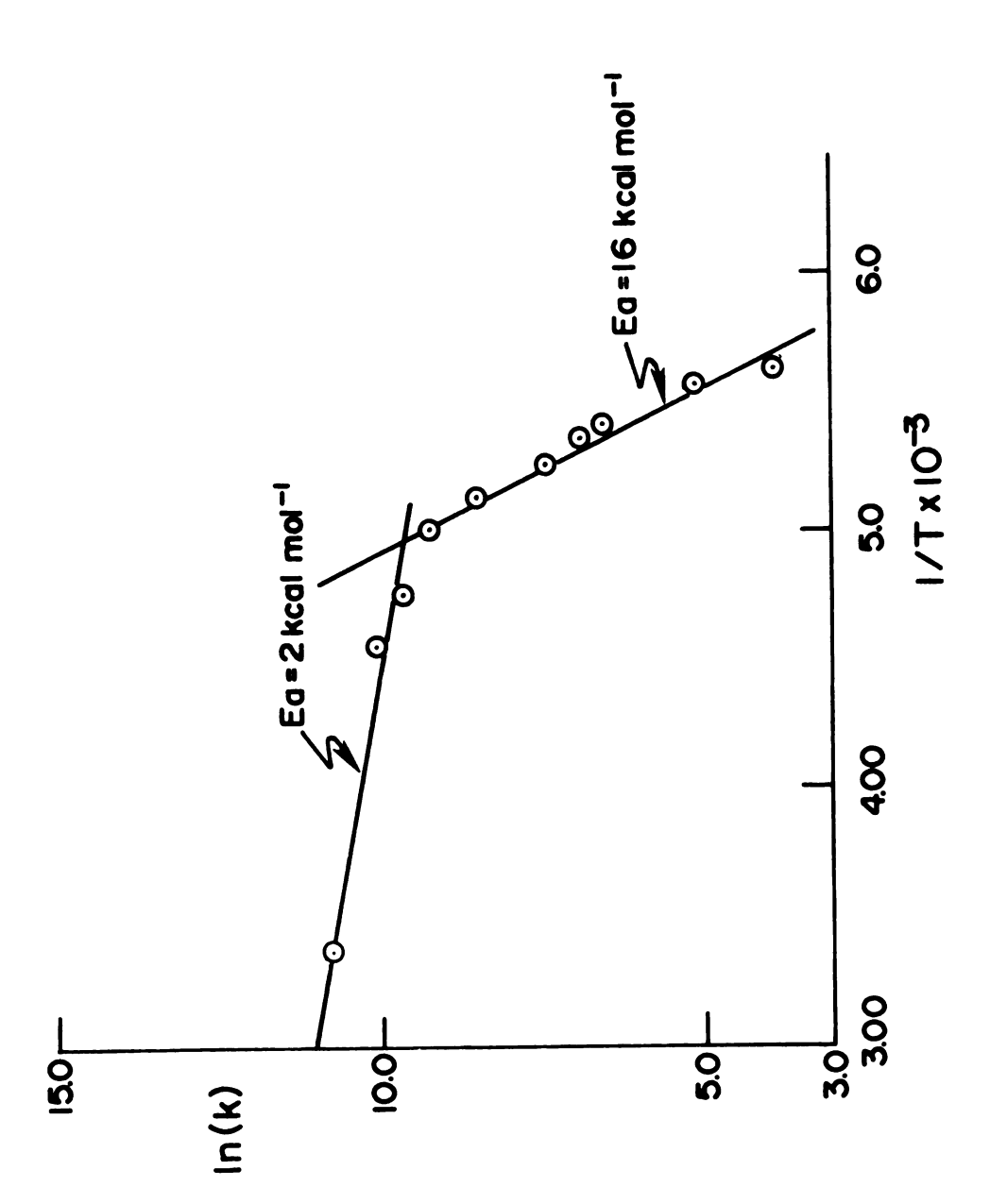


Figure 28. The temperature dependence of the internal proton resonance of Clll $^{\circ}H^{\dagger}$, i in d₆-acetone.



Computer-simulation of the temperature dependence of the internal proton resonance of Clll.H ,1 in d_6 -acetone. Figure 29.



The dependence of $\ln(k)$ on 1/T for the skeletal locking process from the spectra of the internal proton of Clll.H⁺,1. Figure 30.

from that of the other temperature regions. In this intermediate region, both plots indicate the presence of two processes which causes line broadening or narrowing in excess of that predicted by the computer simulation analysis. The high temperature process has already been assigned to the slowing of the vicinal carbon wagging motion. The simulation of the second process yields $E_{a} = 16 \pm 2 \text{ kcal mol}^{-1}$, $\Delta H^{\dagger} = 16 \pm 2 \text{ kcal mol}^{-1}$, and $\Delta S^{\dagger} = +39 \text{ cal mol}^{-1} \text{ deg}^{-1}$. The large activation enthalpy necessitates a concerted proccess, if it involves only conformational changes of the ligand. The nature of the process is highly unusual, because any process with such a large value of $\Delta H^{\frac{1}{7}}$ would be expected to be slow even at room temperature. If the value of ΔH^{\dagger} is correct, then it is the large positive ΔS^{\dagger} which is responsible for the very rapid exchange rates at such low temperatures, but its origin remains a mystery.

This exchange phenomenon might arise from one of three processes. First, a phase transition might have occurred at these temperatures. In order to rule out this trivial explanation, the sample was pulled from the magnet gap and inspected. No abnormality of this sort was noted. In addition, the spectra were duplicated in methanol, and the same kind of splitting was also observed.

A second process which could give rise to the spectra would involve the exchange of the H₁ between two sites inside the ligand, namely, the nitrogens (8.0 ppm) and the oxygens (10.8 ppm). The different populations of these sites would

reflect their relative energies, the nitrogen site being more stable. One discrepancy in this mechanism involves the expected effect on the chemical shifts of the backbone protons when the exchange of the H; is slow. We have shown that the majority of the shift of the backbone protons upon protonation is due to the location of the added proton rather than to a conformational change. Therefore, if the motion of the internal proton was slow, the ${\rm CH_2N}$ proton signals would be shifted about 250 Hz apart, corresponding to protonated and unprotonated sides. If the exchange of the $\mathbf{H}_{\mathbf{1}}$ were slow enough (and simulation suggests that it indeed would be), the CH2N resonances should be vastly broadened at about 185 K and two or more lines should appear which are centered at 3.11 ppm, but separated by 250 Hz at 180 K and The spectra in Figure 25 indicate that this phenomenon is not occurring. Therefore, we must conclude that the exchange of the H, between the nitrogens is always rapid.

The third explanation involves two conformations of the ligand, which possess different cavity sizes and donating abilities to the internal proton. The environment of this proton is determined by the topology of the ligand's cavity, and if it changes, the chemical shift of the H₁ would also change. A process which involves an exchange between the two conformations of the ligand, similar to those shown in Figure 13, might well explain our observations. The cavity size would change by an Angstrom or more in going from one conformation to the other and the conformation with the smallest

8.0 ppm would result from the proton in the small cavity, since this conformation would allow efficient electron donation, whereas that at 10.8 ppm would correspond to the conformation with the larger cavity. The populations of the two sites, reflected by the areas of the respective resonances, suggest that the former conformation is more stable.

This exchange phenomenon could also reasonably explain the unusual thermodynamic parameters, because in a concerted process, the individual thermodynamic components of the processes are additive. Therefore, the ΔH^{\dagger} of 16 kcal mol⁻¹ is unexpected, but the large ΔS^{\dagger} of 39 cal mol⁻¹ deg⁻¹ is still surprising. It may arise from several factors, such as an increase in molecular volume between the products and transition state, several pathways from transition state to products, a greater mobility of the $\mathbf{H}_{\mathbf{i}}$ in the transition state, etc. Proton tunneling might also effect the lineshape in a way which is not described by this classical approach. Whatever its origin, the large value of ΔS^{\dagger} is the dominant factor which allows rapid exchange of this high energy process at such low temperatures. It must be stressed however, that the apparent values of the activation parameters are fairly well determined experimentally. The large values of ΔH^{\dagger} and ΔS^{\dagger} are not the result of large experimental errors. The process which gives rise to these parameters must therefore be unusual. Of course, since the two-site

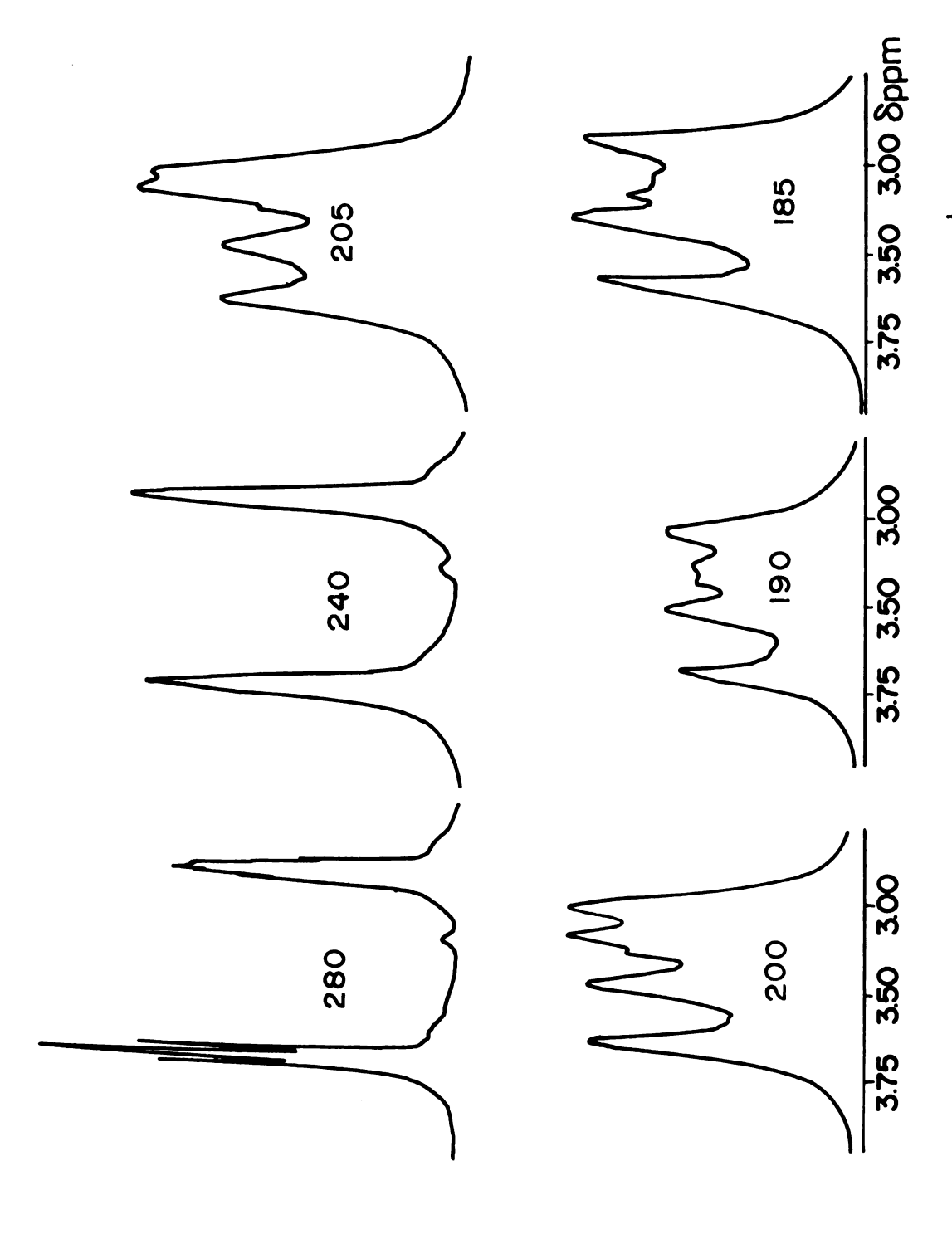


Figure 31. The temperature dependence of the NMR spectra of Clll \cdot H $^+$,1 in d $_{\mu}$ -MeOH.

Table 10. The temperature dependence of the NMR parameters for a 0.04 M solution of Clll 'H $^+$, i 'Br $^-$ in d $_4$ – MeOH.

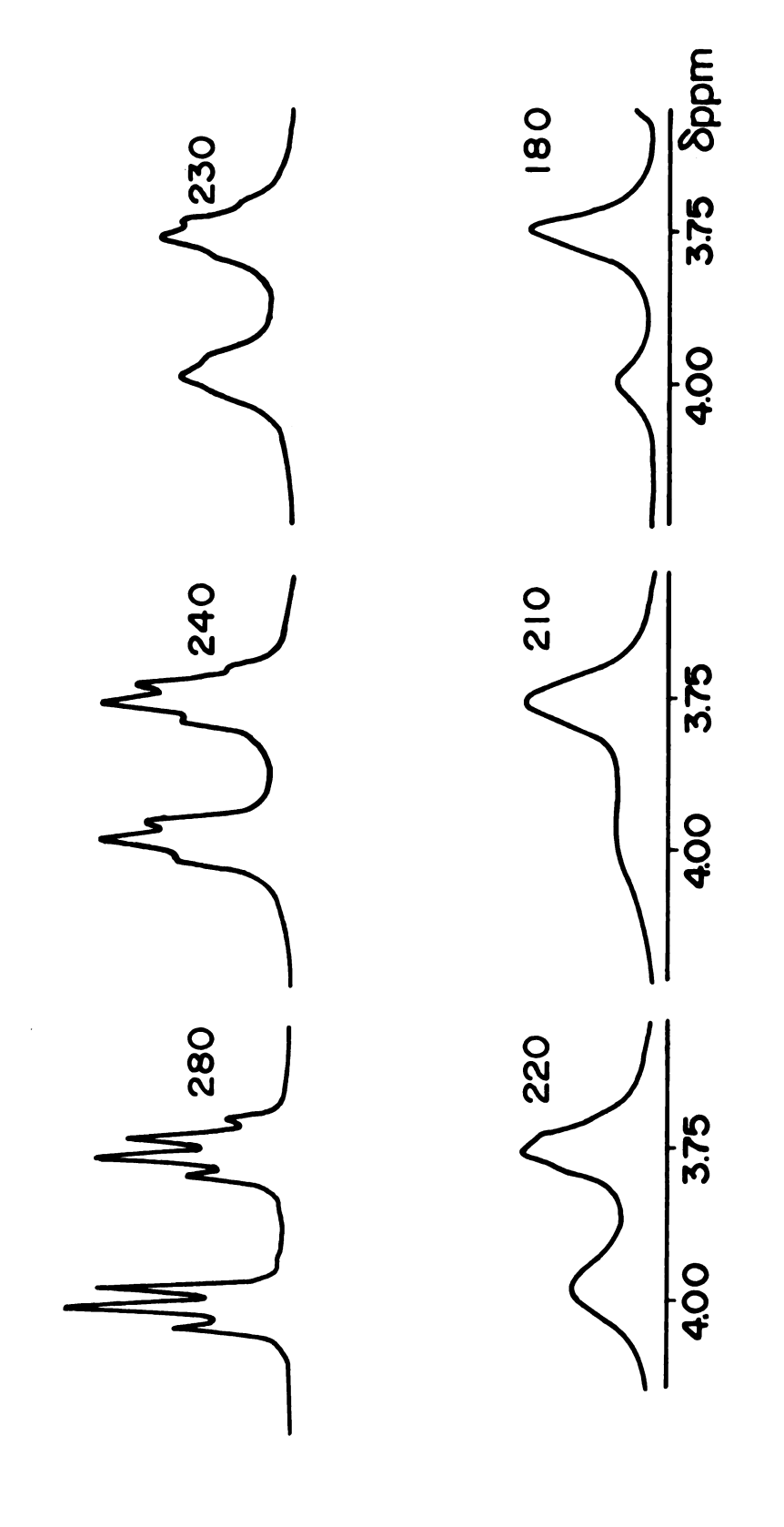
Temp (°K)	δ ^{CH} 2 ^O ppm	δ ^{CH} 2 ^N	δ ^H i ppm	Δυ1/2 ¹ (hz)
300	3.70	3.11	9.03	
280	3.68	3.10	9.02	15
260	3.68	3.10	9.03	14
240	3.67	3.09	9.04	14
220	3.67	3.10	9.10	20
210	3.79, 3.56	3.11	9.14	30
205	3.82, 3.50	3.15, 3.04	9.16	30
200	3.83, 3.48	3.18, 3.01	9.2	50
190	3.82, 3.45	3.17, 2.98	9.1	130
185	3.82, 3.45	3.16, 2.96		
180	3.83, 3.45	3.16, 2.96		
175	3.83, 3.44	3.16 2.94	8.0	200
170	3.82, 3.42	3.16, 2.97	7.9	150
165	3.79, 3.40	3.00	7.9	70

mechanism was used in the simulation, the analysis could be in error if more than two conformations are involved.

Figure 31 and Table 10 describe the exchange in d_{μ} -MeOH, and illustrate that the process is very similar in both solvents. The H_1 splitting is also observed in d_{μ} -MeOH, but the populations of the two sites are somewhat different, probably as a result of different solvation of the ligand.

C) $C111 \cdot 2H^+, i-i \cdot 2C1^-$ in d_{μ} -MeOH

The internally diprotonated cryptand, Clll.2H, i-i, should have a very rigid structure in comparison to Clll or Clll. H, i, because of the crowded nature of the cavity. Proton-proton repulsion inside the cavity would force the ligand to expand to as great an extent as possible, and its temperature characteristics should reflect this strain. Figure 32 shows that the temperature dependence of the NMR spectra of $\text{Clll-2H}^+, \text{i-i}$ in $\text{d}_{4}\text{-MeOH}$ shows behavior similar to those of Clll and Clll·H; ·Br. As the temperature is decreased, the CH₂O lines broaden most rapidly and split into two lines, while the CH₂N proton lines broaden, but neither shift nor split. This pattern is again consistent with an ABXY assignment, except that the breadth of the lines masks the coupling. The chemical shifts are assigned as follows (Table 11): 4.15 ppm (A), 3.75 (B,X,Y). It should be noted that the CH₂N proton and one of the CH₂O proton resonances overlap, an assignment which is confirmed by the relative areas (1:3).



The temperature dependence of the NMR spectra of Clll.2H $^+$,1-1 in d $_{\rm H}$ -MeOH. Figure 32.

Table 11. The temperature dependence of the NMR parameters for a 0.04 M solution of Cll1•2H $^+$,i-i•2Cl in d $_{4}$ -MeOH.

Temp (°K)	δ ^{CH} 2 ^O ppm	$\mathfrak{d}_{\mathbf{ppm}}^{\mathrm{CH_2N}}$	$\mathfrak{d}_{\mathtt{ppm}}^{\mathtt{H}}$	$\Delta v 1/2^{\text{H}_1}(\text{hz})$
305	3.96	3.74	7.33	50
280	3.96	3.74	7.33	50
260			7.31	37
245	3.96	3.76	7.30	
240	3.96	3.74	7.30	30
230			7.28	25
220	3.95	3.76	7.28	21
210	4.15,	3.75	7.24	25
180	4.15,	3.75	7.21	30
170	4.15,	3.74	7.20	30

The extreme breadth of the lines is probably caused by the rigidity of the molecule, which leads to more efficient dipole-dipole relaxation. The chemical shifts of the two H₁ resonances are independent of temperature, which suggests that the topology of the cavity is also temperature independent. The linewidth of the H₁ protons, however, is very temperature dependent, as mentioned in the section which considered spectra at elevated temperatures. This temperature dependence results from efficient scalar relaxation via the nitrogens. This complex provides supportive evidence that

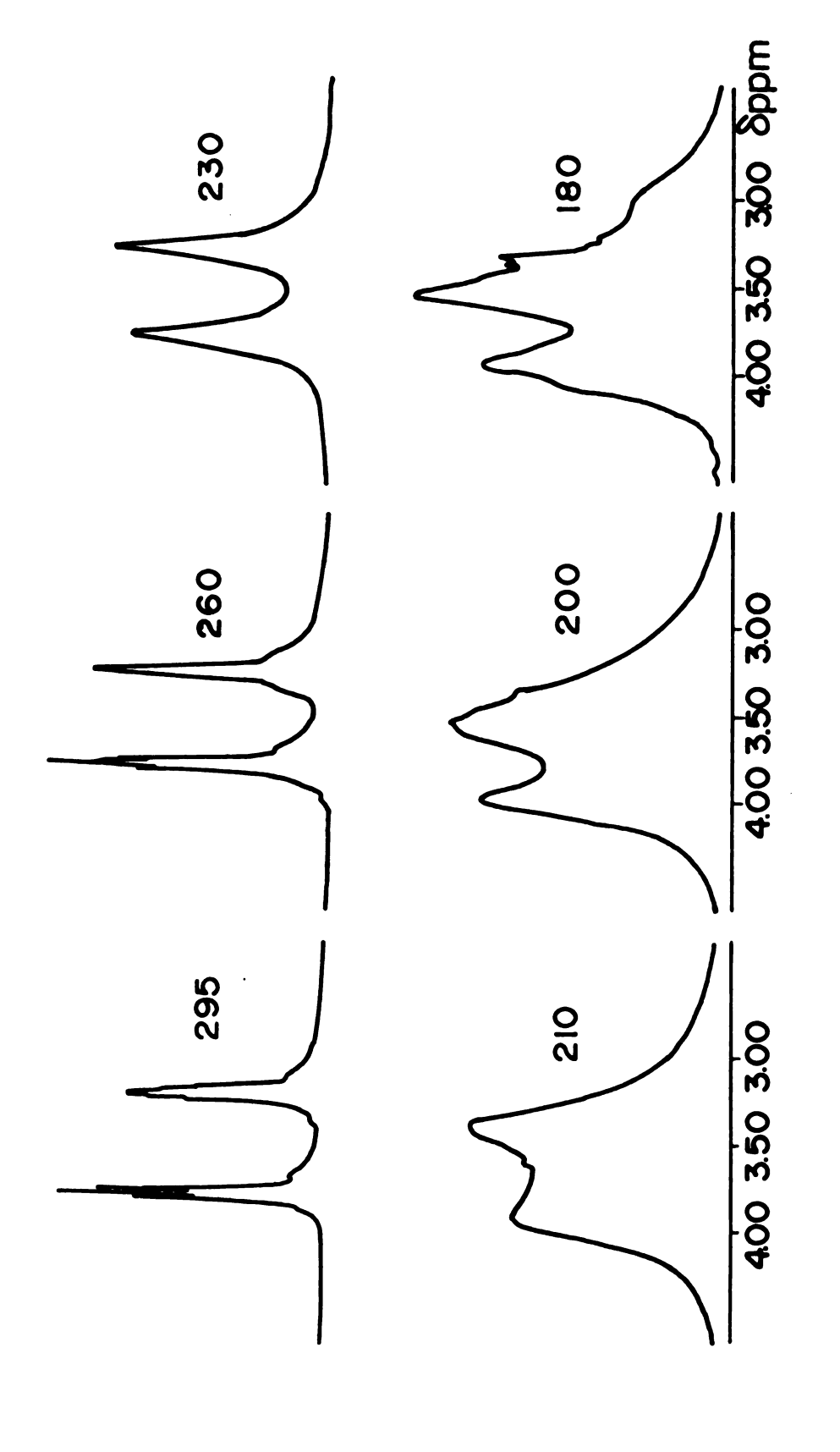
the skeletal locking process described for Clll and Clll·H⁺,i is vicinal carbon locking rather than exo-endo isomerization, because the diprotonated species is not able to undergo nitrogen inversion.

D) Clll•2H $^+$,i-o in d_µ-MeOH

The inclusively monoprotonated ligand, Clll·H⁺,i has an NMR spectrum which is very pH dependent in water, as previously attributed to the formation of the exo-endo diprotonated species, Clll·2H⁺,i-o. This complex is also produced upon the addition of an acid to methanol and, upon the acidification of a solution of Clll in methanol and, as in water, external proton exchange is rapid on the NMR timescale and average D_{3h} symmetry is preserved. As acid is added to the solution, the skeletal protons shift downfield, and broaden slightly (Table 6) in conformity with the following rapid equilibrium:

Clll·2H⁺,i-o
$$\xrightarrow{K_a}$$
 Clll·H⁺,i + H⁺ (29)

The temperature dependence of the process also indicates an equilibrium of this sort, with preference given to the diprotonated form as the temperature is lowered. This is shown in Table 12 and Figure 33 for a solution of 0.04 M Clll·H⁺,i·Br⁻ in d₄-MeOH acidified with excess hydrochloric acid (HCl). As the temperature is lowered, the CH₂N proton resonance broadens more rapidly than that of the CH₂O protons, both sets shifting downfield. The H₁ resonance also shifts with temperature, but it moves upfield simultaneously with



The temperature dependence of the NMR spectra of Clll·H ,1 in $d_{\mu}\text{-MeOH}$, acidified with HCl. Figure 33.

Table 12. The temperature dependence of the NMR parameters for a 0.04 M solution of Clll*H $^{+}$,i in d $_{4}$ -MeOH, acidified with HCl.

Temp (°K)	δ ^{CH} 2 ^O ppm	δ ^{CH} 2 ^N ppm	δ ^H i ppm	Δν _{1/2} (hz)
295	3.72	3.18	8.98	16
280	3.73	3.19	8.96	15
260	3.73	3.21	8.95	15
240	3.74	3.25	8.93	18
230	3.75	3.28	8.91	22
220	3.76	3.29	8.89	40
210	3.85,	3.34	8.84	66
200	3.89, 3.47	obscured by	8.66	50
190	3.89, 3.51	CH ₂ O proton	8.64	45
180	3.87, 3.50	11	8.58	30
170	3.88, 3.51	11	8.59	

the downfield skeletal proton shifts. Below 200 K the CH₂N proton resonances broaden extensively, and are obscured by the CH₂O proton lines. The extreme width of all the lines and the shifts with temperature, which show a more pronounced effect for the CH₂N protons, are consistent with external protonation at the nitrogen, which is fast at room temperature, but slow below 230 K. Comparison of these spectral features with those of the same sample prior to acidification, shown in Figure 31 and Table 10, indicates that the two complexes are indeed different structures. Nitrogen inversion must be slow in order to facilitate this slow proton transfer at low temperatures, thus the molecule is "locked" into the exo-endo isomer. A pseudo-equilibrium constant for protonation, defined by:

$$K = \frac{(C111 \cdot H^{+}, i)}{(C111 \cdot 2H^{+}, i-o)}$$
 (30)

may be obtained from the shift of the $\mathrm{CH_2N}$ proton line and the $\mathrm{H_1}$ line, by using equation (22) to obtain the mole ratio of the two species from the observed chemical shift. The $\mathrm{CH_2N}$ proton chemical shift in the absence of exchange for the diprotonated (i-o) ligand was chosen as 3.74 ppm, the same as $\mathrm{Clll} \cdot \mathrm{2H}^+$,i-i in $\mathrm{d_{4}}\text{-MeOH}$, and Table 10 gives a value of 3.10 ppm for the monoprotonated cryptand. The chemical shift of the internal proton of the diprotonated ligand (i-o) was taken as 8.58 ppm, that of $\mathrm{Clll} \cdot \mathrm{H}^+$,i was taken from Table 10 for each temperature because it shifted slightly with temperature. The values of $\mathrm{ln}(\mathrm{K})$ which were obtained

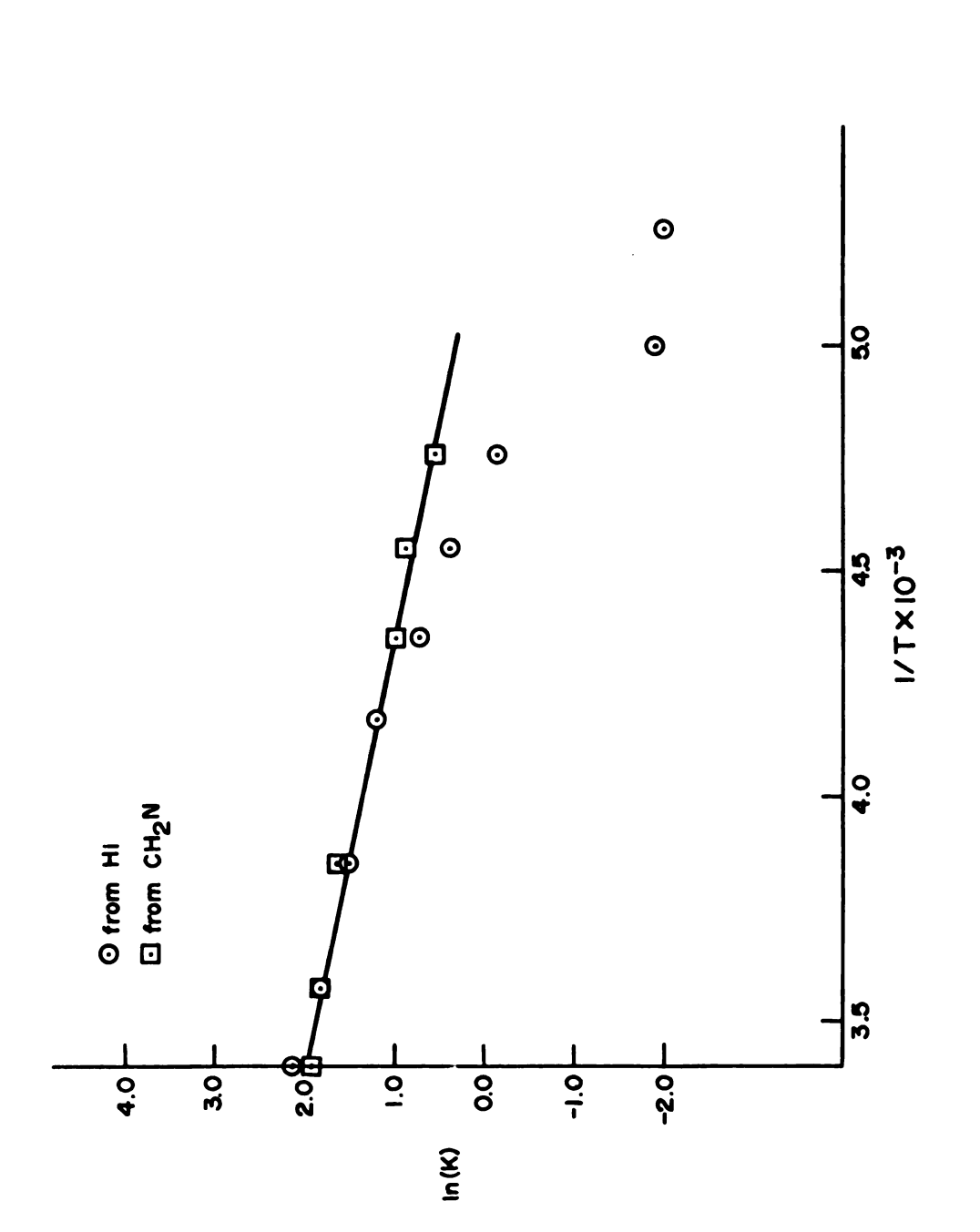
Table 13. The temperature dependence of the equilibrium constant for the conversion of Clll·H⁺,i to Clll·2H⁺,i-o in d_{μ}-MeOH: K^N from the CH-2N protons and K¹ from the internal proton.

Temp.(°K)	(1/T)x10 ⁻³	κ ^N	ln(K ^N)	κ¹	ln(K ¹)
295	3.39	7.0	1.95	8.0	2.1
280	3.57	6.1	1.81	6.3	1.8
260	3.84	4.8	1.57	4.6	1.5
240	4.17	3.3	1.19	3.2	1.2
230	4.35	2.6	0.96	2.1	0.72
220	4.55	2.4	0.88	1.5	0.39
210	4.76	1.7	0.53	0.87	-0.14
200	5.00			0.15	-1.9
190	5.26			0.13	-2.0

(Table 13) from the two sets of resonances are plotted in Figure 34 versus the reciprocal of the temperature. Both sets of data fall on the same straight line, except at very low temperatures, where skeletal locking causes the H_1 points to deviate. The slope of the line and the values of K give $\Delta H^{O} = 2.0 \pm 0.1$ kcal mol^{-1} , and an apparent $\Delta S^{O} = 11 \pm 1$ cal mol^{-1} deg⁻¹ is obtained. Since the study was done only at one acidity, the true value of ΔS^{O} was not determined.

The two forms are very similar in energy, although the diprotonated complex is slightly preferred, but the monoprotonated form has a more favorable entropy at this acidity.

The increase in entropy might be attributed to greater



The dependence of ln(K) on l/T for the equilibrium between Clll·H⁺, and Clll·2H⁺,i-o in d $_{\rm H}$ -MeOH. Figure 34.

vibrational freedom for the endo-endo complex, both for the internal proton and the strands of the ligand. Much of this vibrational freedom is lost in the exo-endo complex, as indicated by the very broad lines at low temperatures. This loss of vibrational freedom is also indicated by the H₁ resonance, which does not split at low temperatures, in contrast to the monoprotonated ligand.

A pH titration of Clll·H⁺,i was performed in d_{μ} -MeOH, using NMR techniques to measure the amount of diprotonated species formed. HCl was generated by preparing a solution of \sim 10% acetyl chloride in d_n -MeOH, which reacted with water to give HCl and acetic acid, or with methanol to give HCl and methyl acetate. This solution was added dropwise to a solution of Clll·H⁺,i·Br⁻ (0.02M) in d_4 -MeOH, and the acetyl moiety served as an internal standard for acid determination (This titration was also attempted with TFAA, but it was not a strong enough acid to externally protonate the internally monoprotonated ligand.) Figure 35 depicts the behavior of the H_{\bullet} resonance at 200 K as acid is added. It goes from a single line in the absence of acid to two lines, when less than one equivalent of acid is added. These lines correspond to Clll·H⁺,i (9.2 ppm) and Clll·2H⁺,i-o (8.6 ppm). Figure 36 shows the temperature dependence of the system when the mole ratio of acid to ligand is about 0.5. It shows the same skeletal locking process which causes splitting of the H4 resonance in Clll.H, i, while the H, resonance of Clll.H, i-o remains unchanged. These data confirm the conclusion reached

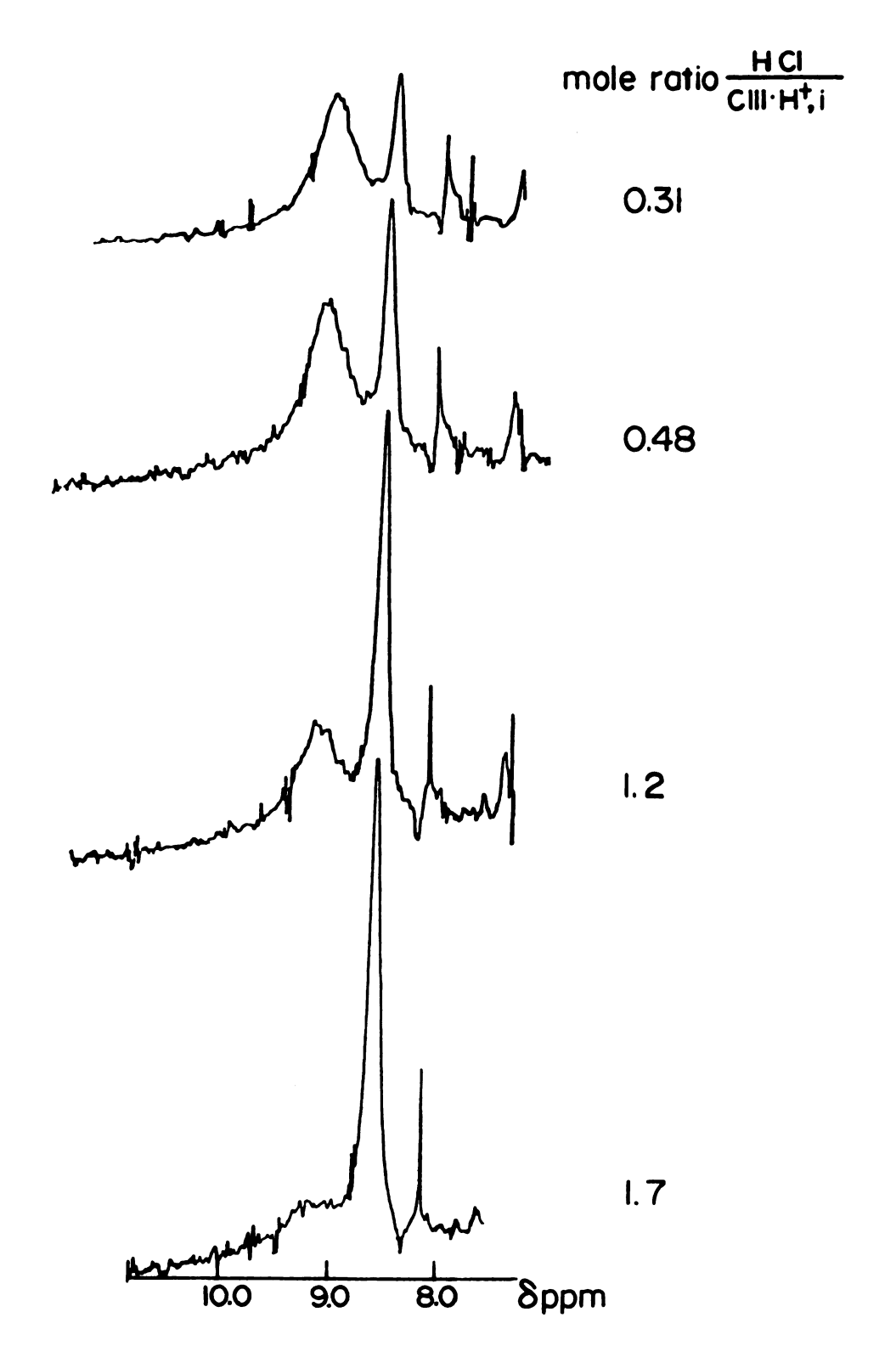


Figure 35. The variation in the NMR spectrum of the internal proton of Clll*H*,i in $\rm d_4$ -MeOH with the addition of HCl at 200 K.

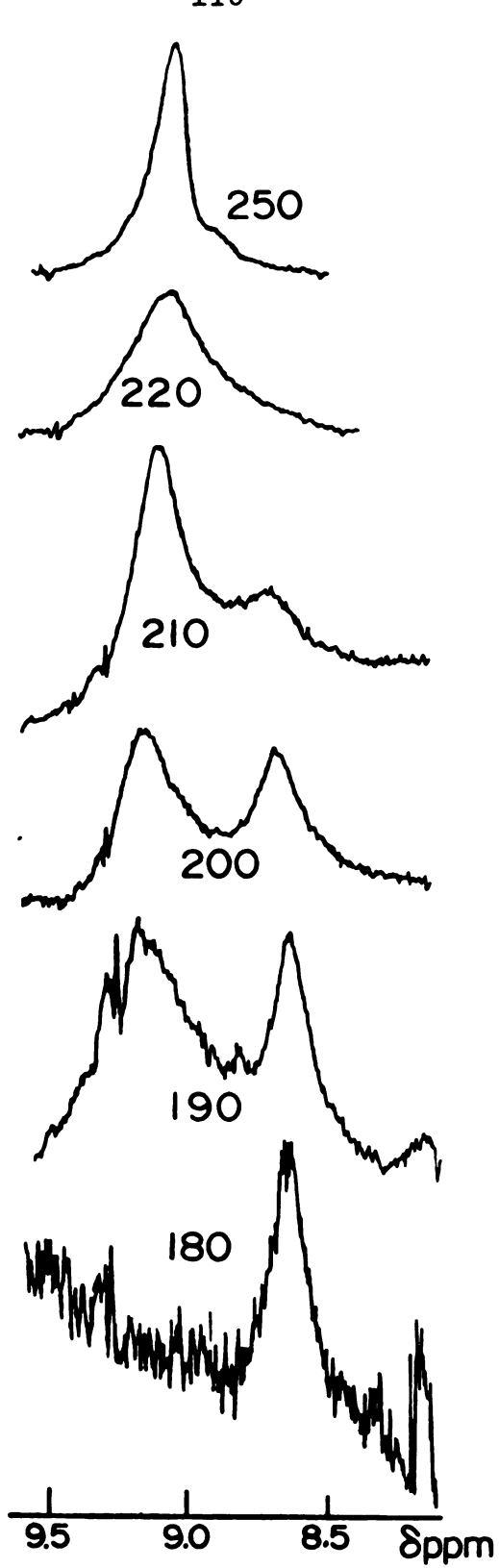


Figure 36. The temperature dependence of the NMR spectrum of the internal proton of Clll+H ,i in d $_4$ -MeOH with about 50 mole % HCl added.

previously, that the exchange between the mono and diprotonated ligand is fast at elevated temperatures, but slows greatly as the temperature is lowered and shifts toward the diprotonated form. The relative areas of the H_i resonances at 200 K provide an estimate of the equilibrium constant for the process:

Clll·2H⁺,i-o
$$\xrightarrow{K_a}$$
 Clll·H⁺,i + H⁺ (31)

yielding $K_a = 7.0 \pm 1.0 \times 10^{-3}$ M. Using $\Delta H^o = 2.0$, the equilibrium constant may be extrapolated to 298 K, giving a value of about 0.06 M. The true ΔS^o may also be calculated since the acid concentration is known, thus $\Delta S^o = 1$ cal mol⁻¹ deg^{-1} .

The monoprotonated ligand, Clll·H⁺,i, may be recovered from Clll·2H⁺,i-o by evaporating the solvent and evacuating the ligand in a vacuum desiccator with the aid of a roughing pump, provided the acid is volatile and the concentration process does not cause cleavage of the ligand (as with HNO₃).

E) Clll·H⁺,o in d₆-Acetone

The temperature dependence of Clll·H⁺,o protonated with TFAA in d₆-acetone gives rise to very complex patterns, due to the presence of two or more species in solution. As the temperature is lowered, the equilibrium tends to favor the mono and di externally protonated Clll, as shown in Figure 37, for a mole ratio of acid to Clll equal to 1.7. With increasing acid concentration, the equilibrium is also

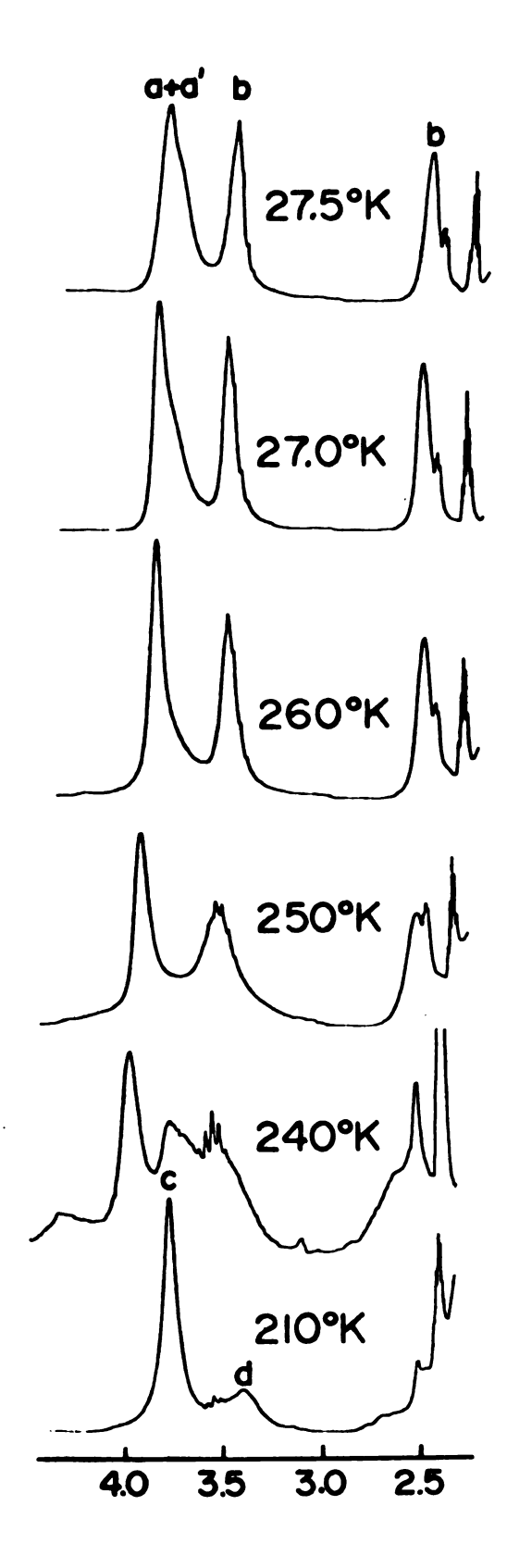


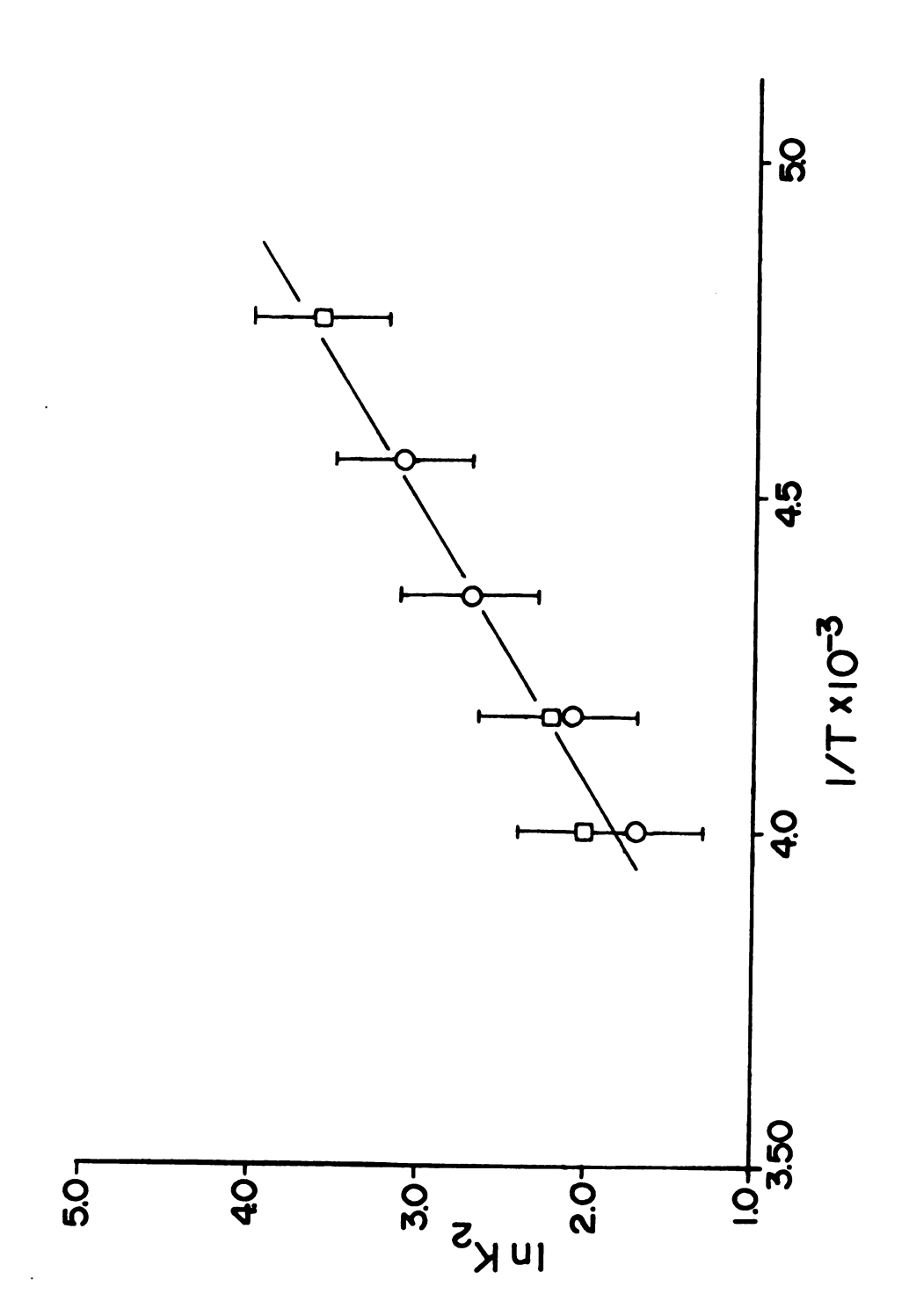
Figure 37. The temperature dependence of the NMR spectra of Clll+H+,0 in d₆-acetone, acidified with TFAA.

forced toward the diprotonated form in accordance with the following scheme:

C111 +
$$2H^{+} \xrightarrow{K_{1}}$$
 C111. H^{+} , $o + H^{+} \xrightarrow{K_{2}}$ C111. $2H^{+}$, $o - o$ (32)

The first external protonation is very efficient and K_1 is large, whereas K_2 is small and the rate of deprotonation of $\text{Clll} \cdot 2\text{H}^+$, o-o is very rapid. Therefore, as the temperature is decreased, the line corresponding to the diprotonated species at 3.8-4.0 ppm grows in intensity. The other lines of Figure 37 correspond to the externally monoprotonated species. A rough calculation from the relative areas of the resonances provides the temperature dependence of the pseudo-equilibrium constant, $K_2([\text{H}^+])$, which is shown in Table 14 for mole ratios of 1.4 and 1.7 acid/Clll. A plot of $\ln K_2$ with 1/T is presented in Figure 38, which gives a value of $\Delta H^\circ = -5 \pm 1$ kcal mol^{-1} , $\Delta S^\circ = -16$ cal mol^{-1} deg⁻¹, $\Delta G^\circ_{298} = -0.2$ kcal mol^{-1} , $K_2 \approx 1.0$ at 298 K and ≈ 20 at 220 K.

The same process may be followed at a single temperature by addition of acid. For example, at 220 K the line at 3.8-4.0 ppm shifts from about 3.82 to 3.91 ppm upon addition of acid (Table 15). From this shift, the ratio of Clll·2H⁺,o-o to Clll·H⁺,o may be obtained, assuming that their chemical shifts in the absence of exchange are 3.99 and 3.82 ppm respectively. The plot of this ratio versus acid strength (Figure 39) gives a straight line of slope = $\frac{1}{K_2C_t}$, where C_t is 0.005 M, the total concentration of Clll.



The variation of $\ln(K_2)$ with 1/T for the formation of Clll.2H⁺,o-o in d_6 -acetone upon the addition of TFAA. Figure 38.

Table 14. The temperature dependence of the equilibrium constant for the formation of Clll \cdot 2H $^+$,o-o in d $_6$ -acetone with the addition of TFAA.

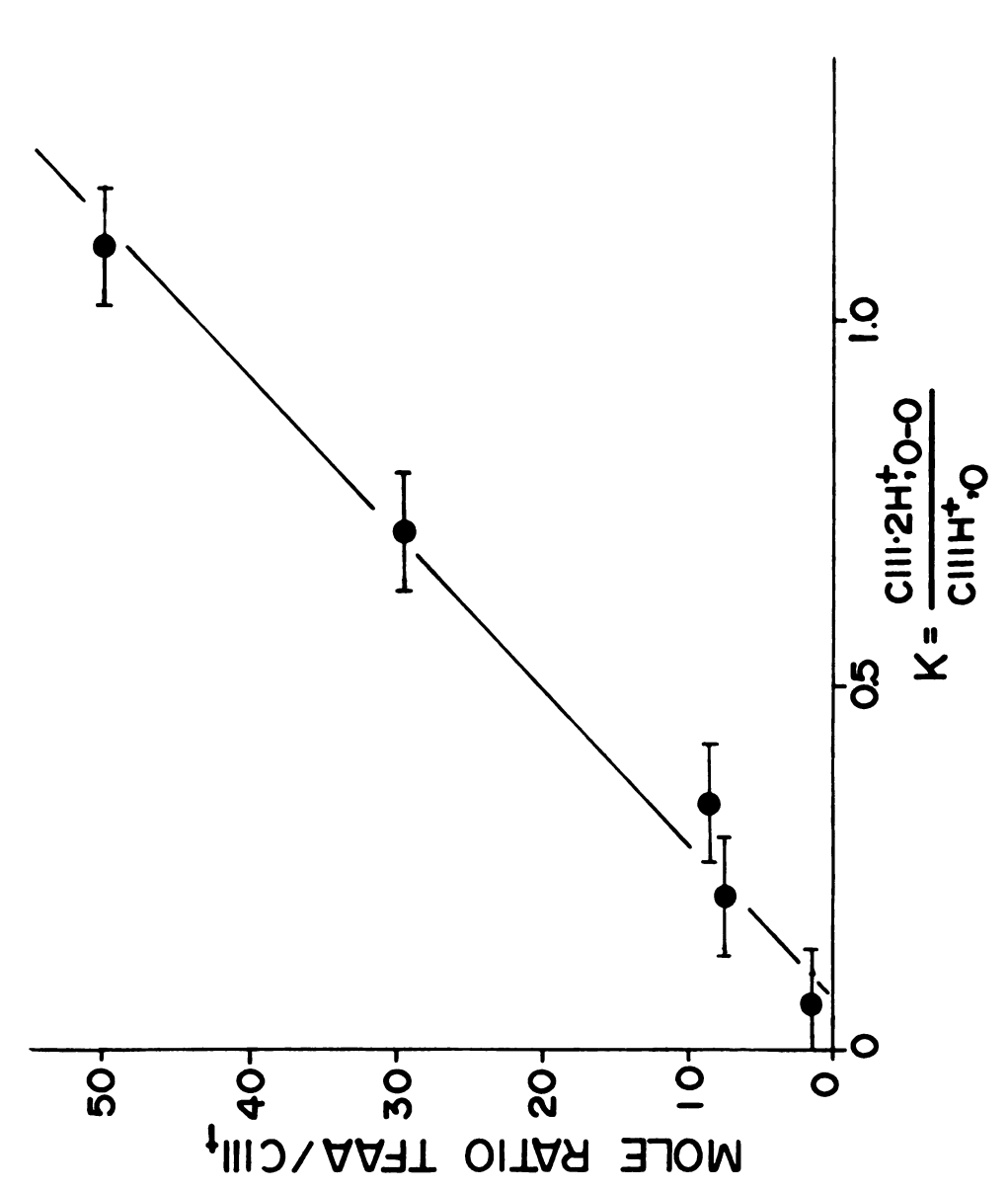
Mole ratio $\frac{\text{acid}}{\text{Clll}}$	Temp (°K)	1/Tx10 ⁻³	к ₂ [н ⁺]	к ₂	ln K ₂
1.4	220	4.55	0.16	23	3.1
1.4	230	4.35	0.10	14	2.7
1.4	240	4.17	0.06	9	2.1
1.4	250	4.00	0.04	6	1.7
1.7	210	4.76	0.30	35	3.6
1.7	240	4.17	0.08	9	2.2
1.7	250	4.00	0.06	7	2.0

This yields a value of $K_2 = 5.0$ at 220 K compared to 20 by the first method. The discrepency between the values of K_2 obtained by the two methods is probably due to large systematic errors in both methods, especially the first, since the lines of the monoprotonated ligand are too broad to measure accurately. Therefore, the agreement is satisfactory and supportive of the previous assignments.

F) Summary

- 1) Clll exists in the endo-endo configuration which is preferred by a factor of 50 over the exo-endo form in water at 298 K.
- 2) Clll protonates externally (exo-endo form) with a pK_a at 298 K in water of 7.1. Protonation occurs at the nitrogen.

C111.H⁺,o[H⁺] The dependence of the equilibrium constant for the conversion of Clll. Ht.o to Clll. 2Ht.o-o on the concentration of TFAA. C111.2H+ 7.5 5.5 9.7 4.9 4.4 C111.2H+,0-0 C111.H⁺,o 0.064 0.064 0.21 0.32 0.71 1.11 3.83 3.83 3.85 3.86 3.89 3.91 ^{2H}⁺ ⁶ppm TFAA C_tClll Mole ratio 9.7 ₹.8 Table 15. 1.7 29 50



The dependence of the equilibrium constant for the conversion of Clll+H⁺,o to Clll+2H⁺,o-o in d_6 -acetone on TFAA concentration. Figure 39.

- 3) Clll will protonate a second time externally at the unprotonated nitrogen (exo-exo) with a pK_a (in water) of between 0 and 1.5.
- 4) Internal protons bind most strongly to the nitrogens and the proton exchanges rapidly between them.
- 5) The barrier (ΔH^{\dagger}) to vicinal carbon wagging motions is about 9 ± 0.5 kcal mol⁻¹ with ΔS^{\dagger} = -6 cal mol⁻¹ deg⁻¹ for the internally monoprotonated species.
- 6) Another motion freezes out at temperatures below those which freeze out the vicinal carbon wagging. This process has $\Delta G^{\frac{1}{7}} = 8.4 \text{ kcal mol}^{-1}$ at coalescence and apparent values of $\Delta H^{\frac{1}{7}}$ of $16 \pm 2 \text{ kcal mol}^{-1}$ and $\Delta S^{\frac{1}{7}}$ of -39 cal mol^{-1} deg⁻¹. It probably originates from a concerted torsional motion of the skeleton of the cryptand.
- 7) The structure, Clll·H⁺,i, protonates externally at the nitrogen with a pK_a value at 298 K in water of roughly 0.4. This low pK_a value indicates that the endo-endo form of Clll·H⁺,i is favored by a factor of about 10⁸ over the exo-endo form.
- 8) Clll·2H⁺,i-i exists in the endo-endo form with very slow or no exchange of the H_i protons.
- 9) For the external protonation of Clll·H⁺,i in d_{μ} -MeOH, $\Delta H^{\circ} = 2 \pm 0.1 \text{ kcal mol}^{-1} \text{ and } \Delta S^{\circ} = 1. \text{ cal mol}^{-1} \text{ deg}^{-1}.$
- 10) For the second external protonation of $Clll \cdot H^+$, o in d_6 -acetone, $\Delta H^\circ = 5 \pm 1 \text{ kcal mol}^{-1}$ and $\Delta S^\circ = -16 \text{ cal mol}^{-1}$ \deg^{-1} .

CHAPTER 4

THE KINETICS OF INTERNAL PROTONATION OF C111

I) INTRODUCTION

Cryptand lll has the remarkable ability to irreversibly bind protons. It does so by encapsulating them inside its cavity so as to exclude solvent interactions and to provide a very thermodynamically favored environment for the proton. The internally monoprotonated complex, for example, is not significantly deprotonated even upon heating for days at 60°C in 5 M KOH! Neither do sodium in liquid ammonia or ion exchange methods accomplish deprotonation, except when the ligand is destroyed. The second internally protonated complex is also very stable to base at room temperature. At elevated temperatures, however, one of the two protons may be removed, but only at a slow pace.

In light of the apparent stability of the internally protonated complexes, it is unusual that their rates of formation are slow. It was shown earlier that proton transfers between donors of quite different pK_a values proceed very rapidly and favor the one of largest pK_a . Yet the rate of formation of the internally monoprotonated complex proceeds with a half-life of several hours at room temperature at a pH of 7 indicating that the mechanism is more complex than for normal proton transfers. This is confirmed by the disclosure that internal protonation occurs with an enormous activation energy of 25 to 27 kcal mol⁻¹. This large

activation energy causes the rates of proton transfer to be slow. Therefore, the long life-time of the complex is not completely thermodynamic in origin, but is also strongly affected by this kinetic phenomenon.

The rates of internal protonation provide estimates of the thermodynamic stability of the internally protonated complexes. Their pH dependence also sheds light on the mechanism of proton transfer. These and other topics will be discussed in the ensuing sections upon presentation of the kinetic data.

II) THE FIRST INTERNAL PROTONATION OF C111

The rate of the first internal protonation of Clll was studied as a function of pH and temperature in D_2O , using buffers to obtain the desired pH. The pD value of the buffers was measured using a calibrated radiometer with a type GK2321C electrode, the values being shifted upward by 0.4 pH units to give a correct pH reading $^{(67)}$. About 1 mg. of Clll was utilized for each sample, this amount being 5% or less of the buffer content and insignificant to the final pH. Table 16 presents the buffers utilized to achieve various pH values and their ionic strengths.

The rates of internal protonation, which were measured at constant temperature (checked periodically) and pH proceeded with first order dependences on the ligand in all cases and also depended heavily on both pH and temperature as shown in Table 17. A typical rate analysis is shown in

Table 16. Buffer compositions and their ionic strengths in D_2O .

рН	Composition	Ionic Strength
8.65	KH2PO4-NaOH	0.29
7.47	KH ₂ PO ₄ -NaOH	0.37
6.46	KH2PO4-NaOH	0.33
4.93	KHP-NaOH	0.34
4.04	KHTartrate	0.22
4.00	KHP-HC1	0.29
3.19	KHP-HC1	0.29
2.60	KC1-HC1	0.30
1.78	KC1-HC1	0.36
1.44	KC1-HC1	0.41
1.25	KC1-HC1	0.38
1.11	KC1-HC1	0.55

Figure 40 in which the natural log of the reactant concentration is plotted versus time. It should be emphasized that these rates were extremely slow, each reaction requiring several hours to go to completion.

The temperature dependence of the rate of internal protonation has been studied at pH values of 7.5 and 4.9, both of which provide similar Arrhenius activation plots which are depicted in Figure 41. The temperature dependence of the rates at the pH values provide straight line plots of nearly equal slope, giving values for the activation parameters at 299 K of $E_a = 26 \pm 2$ kcal mol⁻¹,

Table 17. The dependence of the rate of internal monoprotonation of Clll upon pH and temperature.

pH (buffer)*	Temp.	k(sec ⁻¹)	σ [†]	ln k	log ₁₀ k
unbuffered (~9)	299	4.27x10 ⁻⁶	2.7x10 ⁻⁷	-12.36	-5.37
8.7	299	1.57x10 ⁻⁵	3.0×10^{-7}	-11.06	-4.81
7.5	299	8.70×10^{-5}	3.0×10^{-6}	-9.35	-4.06
7.5	310	3.65×10^{-4}	$8.3x10^{-6}$	-7.92	-3.44
7.5	320	1.25x10 ⁻³	5.0×10^{-5}	-6.69	-2.90
6.5	299	1.14x10 ⁻⁴	8.0×10^{-6}	-9.08	-3.95
4.9	299	1.70×10^{-4}	1.2×10^{-5}	-8.68	-3.77
4.9	320	2.08×10^{-3}	$2.0x10^{-4}$	-6.17	-2.68
4.0 (tartrate)	299	$2.02x10^{-4}$	1.9×10^{-5}	-8.59	-3.73
4.0 (HC1-KC1)	299	1.95x10 ⁻⁴	$1.2x10^{-5}$	-8.48	-3.68
3.2	299	2.25×10^{-4}	1.0x10 ⁻⁵	-8.33	-3.62
2.6	299	4.22x10 ⁻⁴	7.3×10^{-5}	-7.47	-3.24
1.8	299	6.40×10^{-4}	$1.7x10^{-5}$	- 7.35	-3.19
1.5	299	8.53×10^{-4}	1.3x10 ⁻⁵	-6.67	-2.90
1.3	299	9.42×10^{-4}	1.8×10^{-5}	-6.65	-2.89
1.1	299	1.03x10 ⁻³	1.1x10 ⁻⁵	-6.49	-2.82
1.1	E 3 J		I . INIO	10 • 17	2 . 0 2

^{*} pH values measured by calibrated radiometer and corrected up 0.4 pH units for deuterium isotope effect.

[†] Some values corrected to 299 K using $E_a = 26.4$ kcal/mole.

t Linear estimate of the standard deviation on k.

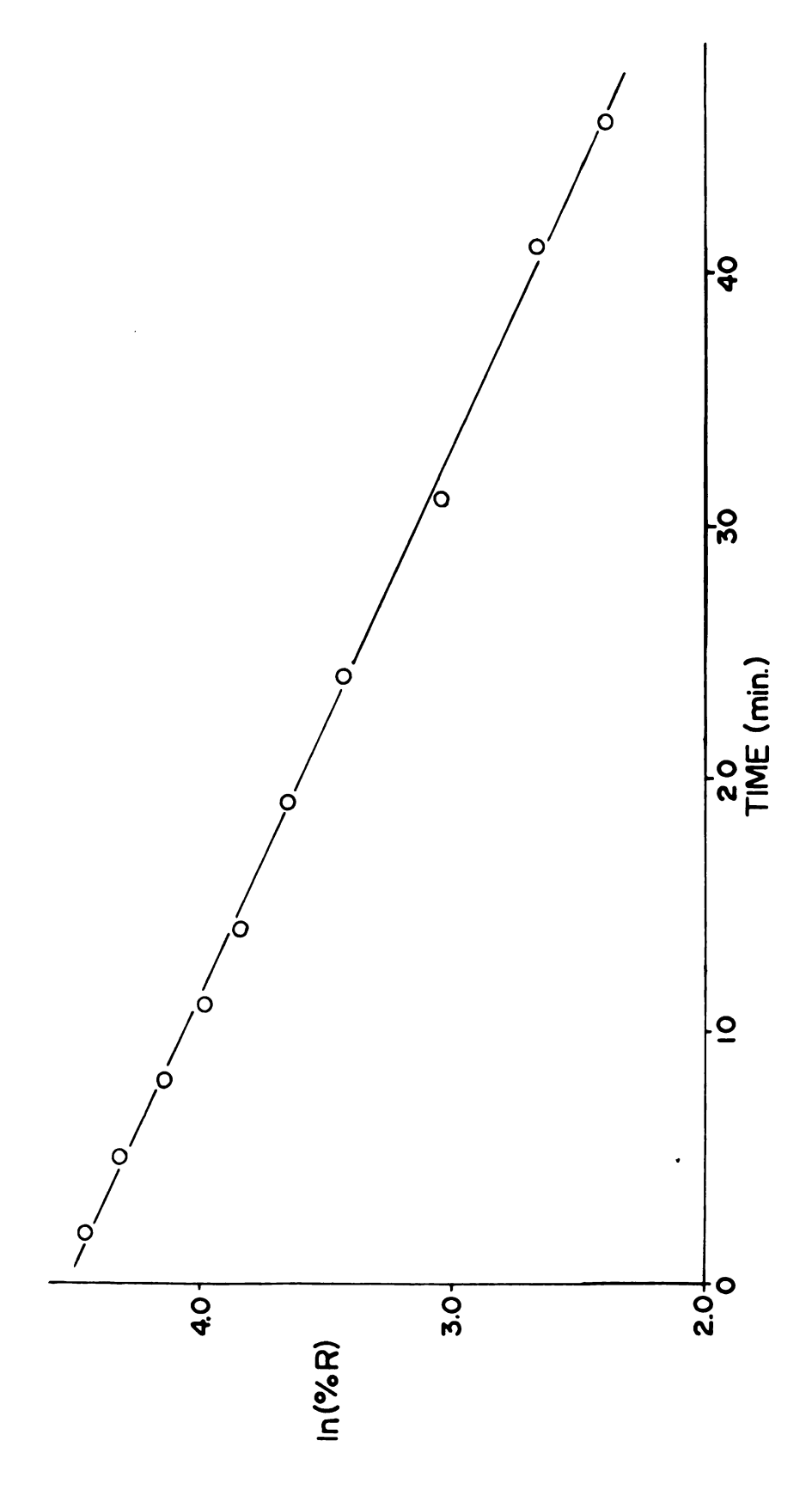
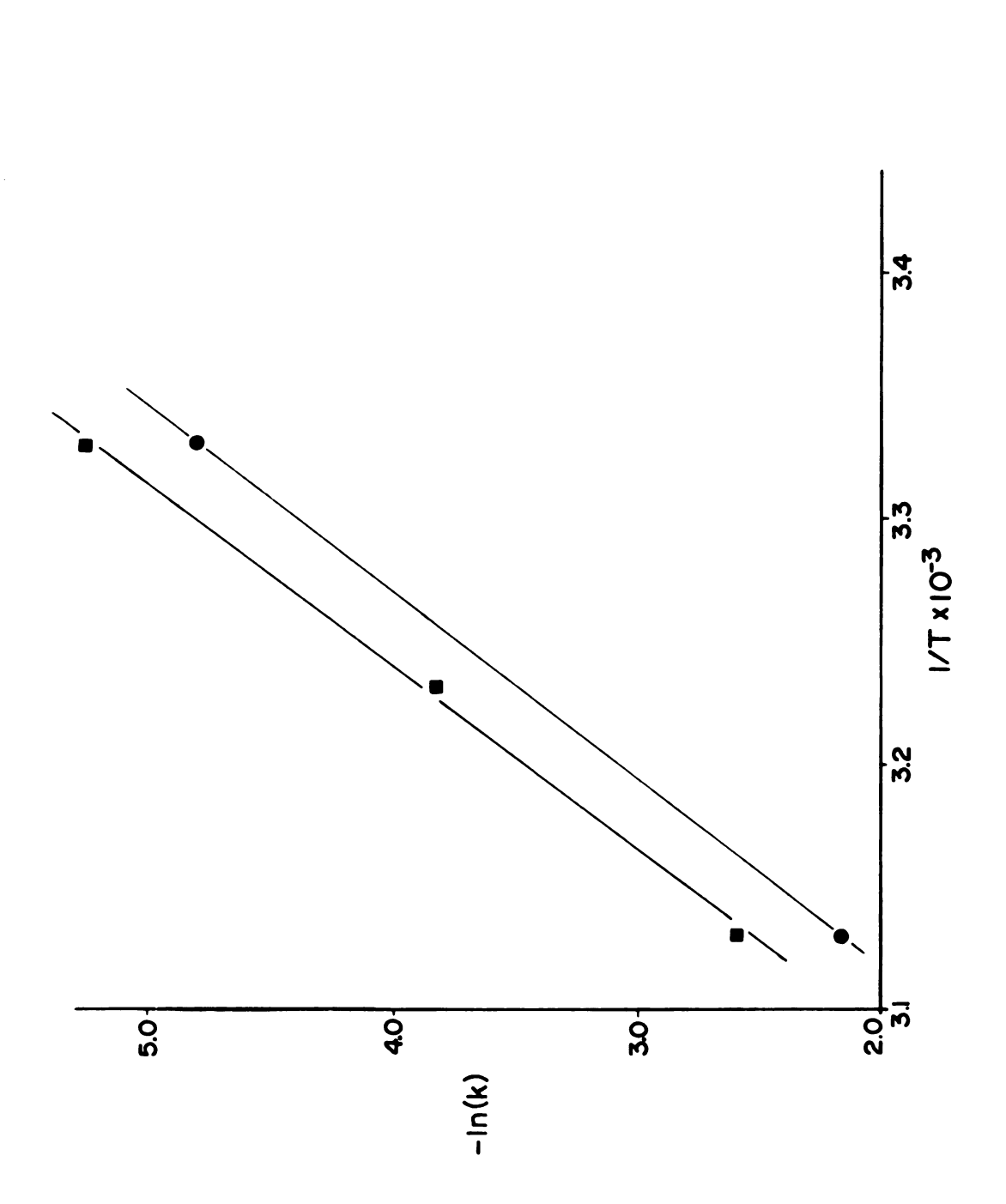


Figure 40. A typical rate analysis for internal protonation of Clll in water.



The dependence of $\ln(k)$ on 1/T for the internal protonation of Clll in water at two different pH values: squares; pH = 7.5 and circles; pH = 4.9. Figure 41.

 ΔG^{\dagger} = 23 kcal mol⁻¹ and ΔH^{\dagger} = 25 kcal mol⁻¹ and ΔS^{\dagger} = +7 cal deg⁻¹ mole⁻¹⁽⁷³⁾. The large free energy of activation originates mainly from the enthalpy term. This is presumably the energy required to distort the face of the ligand, which allows the proton access to the cavity. This topic will be discussed further when the activation parameters of the other internal protonation processes have been documented. It is clear, however, that the slow rates of internal protonation are dominated by a large enthalpy barrier which results from ligand deformation.

The large activation barrier is somewhat unexpected, since a proton possesses negligible size and should easily fit into the holes of the ligand's faces. However, in solution (as ${\rm H_30}^+$) the proton possesses electron density obtained from its hydrogen bonded counterpart and has a finite size. As the proton interacts with the nitrogen and the oxygen atoms of Clll, it accumulates considerable electron density from this source which also imparts significant size to the proton. Therefore, the same interaction which induces proton binding also restricts the proton from entering into the cavity of the ligand. Once inside, it accumulates even more electron density as it interacts with the nitrogen and oxygen lone pairs and its effective size becomes larger. This phenomenon probably contributes most to the resistance of the complex to deprotonation.

The conformation of Clll is very much influenced by the pH of the medium, since it may bind either one or two

protons externally. Such changes in conformation also seem to correlate with the pH dependence of the rate of internal protonation. Table 6 (Chapter 3) lists the chemical shifts of Clll as a function of pH in water, the $\mathrm{CH}_{2}\mathrm{N}$ proton shifts being plotted in Figure 22 (also in Chapter 3). A break is observed in this curve at a pH value of about 6, above which Clll and Clll. H, o are the predominant forms of the ligand in solution. Below a pH value of 6, the ligand is fully monoprotonated externally and begins to add a second proton (also externally). However, even at a pH value of 1, only about half of the ligand is diprotonated externally, if it is assumed that the chemical shifts of these species in D_2O are similar to those in d_6 acetone (as they appear to be). The reversal of the CH2N proton shifts after complete formation of the externally monoprotonated form (at a pH value between 5 and 6) is also observed in d₆-acetone upon the formation of the externally diprotonated complex. This reversal is probably a result of less effecient proton binding as the ligand must accomodate a second positive ion.

This NMR titration agrees qualitatively with a pH titration done in a conventional way with a calibrated radiometer, as shown in Figure 42. This titration gives an endpoint at a pH value of about 5 and a value of pK_a = 7.1 ± 0.3 at 299 K for the first external protonation. A second break has not been observed, even at pH values as low as 1.2, but the second pK_a may be estimated at ≤ 1.5 .

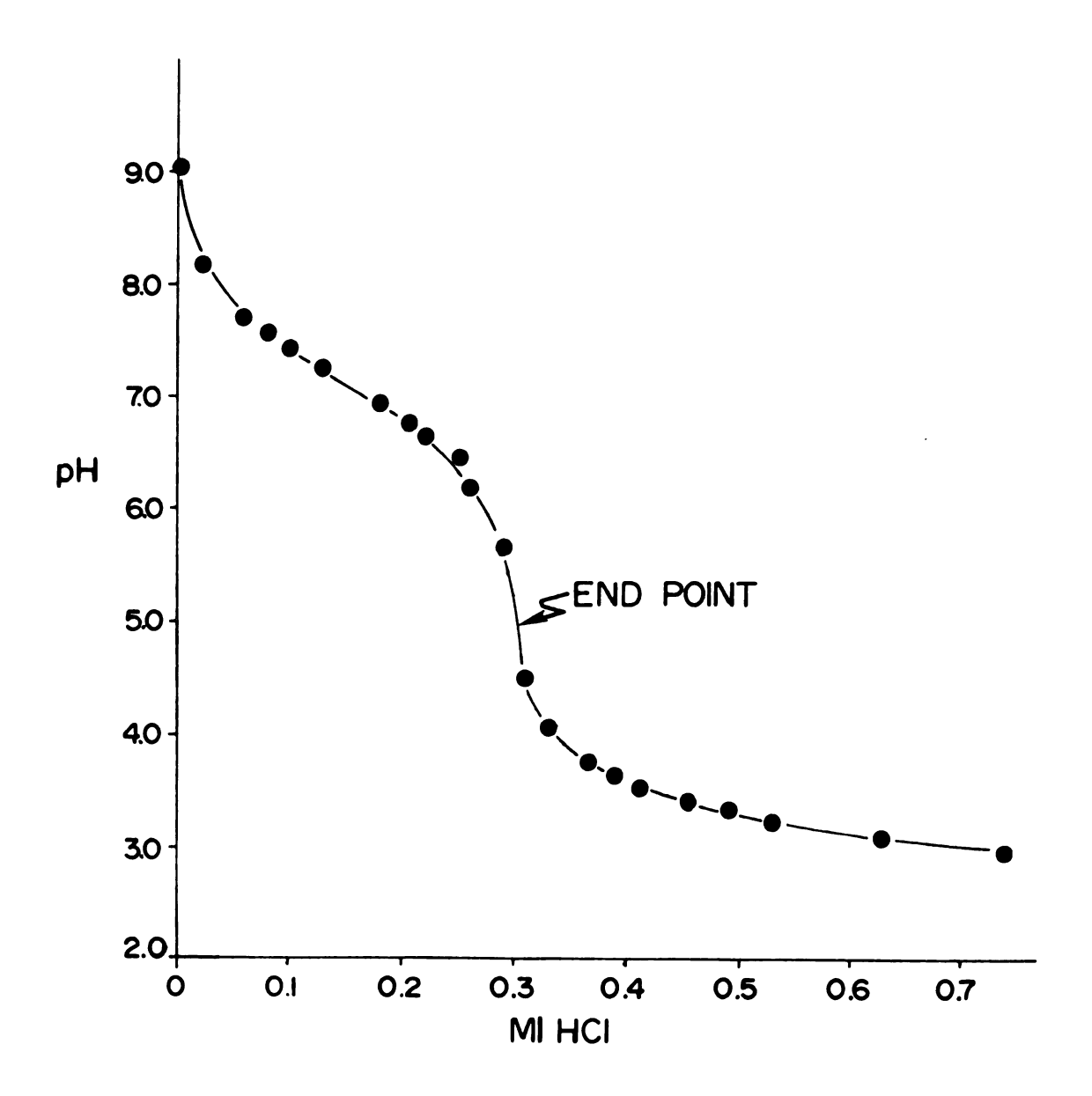


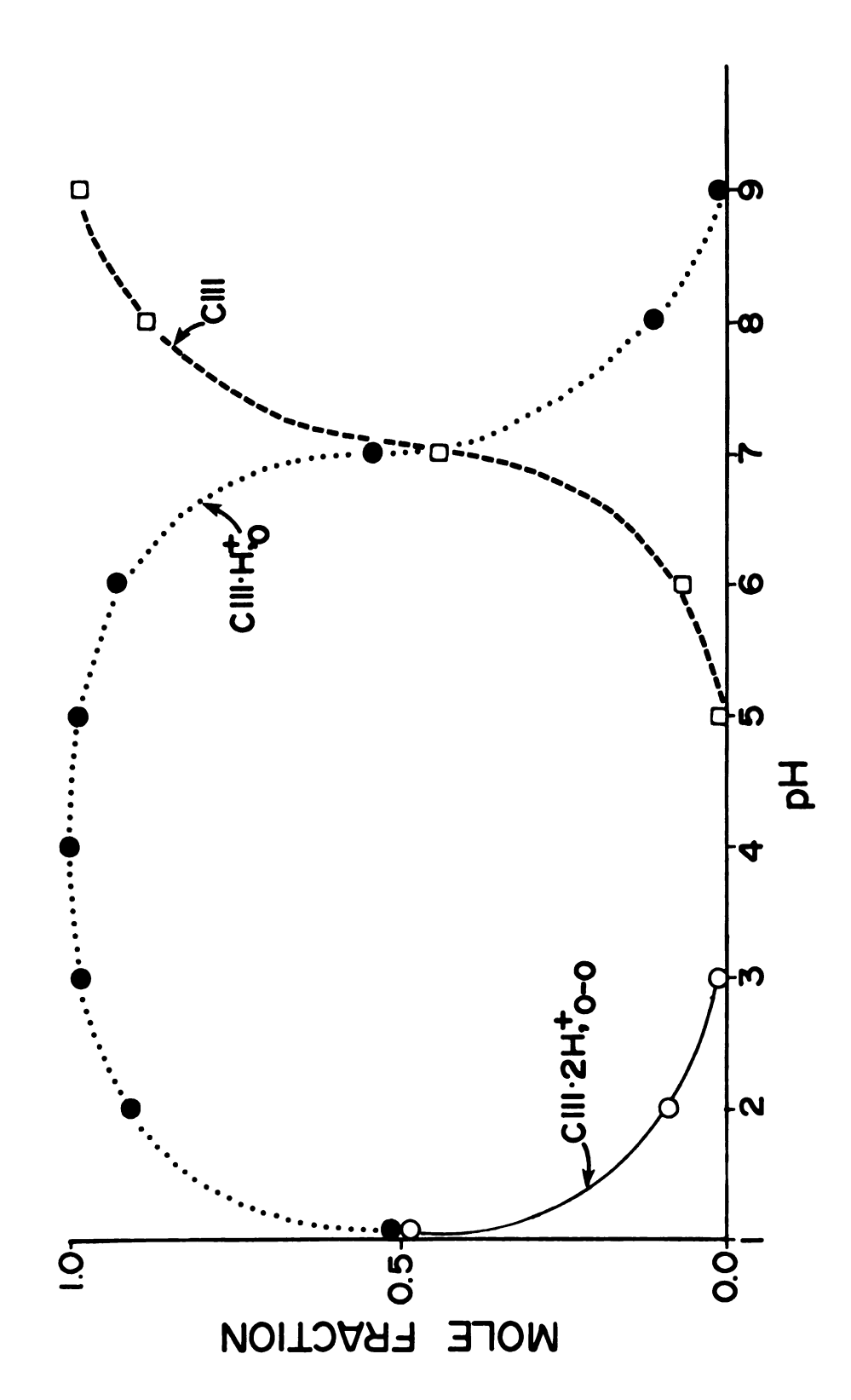
Figure 42. The pH titration of Clll with HCl in water (only external protonation occurs).

(The NMR data indicate a pK_a value of between 0 and 1.5.)

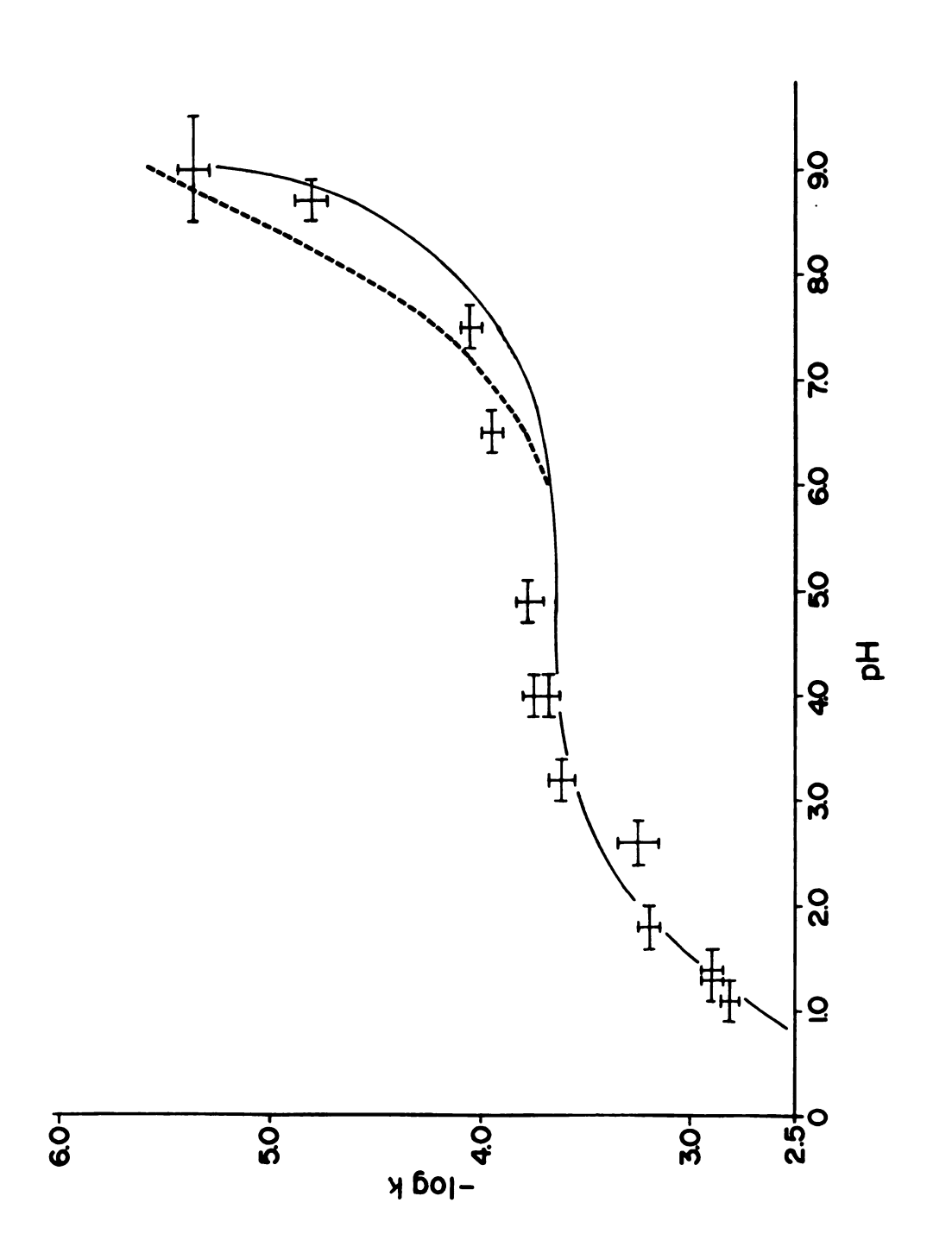
The relative concentrations of the various forms of the ligand in solution may be calculated as a function of pH by using pK_a values of 7.1 and 1. for the two external protonations (Figure 43). The externally monoprotonated complex is the predominant structure over a very wide pH range, 2 to 7, above and below which the other forms are important.

The rate of internal protonation correlates well with the form of the ligand in solution. Figure 44 depicts the dependence of this rate upon pH. It shows a nearly linear curve between pH values of 3 and 7 where the monoprotonated species is predominant and in fairly constant concentration. Below a pH value of 3, the rate increases and approaches a first-order dependence on the hydrogen ion concentration simultaneous with the build-up of the externally diprotonated complex. Above a pH value of 7, the rates are very slow, decreasing markedly as the mole ratio of Clll·H⁺, o decreases.

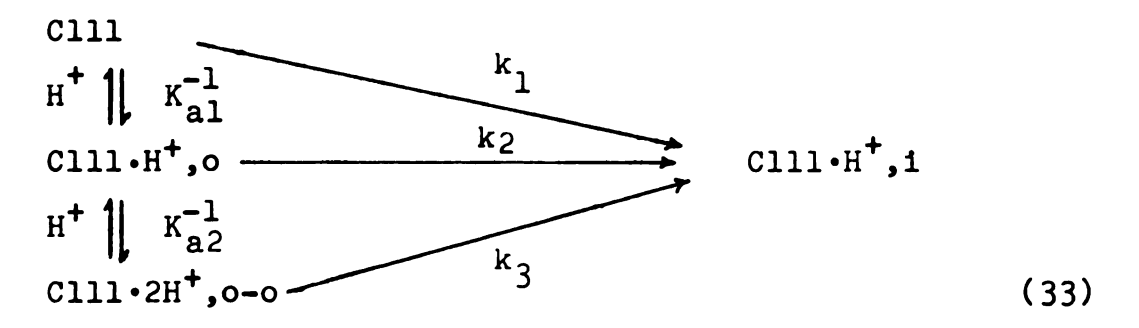
The correlation of the rates of internal protonation with the form of the ligand suggests that it is easiest to internally protonate the externally diprotonated ligand. The externally monoprotonated form, Clll·H⁺,o will internally protonate, but with difficulty and the free ligand is even more difficult, if not impossible to internally protonate. This observation is represented schematically as follows:



The variation of the relative concentrations of the various forms of Clll in water with $\ensuremath{\mathrm{pH}}\xspace$. Figure 43.



The dependence of the rate of internal monoprotonation of Clll on pH: dashed line; $pK_a = 7.1$ and solid line; $pK_a = 7.5$. Figure 44.



in which $k_1 << k_2 < k_3$.

If we assume that this is a valid mechanism for internal protonation, we can write a rate expression as follows:

rate =
$$k_1$$
 [C111][H⁺] + k_2 [C111•H⁺,o] + k_3 [C111•2H⁺,o-o] (34)

The rate observed from the NMR analysis is equal to some rate constant multiplied by the total Clll concentration, C_+ , or:

$$rate = k_{obs} C_{t}$$
 (35)

Solving for K_{obs} , one obtains for the expression of equation (34):

$$k_{obs} = \frac{k_3(K_{a1}) + k_2 + K_{a2}k_1(H^+)}{H^+/K_{a1} + 1 + K_{a2}/(H^+)}$$
(36)

This equation has been used to computer fit the pH dependence of the rate of internal protonation of Clll. The values of K_{al} and K_{a2} were taken as 7.9×10^{-8} and 0.1. The rate of internal protonation of the free Clll, k_1 , was taken to be zero and the other two rate constants were the variables.

A computer fit (using KINFIT) of the data is shown in Figure 44 (dashed line) and gives values for the rate constants, k_3 and k_2 , of $3.8 \pm 0.6 \times 10^{-3} \, \mathrm{sec}^{-1}$ and $2.3 \pm 0.3 \times 10^{-4} \, \mathrm{sec}^{-1}$. Thus the experimental points are fit rather well by this rate expression. If K_{al} is given a value of 3.1×10^{-8} , the fit is even better (solid line). The values of k_3 and k_2 do not change appreciably when the latter value of K_{al} is used, however.

It should be pointed out that several rate expressions would yield the same form of $k_{\mbox{\scriptsize obs}}$ as given in equation (36). These include:

rate =
$$k_1^{\dagger}$$
 [Clll·H⁺,o][H⁺] + k_2 [Clll·H⁺,o] (37)

rate =
$$k_1^{\dagger}$$
 [Clll•H⁺,o][H⁺] + k_2^{\dagger} [Clll][H⁺] (38)

rate =
$$k_1'$$
 [Cll1] + k_2 [Cll1•H⁺,o] +
 k_3 [Cll1•2H⁺,o-o] (39)

Therefore, a mechanism for internal protonation may not be determined from the rate expressions.

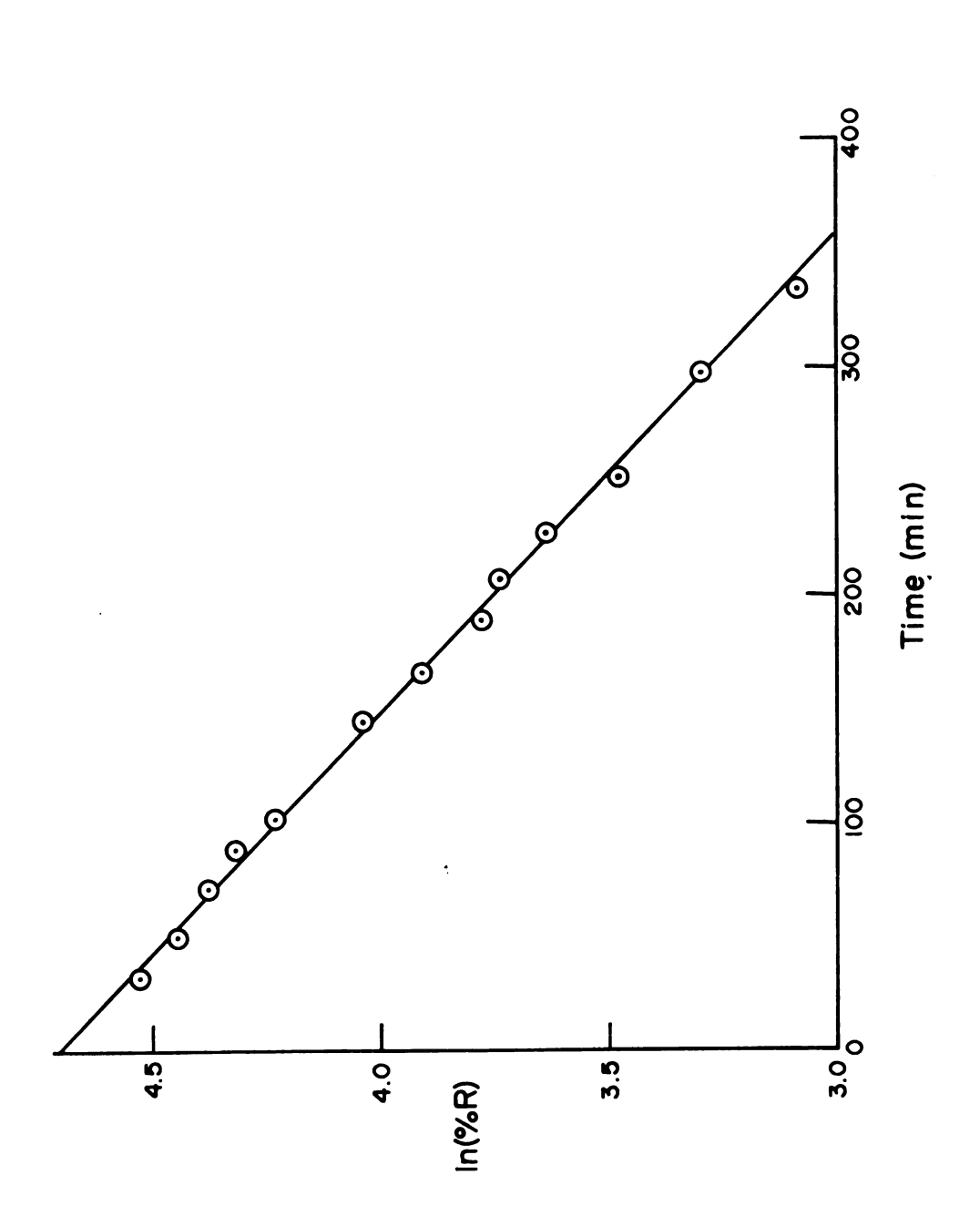
III) THE KINETICS OF THE SECOND INTERNAL PROTONATION OF C111 IN WATER

The species Clll·H⁺,i may be internally protonated a second time, but only under more rigorous conditions than those used for the first internal protonation. For example, the free ligand at a pH of l and room temperature converts to the internally monoprotonated ligand in minutes, but forms no internally diprotonated complex for days. In 1 M HCl, the

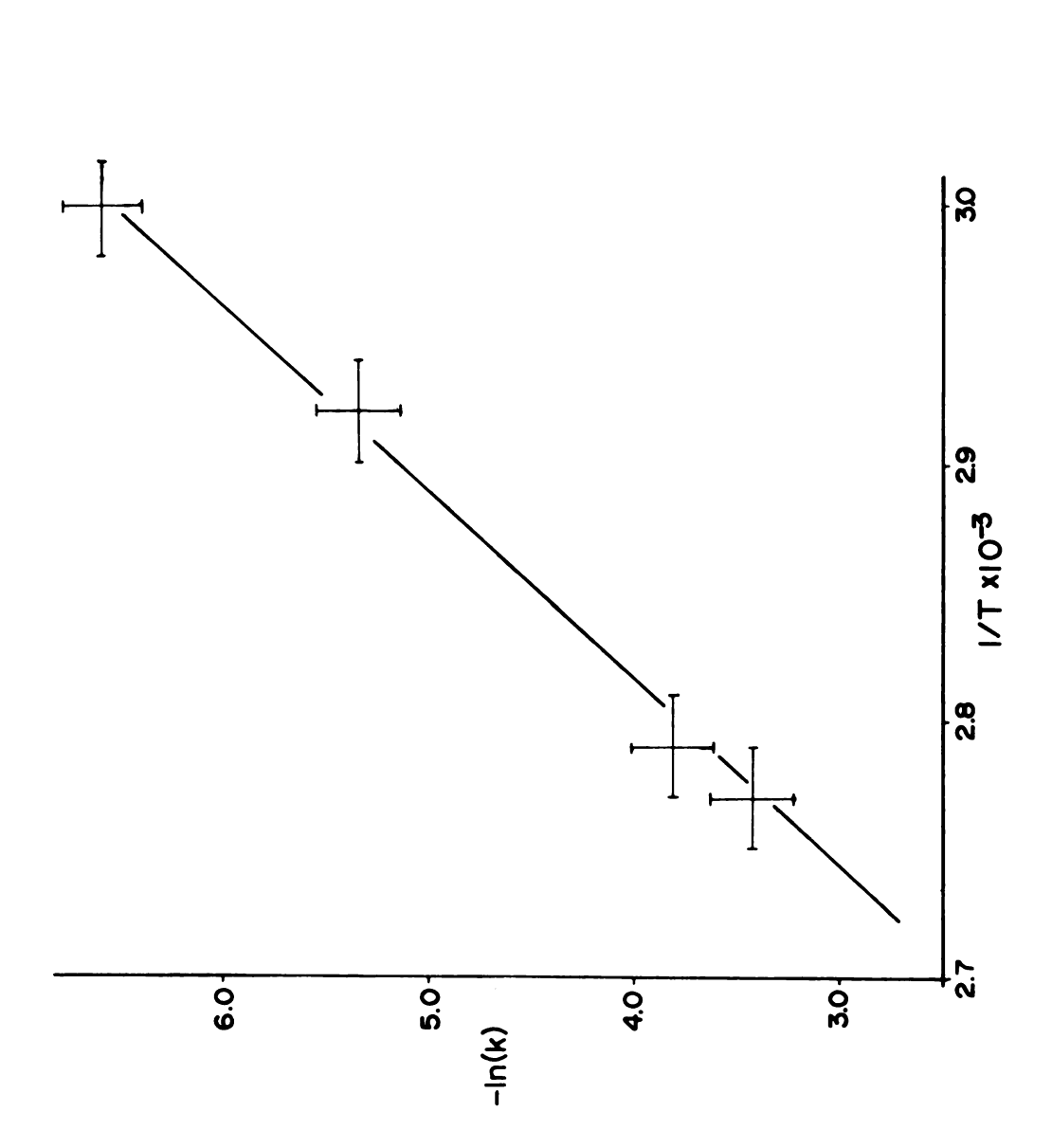
second internal protonation proceeds with a time-scale of several weeks at room temperature and is accompanied by considerable decomposition of the ligand. At elevated temperatures, the rates are much faster and decomposition is minimized.

The internal protonation of $\text{Clll} \cdot \text{H}^+$, i has been studied as a function of temperature in 1 M HCl in D_2O . The data obtained for a typical rate study are shown in Figure 45. Just as for the first internal protonation, the rates show a first order dependence on the ligand concentration but are slower than the former under similar conditions. Table 18 gives the rates as a function of temperature in 1 M HCl and an Arrhenius plot of these data is shown in Figure 46. The plot shows a linear dependence of $\ln(k)$ on 1/T and gives $E_a = 26.4 \pm 2 \text{ kcal mol}^{-1}$, ΔG^{\dagger} at $298 \text{ K} = 26.5 \text{ kcal mol}^{-1}$, $\Delta H^{\dagger} = 25.8 \text{ kcal mol}^{-1}$, and $\Delta S^{\dagger} = -2.4 \text{ cal deg}^{-1} \text{ mol}^{-1}$.

These values are strikingly similar to those for the first internal protonation and lend credence to the theory that ligand deformation is responsible for the majority of the energy barrier, since $\Delta H^{\frac{1}{7}}$ is as large as for the first internal protonation. This rate analysis was performed at only one pH, but a pH dependence of the rate similar to that of the first internal protonation is also expected for the process.



A typical rate analysis for the second internal protonation of Clll.H '1 in 1 M HCl. Figure 45.



The dependence of ln(k) on l/T for the second internal protonation of Cill.H⁺,1 in 1 M HCl. Figure 46.

Table 18. The dependence of the rate of the second internal protonation of Clll H, i upon temperature in 1 M HCl.

Temp.(°K)	1/Tx10 ⁻³	k(sec ⁻¹)	σ#	ln(k)
333	3.00	2.27x10 ⁻⁵	1.6x10 ⁻⁶	-10.69
343	2.92	8.00×10^{-5}	1.1x10 ⁻⁶	-9.43
359	2.79	3.65×10^{-4}	1.2x10 ⁻⁵	-7. 92
361	2.77	5.28×10^{-4}	1.6x10 ⁻⁵	-7. 53

^{*} Linear estimate of the standard deviation.

IV) THE KINETICS OF DEPROTONATION OF C111.2H,1-1

The rate of proton extraction from Clll·2H⁺,i-i has been studied as a function of temperature in 5 M KOH in D₂O. The rates were again first order in ligand as shown in Figure 47 and were very slow. For example, at room temperature the complex was stable for weeks in 5 M KOH, while at elevated temperatures, the reaction proceeded with the extraction of only one of the two internal protons. At very high temperatures (386 K), the reaction was accompanied by considerable decomposition of the ligand.

The temperature dependence of the rates of deprotonation are shown in Table 19. Figure 48 presents an Arrhenius plot of the of the three data points which give a linear dependence of $\ln(k)$ versus 1/T, resulting in values of $E_a = 24.8 \pm 2$ kcal mol^{-1} , $\Delta G^{\dagger} = 27.4$ kcal mol^{-1} , $\Delta H^{\dagger} = 24.1$ kcal mol^{-1} , and $\Delta S^{\dagger} = -11$ cal mol^{-1} deg⁻¹. Again, the similarity of these activation parameters with those for internal

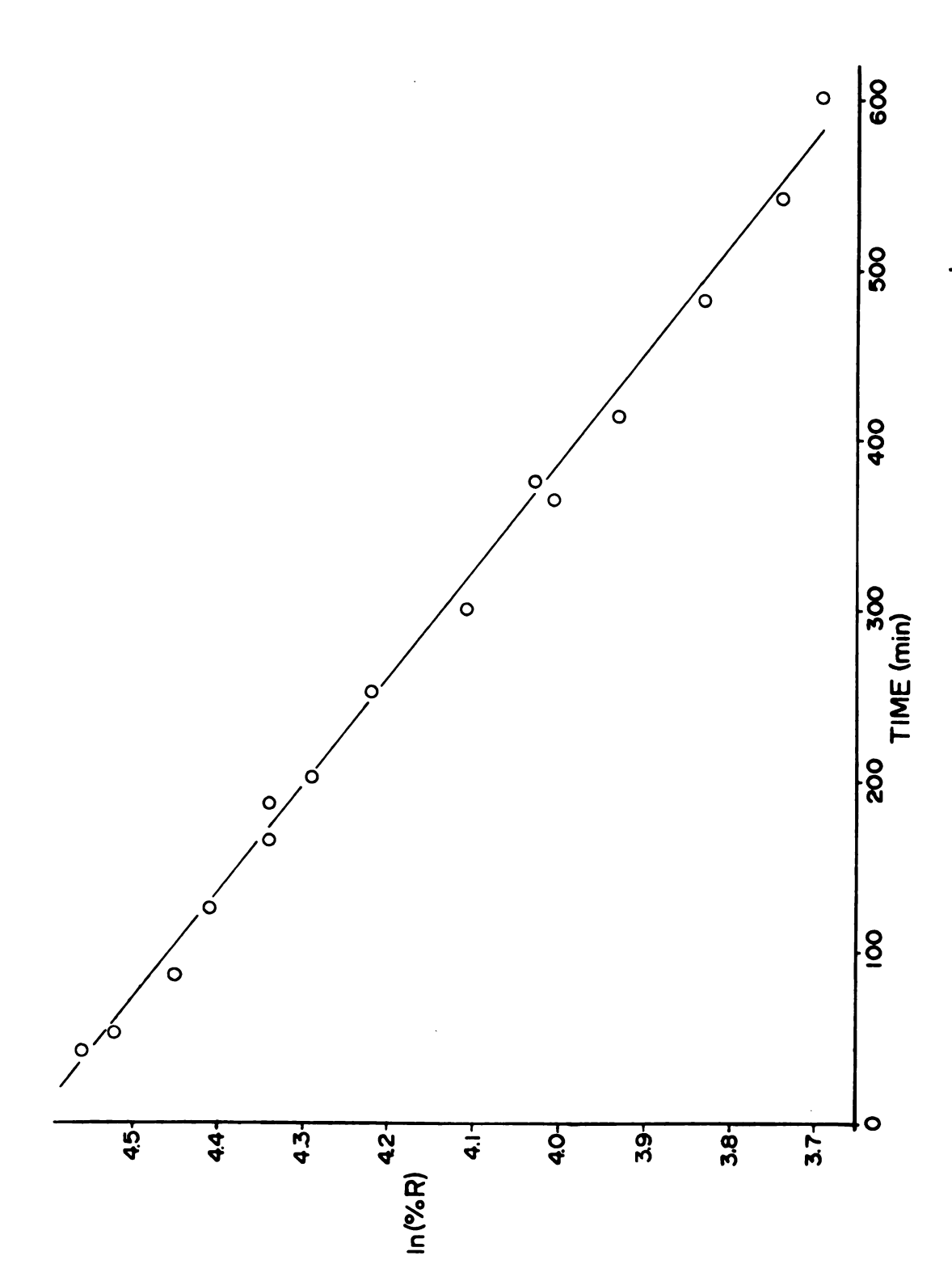
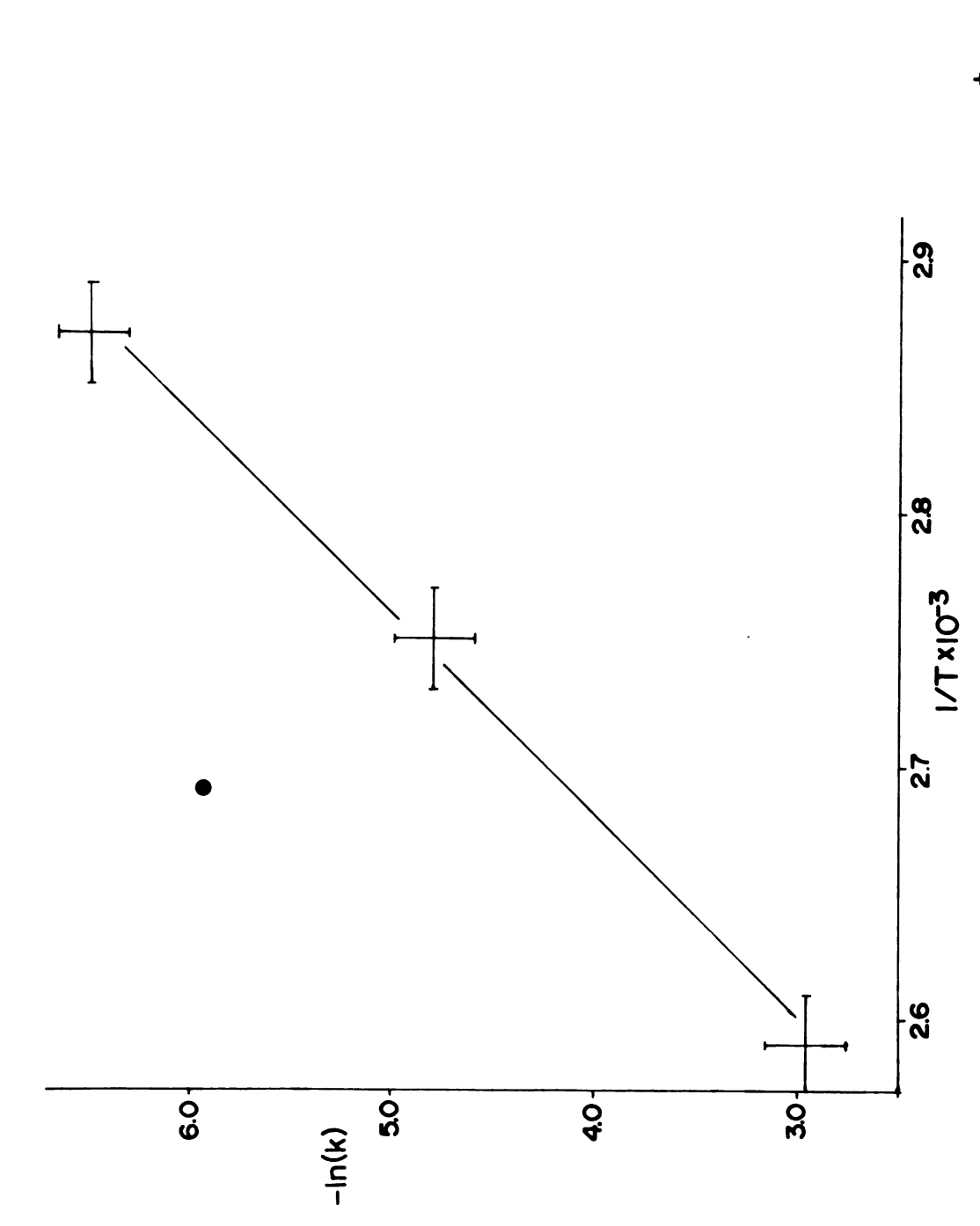


Figure 47. A typical rate analysis for the deprotonation of Clll.2H,1-1 in 5 M KOH.



The dependence of ln(k) on 1/T for the deprotonation of Clll.2H,1-1 in 5 M KOH (crosses) and 1 M KOH (circle). Figure 48.

protonation is striking, but it may only be coincidental, since deprotonation may proceed by a very different pathway than the protonation.

Table 19. The dependence of the rate of deprotonation of Clll.2H, i-i upon temperature in 5 M KOH.

Temp.	1/Tx10 ⁻³	k(sec ⁻¹)	σ *	ln(k)	Base Strength
349	2.87	2.55x10 ⁻⁵	3.9x10 ⁻⁷	-10.57	5 M
363	2.75	1.40×10^{-4}	6.7×10^{-6}	- 8.87	5 M
386	2.59	1.04×10^{-3}	8.2×10^{-5}	- 6.87	5 M
372	2.69	4.33x10 ⁻⁵	4.5x10 ⁻⁷	- 10.05	5 M

^{*} Linear estimate of the standard deviation.

This process would be expected to depend upon base concentration just as the internal protonation depends on acid strength. In order to check this, the deprotonation rate was determined in 1 M KOH at 372 K. This rate, in comparison with those obtained in 5 M KOH (Figure 48), gives a 0.7 order dependence on base strength.

V) METHOD OF ANALYSIS

The samples utilized in the analysis were prepared by weighing the ligand into an NMR tube and adding about 2 ml of $\rm D_2O$ at the appropriate pH. The samples were then brought to temperature in the probe of the NMR and analyzed by taking several scans in the pulse-FT (PFT) mode. The spectra were then stored on a magnetic disk and plotted if time permitted

and subsequent spectra taken. These spectra provided an accurate time profile of the reaction. The relative areas of the resonances of the products and reactants were obtained by tracing the spectra onto tracing paper, the images being cut and weighed.

Nuclear magnetic resonance, as a method of analysis, has several inherent shortcomings which could cause attenuation of one or all resonances, and thereby undermine its accuracy. Delay time attenuation, filtering and imcomplete relaxation could each contribute to instrumental errors and overlapping resonances could further complicate the analysis. Care was taken to insure full relaxation and in many cases a calibration chart was developed for pulse repetition rates near the saturation limit, to be certain that attenuation from this source was not occurring. Delay times and filtering did not present a problem because the lines utilized for the analysis were narrow and of similar width, and were centered in the middle of the spectrum. The largest errors originated with overlapping lines which were often of slightly different linewidth. The poorest of these analyses, however, provided rate constants with standard deviations of 20% or less, and usually less than 10%. Linear estimates of the standard deviation, obtained from KINFIT data analy $sis^{(72)}$, have been given with all rate constants.

VI) SUMMARY

The ultimate goal in this analysis is to develop a mechanism for internal protonation and deprotonation of Clll. It is not possible to determine a mechanism from the rate expression for the internal protonation of Clll since the form of this expression can be produced by several mechanisms. However, the rates of the internal protonation-deprotonation processes do provide an estimate of the thermodynamic stability of the complexes when some assumptions are made. The activation parameters for the internal protonation processes are summarized in Table 20. Using these values and the rates obtained for internal protonation, one can estimate the thermodynamic stability of Clll·H⁺, i in the following way.

For the reaction:

$$H_{2}O + C111 \xrightarrow{k_{1}} C111 \cdot H^{+}, i + OH^{-}$$
 (40)

 k_1 has been measured in pure D_2O , giving a value of 4.3 x 10^{-6} at 299 K. k_1 may also be calculated by the following scheme:

$$H_{2}O + C111 \xrightarrow{K_{a1}} C111 \cdot H^{+}, o + OH^{-}$$

$$\downarrow^{k}_{2}$$

$$C111 \cdot H^{+}, 1$$
(41)

k was calculated by computer fitting the pH dependence of the rate of internal protonation and its value is

The activation and thermodynamic parameters for internal protonation processes at $298~\mathrm{K}.$ Table 20.

1					
Process	Eal mol-1)	$\Delta_{\mathrm{H}}^{\dagger}$ (kcal mol ⁻¹)	ΔG [†] (kcal mol ⁻¹)	ΔS [‡] (cal mol ⁻ l deg ⁻ l)	ΔG° (κcal mol ⁻ 1)
C111+H++C111.H+,1	26±2	25	23	- 7 -	
C111.H1+H++ C111.2H+,1-1	26.4±2	25.8	26.5	- 2.4	
он-+с111.2H ⁺ ,1-1+ с111.H ⁺ ,1+H ₂ 0	24.8±2	24.1	27.4	-11.	
C111+H20+ C111·H+,1+OH-			25		140
c111.H ⁺ ,1+OH ⁻ + C111+H ₂ O			≥30		
C111+H20 Kpl C111.H+120 C111					<u>-</u> -5.
C111.H ⁺ ,1+H ₂ 0 K _{b2} C111.2H ⁺ ,1-1+OH	41 1				• 8+
H ₂ 0 LW H+OH-					+19.
H_3 0 $\stackrel{\longleftarrow}{\longleftarrow}$ H^{+} + H_2 0					• 0

 2.3×10^{-4} . k_1 is the overall rate constant for the process given by:

$$k_1[C111] = \frac{k_2K}{[OH^-]}[C111] \tag{42}$$

at a pH value of 9, where only Cll1 and the externally monoprotonated complex are present:

$$k_1 = \frac{(2.3 \times 10^{-4})(10^{-7.1})}{(10^{-5})} = 1.8 \times 10^{-6}$$
 (43)

This value of k_1 is very similar to that calculated by the other method.

 \mathbf{k}_{-1} is too slow to be observed, but upper limits can be estimated from:

$$clll \cdot 2H^+, i-i + OH^- \xrightarrow{k_{-2}} clll \cdot H^+, i + H_2O$$

 k_{-2} equals 4.3×10^{-5} at 372 K for 1 M KOH, which may be extrapolated to 299 K using $E_a = 24.8$ kcal mol⁻¹ to give $k_{-2} = 1.4 \times 10^{-8}$. The formation of the free ligand must be slower than 5% of this rate or else it would be detected, so k_{-1} may be estimated at less than 5% (k_{-2}) , giving $k_{-1} \le 7.0 \times 10^{-10}$. Therefore:

$$K_b = \frac{k_1}{k_{-1}} \ge \frac{4.3 \times 10^{-6}}{7.0 \times 10^{-10}} \ge 6.1 \times 10^{-3}$$
 (44)

pK_b \leq -3.8 and pK_a \geq 17.8. For reaction (43) as written above, $\Delta G^{\circ} \leq$ -5. kcal mol⁻¹ which indicates that because of encapsulation, the first internal protonation is

thermodynamically stable as opposed to possessing only kinetic stability; that is, Clll is a very good base thermodynamically but a poor one kinetically. For the second internal protonation,

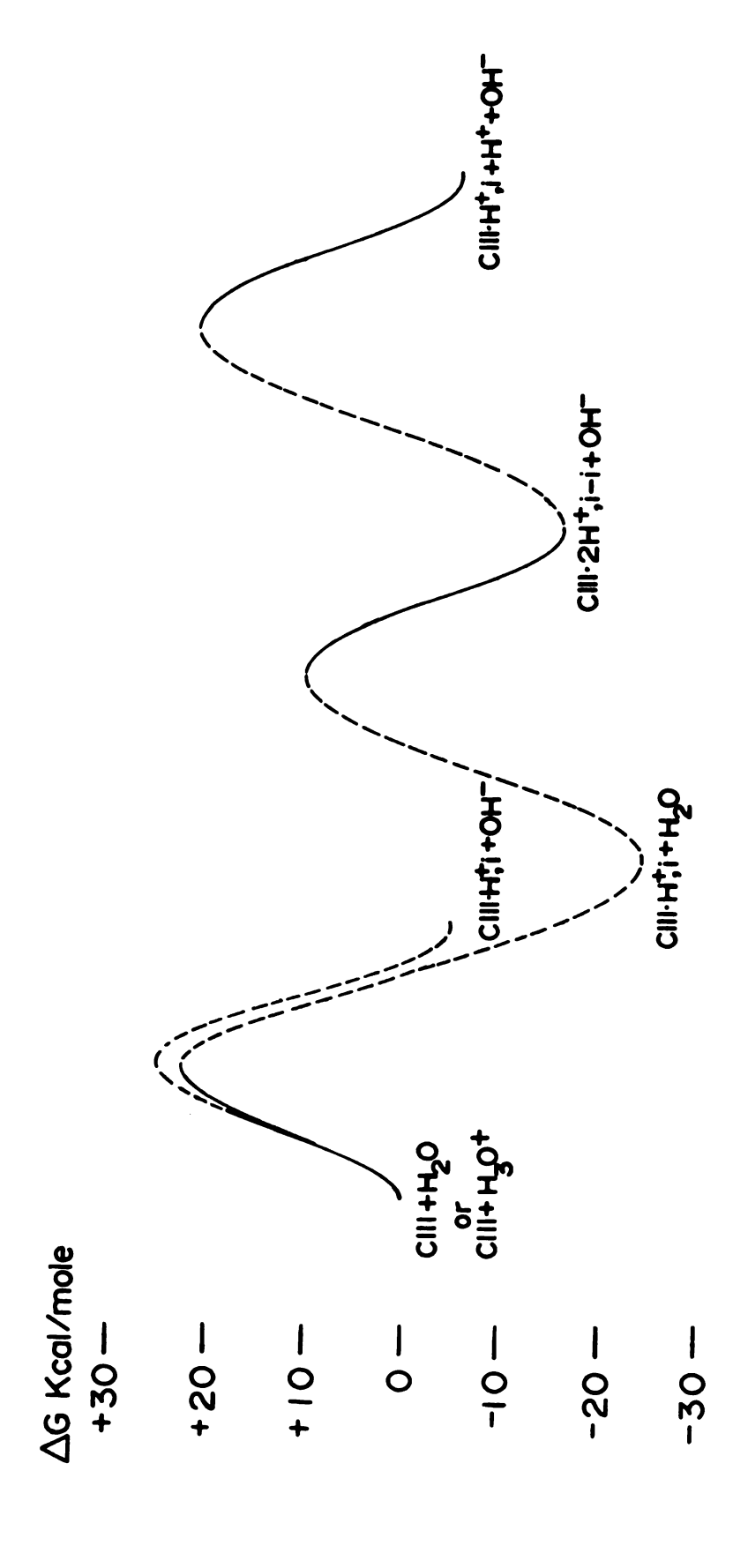
$$\text{C111} \cdot \text{H}^+, \text{i} + \text{H}_2\text{O} \xrightarrow{\frac{k_2}{k_{-2}}} \text{C111} \cdot 2\text{H}^+, \text{i-i} + \text{OH}^-$$
 (45)

 $k_2 = 3.1 \times 10^{-7}$ at 300 K and [H⁺] = 1 M. Assuming a first order dependence on [H⁺], the rate may be extrapolated to pH = 7, giving $k_2 = 3.1 \times 10^{-14}$. $k_{-2} = 1.4 \times 10^{-8}$ at 300 K, and [OH⁻] = 1 M as before. Therefore:

$$K_{b_2} = \frac{k_2}{k_{-2}} = \frac{3.1 \times 10^{-14}}{1.4 \times 10^{-8}} = 2.2 \times 10^{-6}$$
 (46)

 $pK_{b_2} = 5.7$, $pK_{a_2} = 8.3$, and $\Delta G^{\circ} = +8.0$ kcal mol⁻¹. The stability of the second internal protonation is similar to that of Dabco, thus not as thermodynamically favored as the first. Its apparent stability, as indicated by the slow rates of proton transfer from the cavity, does not originate from a thermodynamic source. Rather, the slow proton transfer processes are due solely to the large activation barrier which must be surmounted in order for the proton to escape from the cavity.

A fairly complete potential energy diagram may be constructed from the kinetic and thermodynamic parameters which have been accumulated. This diagram, presented in Figure 49, utilizes free energies for consistency, since the ΔH values of some processes are not known. The



The potential energy diagram for the internal protonation processes. Figure 49.

direction of the plot, indicated by a solid line, has been determined experimentally, whereas the dashed line merely joins the transition state with the products, and has not been measured experimentally. The diagram may be somewhat misleading because the pathway between reactants and transition state is represented by a smooth curve, and is probably in error. The route more likely goes via a series of intermediates, but the one(s) of highest energy determines the rate of the reaction. The shape of the dashed line profile is also not known. It has been assumed that the reverse reaction follows the same profile as that of forward reaction in order to join the reactants and products.

The value of ΔG^{\dagger} has no physical interpretation since it is the difference of ΔH^{\dagger} and $T\Delta S^{\dagger}$ which do possess a physical interpretation. Rather, the value of ΔG^{\dagger} is only a measure of the reaction rate at a given temperature. Therefore, the difference in the values of ΔG^{\dagger} for the first internal protonation of Clll by acid and by water merely reflects the pH dependence of the rates and does not suggest a different reaction profile for the two processes. The mechanism for this protonation has not been established but a definate pH dependence for the rate of internal protonation has been observed.

VII) THE REACTION OF Clll. H, 1 WITH Na C222 Na

The reaction between the internally monoprotonated Clll (with a hydroxide counter-ion) and Na⁺C222•Na⁻ was

studied by mixing approximately stoichiometric amounts (2.x10⁻⁵ moles) of Na⁺C222•Na⁻ and Clll•H⁺,1 in methylamine. The sample was prepared by using the technique described in the Experimental section in a vessel similar to that shown in Figure 8. The vessel had two side-arms, one for the Na metal and one for the cryptand. The solution of Na⁺C222•Na⁻ was prepared first and then was poured over the Clll•H⁺,1. The temperature was held at about 0°C. As the Clll•H⁺,1 dissolved, the solution went from deep blue to clear, an evidence of decomposition. An NMR spectrum of the products of the reaction revealed complete decomposition, except for some starting material which did not dissolve. No free Clll was obtained.

VIII) THE REACTION BETWEEN Clll-2H+,1-1 AND ES

The reaction between ${\rm Clll \cdot 2H}^+, i-i$ and $\bar{\rm e}_{\rm S}$ was studied by the addition of Na metal in liquid NH₃ to a solution of ${\rm a3.x10}^{-5}$ moles of ${\rm Clll \cdot 2H}^+, i-i$ in liquid NH₃. The sample was prepared in a vessel equipped with an EPR tube. The solution of Na⁺ and $\bar{\rm e}_{\rm S}$ in liquid NH₃ was prepared first (an excess of about 3 to 1 metal was present) and the entire vessel cooled in a dry ice, isopropanol bath. The dark blue solution was then poured over the ligand upon which considerable effervescence was observed. The dark blue sample was quickly transferred into a 3mm EPR cell, frozen in liquid nitrogen and its EPR spectrum taken. Only the signal of precipitated sodium metal with a linewidth of about

20 gauss was observed. The sample was transferred back and forth over the undissolved ligand (probably decomposed), frozen and analysed several more times in like manner.

Again, only the precipitated sodium metal line was observed.

The NMR spectrum of the chloroform soluble portion of the resulting sample showed mostly decomposition, but some free Clll (\approx 10%) was present. The reaction between \bar{e}_S and the internally diprotonated ligand must have occurred very rapidly and the effervescence observed upon mixing was probably hydrogen gas being evolved. A rapid EPR mixing cell would be valuable for this experiment since electron transfer into the cavity of the ligand appears to be facile and very rapid.

The speed of these deprotonation reactions indicates that a very different mechanism is operative than in the case of proton abstraction by base. The reaction products substantiate this belief since the free amine cannot be prepared from either of the internally protonated complexes by base in water. Therefore, the deprotonation probably proceeds via the production of a hydrogen atom inside the cavity of the ligand, which in the case of the diprotonated complex, may unite with the other proton to form ${\rm H_2}^+$. The transfer of a second electron produces molecular hydrogen and the free ligand is generated. In the case of ${\rm Clll} \cdot {\rm H}^+$, i, the H $^{\circ}$ has nothing to react with except the ligand, which is therefore completely destroyed. In either case, H $^{\circ}$ is a very reactive species and causes considerable decomposition.

These experiments verify the findings of Lehn and Cheney who conducted very similar reactions (27).

CHAPTER 5

DISCUSSION

Cryptand lll has been shown to be unique in its ability to bind protons. It irreversibly binds protons by encapsulating them and isolating them from solution. The pKa for the first internal protonation is greater than 18, which illustrates the tremendous thermodynamic stability for a proton inside the cavity of Clll. The complex derives most of its stability, however, from a kinetic source, because the activation barrier to internal protonation-deprotonation processes is at least 25 to 28 kcal mol. The activation barrier results from the difficulty in opening the face of the ligand so as to expose its cavity to the proton-donor. Thus, internal protonation proceeds slowly, with a half-life at 26°C of roughly 800 sec at a pH of 1. However, the half-life for deprotonation in 5 M KOH at 26°C is greater than six years.

The internally monoprotonated complex, as mentioned, gains the bulk of its stability from two sources. First, the interaction of the donor atoms of the cavity of Clll with the H_i provide stability of a thermodynamic nature. Second, as the proton approaches the cryptand from a protondonor in solution, it interacts with the nitrogen and oxygen atoms, thus accumulating electron density. Therefore its size increases as the interaction becomes stronger and the proton becomes sterically restricted from entering the cavity of the cryptand. Once inside, the proton attracts almost an entire electron from the donor atoms, and its size increases to about an Angstrom. This large increase in size

makes proton abstraction nearly impossible, because the ligand is physically unable to distort itself enough to allow the proton to exit. Proton acceptors are also sterically restricted from approaching the encapsulated proton. Therefore, it is likely that physical encapsulation provides the majority of the kinetic stability for internal complexation.

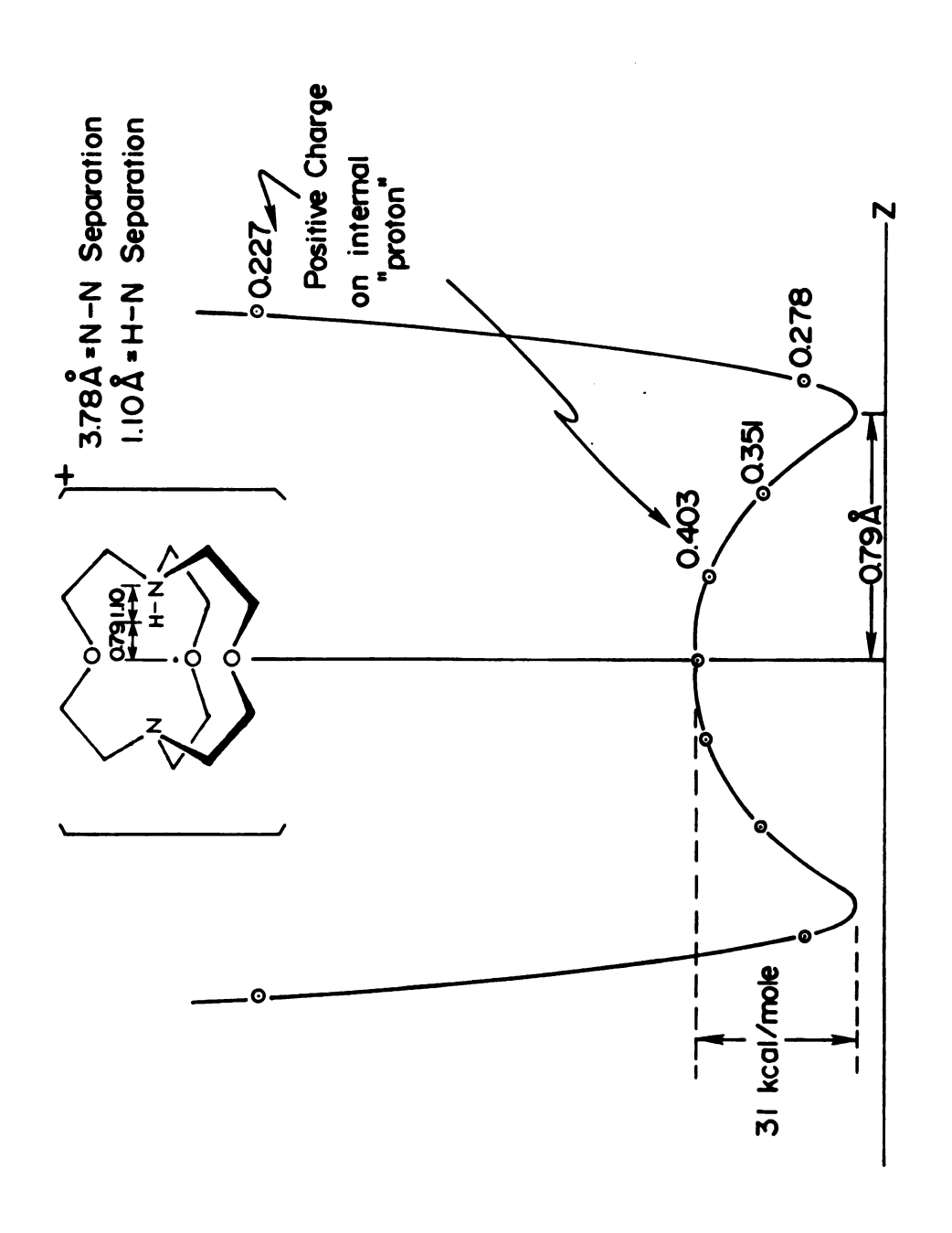
Quantum calculations have been utilized to gain insight into these characteristics of proton binding by Clll. Clll is an excellent candidate for a theoretical analysis because it possesses properties which are similar to the larger cryptands, thus making the study of ion binding by this class of ligands possible. It is also a relatively small molecule whose topology and conformations are well characterized. Clll is a huge molecule for INDO and especially ab initio calculations, but it fortunately possesses only atoms whose atomic wave functions are relatively well known.

The calculations are based on the linear combination of atomic orbitals (LCAO) technique to construct the basis set. The energies of the ensuing molecular orbitals are determined by the self-consistent molecular orbital theory using some semiempiracal approximations which decrease the number of matrix elements to be evaluated. The INDO (84) (intermediate neglect of differential overlap) method has been utilized for these calculations. This technique ignores interactions except between neighboring atoms and those two

bonds away. Clll possesses 93 atomic orbitals which are important to the calculation (only valence electrons are considered). The large number of matrix elements to be evaluated would render the calculation nearly impossible if these approximations were not made but in doing so, the accuracy of the energy values of the molecular orbitals is sacrificed. The INDO calculations are most valuable as models to guide our intuition and are only to be interpreted in light of experimental results.

The calculations reveal that the inclusive proton's lowest energy position along the C_3 axis is about 1.1A from the nitrogen (Figure 50). The charge on the proton is given beside each point. (Typical N-H bond distances are about 1A.) The barrier to proton jump from one nitrogen to the other, along the C_3 axis is indicated to be 31 kcal mol^{-1} , but a known weakness of the INDO calculations is that it gives energy values which are much too large. The barrier may also be much lower if the proton leaves the C_3 axis, because the oxygens may also participate.

The sites of lowest energy seem to be nearest to the nitrogens and the INDO calculation shows that the proton in this position has accumulated 0.7 electrons. Therefore, its size is between 0.6 and 1Å, which is very large for the cavity. Its large size not only makes it impossible to remove the proton from Clll, but it may also restrict participation of the $\rm H_1$ with the oxygens. The topology of the inside of the cryptand is such that there are two large



The dependence of the total energy of the complex on the location of the H proton along the C $_3$ axis for Clll*H $^+$,1 in D $_3\mathrm{h}$ symmetry. Figure 50.

chambers between the nitrogens and oxygens, which are large enough to contain this ion. The cavity is restricted at its center by the oxygens, and in order for the proton to exchange between the nitrogens, it must squeeze through this orifice at the center. The resulting steric barrier may explain why the H_i does not interact appreciably with the ether oxygens inside the cavity.

If the energy barrier to proton exchange is substantial due to steric restriction by the ether oxygens, the exchange would be expected to be easily slowed to the NMR time-scale at low temperatures. Since this does not occur, a tunnelling mechanism is suggested for proton exchange. The expected tunnelling frequency may be calculated using the mass of the proton, a barrier height of about 30 kcal mol⁻¹ and a proton jump distance of 1.58Å (3.0au). This frequency, which is typically 10⁻⁸ seconds or less for symmetric potentials, is much faster than the NMR time-scale and is theoretically independent of temperature (86). If the cavity were smaller due to the concerted twist about the nitrogens, the tunnelling rate would be expected to be even faster.

The fact that Clll is small and rigid, and has a well defined cavity topology makes it a favorable model for testing several NMR theories. Its ability to shield solvent from its internally complexed protons magnifies this utility. Musher's theory (30), for example, was shown to predict shifts which were in the right direction and relative

magnitude although they were too large. However, if the correct charge density on the nitrogen is utilized for the calculation, 0.7 (as obtained in the INDO calculations), rather than 1.0, the values are much closer to the observed shifts, -2.5 ppm for the CH_2N protons, -0.9 ppm for the CH_2O protons, and +1.6 ppm for the H_1 . The observed shifts are -1.4, -0.6, and +1.4 ppm respectively. The two former moieties are greatly influenced by solvation, whereas the H_1 is not. Therefore it is interesting that the H_1 shift is much closer to the predicted value.

The theory of nuclear coupling via the Fermi contact interaction is supported by the behavior of the Clll complexes as is that of scalar relaxation between the H₁ and the nitrogens. Both the increase in magnitude of the scalar coupling between the complexes, Clll·H⁺,i and Clll·2H⁺,i-i, and its temperature dependence are in close agreement with theory.

Clll answers several questions concerning metal ion binding by the larger cryptands. The conformational analysis of Clll indicates that the free diamine exists substantially in the endo-endo configuration, but has the flexibility of nitrogen inversion. Even when binding a proton, it may still invert a nitrogen lone pair to the exo configuration, although this process occurs quite infrequently. The larger cryptands are much more flexible than Clll and would therefore be expected to more easily undergo exoendo nitrogen inversion, even when complexed to a metal

cation. The acid catalyzed removal of metal cations complexes by the cryptands, observed by Cox and Schneider (25), probably does proceed by the mechanism which they suggest. Inference from the Clll binding conformations supports their belief that the exo conformation of the nitrogen should be fairly substantial and available for proton binding.

The binding characteristics of Clll also support the findings of Pizer, et. al. (47-48), who attributed the slow rates of complex formation and dissociation of the cryptands to a steric phenomenon arising from the rigidity of the ligand. However, they also attributed part of the slowness to a very low percentage of the "reactive" endo-endo conformation. The preference for this conformation with Clll and the ease of nitrogen inversion (when unprotonated), suggest that this latter argument is not valid.

Future Projects

The most significant experiment left unfinished is the preparation and identification of H_2^+ inside the cavity of Clll by adding \bar{e}_S to Clll·2H⁺,i-i in liquid NH₃. This reaction was attempted once and although H_2^+ may have been formed, the solution decomposed too rapidly to obtain its EPR spectrum. A different experimental design is necessary to accomplish this goal.

The quantum calculations dealing with proton binding by Clll will also be very useful in identifying the most favorable conformation of the ligand, both when bound to a proton and when free. This theoretical analysis may also help to determine the energy barrier to proton exchange inside the cavity of the ligand, the most favorable entrance for a proton into the cavity from solution and many other important questions.

The binding characteristics of Clll and Clll·H⁺,i with other ions would also be interesting. For example, are both protons and Be⁺² or Mg⁺² ions able to coexist inside the cavity of Clll. If not, do any metal cations bind either internally or externally to the internally monoprotonated complex? The kinetics of decomplexation of Li⁺ or Mg⁺² ions from Clll by protons may also prove interesting, since the kinetics of external protonation of Clll are now known. This would help to answer the question of whether acid catalyzed decomplexation of metal ions by other cryptands occurs by external or internal protonation at the nitrogen. Finally, the crystal structures of the protonated complexes of Clll would be of interest, especially Clll·H⁺,i, Clll·H⁺,o and Clll·2H⁺,i-o.

PART II

AN NMR STUDY OF ALKALI METAL ANIONS IN SOLUTION

I) INTRODUCTION

The properties of solutions of alkali metals in liquid ammonia (NH₂) have intrigued investigators for well over one hundred years since the discovery of Weyl in $1863^{(74)}$ that sodium and potassium metals could be dissolved in liquid ammonia to give deep blue colored solutions. solubility of alkali metals was later shown to be as high as 15 to 20 mole per cent in some cases, the resulting blue to bronze solutions being stable for days at room tempera-Electronic and EPR spectra and electrical conductance studies (75,78) indicate that the solutions contain a variety of chemical species, those of major importance being the metal cation (M⁺), the solvated electron (\bar{e}_S) and the neutral ion pair, $M^+ \cdot \overline{e}_S$ or "monomer". Other more exotic species such as e_2^{2-} , alkali metal anions (M⁻) and higher order ionic aggregates have also been postulated to be present⁽⁷⁸⁾.

The study of alkali metal solutions has been limited almost entirely to liquid ammonia, since the alkali metals are quite insoluble and highly reactive toward most solvents. Exceptions to this rule include hexamethylphosphoric triamide (HMPA), ethylenediamine (EDA), and methylamine (MA), which dissolve at least some of the alkali metals to concentrations higher than 0.01 M. In most solvents,

however, the alkali metals are quite insoluble or only slightly soluble without decomposition. The chemistry of solutions of the alkali metals in amines and ethers is superficially similar to that in ammonia, since deep blue, highly reducing solutions result (75,78). The major differences between metal ammonia and metal amine solutions are solubility and stability toward decomposition, both of which decrease in the amines, and the appearance of metal dependent bands in the electronic spectra of the metal amine solutions. Metal ammonia solutions show only one broad electronic band, regardless of the alkali metal, assigned to \bar{e}_S and aggregates containing this species. The electronic spectra of metal amine and ether solutions are characterized by a band whose frequency maximum is greatly dependent on the metal as shown in Figure 51. These bands have been assigned to the alkali metal anions.

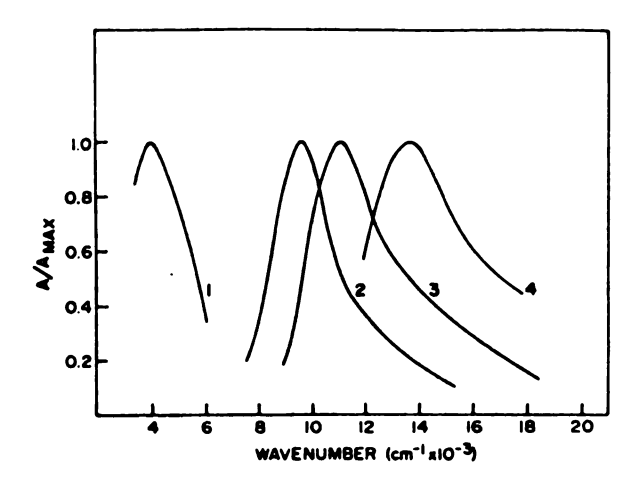


Figure 51. The electronic spectra of the alkali metals in tetrahydrofuran (THF).

Electron paramagnetic resonance spectra of metal ammonia solutions in fairly dilute solutions ($<10^{-1}$ M) show only the \bar{e}_S line with a g-value near that of the free electron. Metal amine solutions often show this line and an overlapping multiplet attributed to the solvated monomer. Thus, the solvent plays a major role in the character of species produced in solutions containing the alkali metals.

The solubility of a particular metal is also greatly influenced by the properties of the solvent. Solubility seems to correlate well with solvent dielectric constant, which decreases in the progression NH₃, HMPA, MA, EDA, ethylamine (EA), isopropylamine (IPA), tetrahydrofuran (THF), and dimethylether (DME). For example, the solubility of sodium in NH₃ is about 15 mole per cent (\approx 5 M), but in THF it is less than 10^{-6} M.

Solvent polarity may also be related to the following equilibrium:

$$M^{-} \xrightarrow{k_{1}} M^{+} + 2\overline{e}_{S}$$
 (47)

The more polar solvents favor the formation of \overline{e}_S , whereas those which are less polar tend to shift the equilibrium to \overline{M} . The character of the metal itself also influences the ratio of metal anion to \overline{e}_S in solution. For example, sodium has a strong preference to form the anion even in MA, but potassium seems to favor the formation of the metal cation and \overline{e}_S . k_1 is so large for lithium, that Li has not yet

been observed in solution. In order of increasing k_1 , the progression seems to follow Na, Cs, Rb, K, Li.

The advent of crown ethers and cryptands has greatly extended the number of solvents in which alkali metal solutions may be studied (76). They provide a great increase in the solubility of the alkali metals for the previously mentioned solvents, as well as for many other nonpolar solvents such as benzene and toluene (77). Cryptands, in particular, fulfill another role in alkali metal solutions. They tend to isolate the cation from the anion, and thereby increase the stability of the anionic species by preventing recombination to form metal. The exchange rates from these ligands are slow, on the order of milliseconds and greater. The cations are therefore encapsulated and insulated from the alkali metal anion by the backbone of the ligand. This can lead to either thermodynamic or kinetic stabilization of M (or both).

The cavity dimensions of the ligand may also be important in determining the products of metal amine reactions and their stability. Since cryptands discriminate between ions by orders of magnitude in their binding constants, the products of mixed metal reactions may be perturbed by the proper choice of cryptand. For example, the reaction with excess metal produces one product via the following scheme:

$$2Na_{(S)} + C222 \xrightarrow{EA} Na^{+}C222 \cdot Na^{-}$$
 (48)

whereas:

$$NaK_{(S)} + C222 \xrightarrow{EA} K^{+}C222 \cdot Na^{-}$$
 (49)

produces a different product⁽²³⁾. The replacement of the Na⁺ by K⁺ in the ligand occurs because C222 binds K⁺ more strongly than Na⁺ by a factor of about 100 in water and presumably also in ethylamine.

The ligand may also influence the products in a different way, namely by stoichiometry. If an equivalent amount of metal and ligand are introduced, the principal anionic species will be \bar{e}_S , whereas if a twofold or greater excess metal is utilized, the reaction will tend further toward the production of M^- .

For a more detailed discussion of the properties of these solutions, the reader is referred to the Ph.D. dissertation of J. M. Ceraso and the references listed in this chapter.

The most definitive methods for characterizing alkali metal solutions in amines and ethers include EPR, NMR, optical spectra, X-ray crystallography (if crystals can be obtained), and magnetic susceptibility. All the alkali metal anions, with the exception of lithium and francium, have been produced in solution or in films (23,75), and have been identified by their optical spectra. The optical spectra of the films produced by rapid evaporation of solvent (MA) from solutions of M c222·M or ē give bands which are very similar to those in solution (Figure 51). The absorbance maxima for Na , K , Rb , Cs , and ē occur at 15,400, 11,900, 11,600, 10,500, and 3,000 to 7,000 cm respectively, in the film spectra.

Crystals of Na⁺C222 Na⁻ have been successfully grown and an X-ray structure performed (21,22). The crystal structure indicates that Na⁻ is a large anion, about the size of I⁻, and that Na⁺ is trapped inside the ligand. The structure is essentially a hexagonal closest-packed type with a closest (Na⁺) to (Na⁻) distance of 7.06Å and (Na⁻) to (Na⁻) distance of 8.83Å. The films and crystals of Na⁺C222·Na⁻ are diamagnetic, whereas those of K⁺C222·ē produced by evaporation of MA from a solution of K⁺C222 + ē are strongly paramagnetic (76).

Perhaps the strongest evidence that the alkali metal anions are indeed anions with electrons in the outer sorbitals, rather than contact ion pairs between the cation and electrons, comes from the NMR spectra of these species in solution (20). The spectra present very narrow lines for the anions (except for potassium which has not been observed), which are diamagnetically shifted very near to the position of the gaseous neutral atom. This observation demands that the solvent be excluded from contact with inner p-electrons by filled outer s-orbitals. The extreme narrowness of the lines also indicates a very symmetrical electron distribution, since the relaxation of alkali metals is governed by quadrupolar effects. Quadrupolar relaxation is very sensitive to the symmetry of the electronic environment of the nucleus, thus the NMR spectra of the alkali metal anions provide strong evidence that they are indeed anions, with a symmetrical electron distribution, rather

than contact ion pairs between the cation and electrons which would produce large anisotropies in the electronic distribution.

This chapter is devoted to the characterization of alkali metal amine and ether solutions with special emphasis on the relative thermodynamic stability of the alkali anions and the preparation of new structures. which will be presented have been obtained from alkali metal NMR spectra using the DA-60 spectrometer described in the Experimental section. The NMR spectra provide a definitive method by which to characterize the species in these solutions. Table 21 gives the chemical shifts of several alkali metal cations and anions in solution, with each chemical shift value referenced to the free metal atom in the gas phase (79). Of particular interest is the fact that the CsC222 chemical shift may vary from -590 ppm to -400 ppm depending on the temperature and solvent (55). This phenomenon has been ascribed to a rapid exchange between inclusive and exclusive complexes (as described in the Introduction to Chapter 3), the shift of the inclusive complex being -590 ppm, and that of the exclusive crown-type complex being about -400 ppm.

The samples have been synthesized by the procedure described in the Experimental section, except that metal alloys have been utilized sometimes rather than single metal films. Common characteristics of all samples are their blue to black colors, an evidence of the presence of M and $\bar{\bf e}_S$ in

0.02 8.0 9.0 17.9 23.0 30.8 120-170 2H 91. 158 1300 4000 220 selected list of chemical shifts and linewidths in alkali metal NMR. σ(M_{solv} vs. M_g) (calcd) Solvent H20 CH30 CH30H EA THF THF THF Temp, 0.3 NaI 0.25 NaI 0.15 Na to Sat NaCl Conc., 0.1 0.1 0.08 0.05 ∞dil ∞dil ∞d11 ¥ 21 Table Ion

solution, and considerable bronze to gold colored films upon solvent evaporation. M^- and \bar{e}_S absorb in the red, therefore their solutions appear blue. Films of these species are gold and metallic-looking because they absorb strongly in the near-infrared and have a sharp cut-off in the visible, similar to the absorption spectra of metals.

II) THERMODYNAMIC STABILITY OF THE ALKALI METAL ANIONS

The measurement of the relative thermodynamic stability of the alkali metal anions involves several complex factors. It is very difficult to determine whether the products of these reactions are the most thermodynamically stable, or whether they possess kinetic stability, e.g., the kinetics of the reaction may favor one product which is much less thermodynamically stable than another. The lattice energy of the metal, alloying effects, the formation constant of the cation and ligand, the desire of the anion to dissociate to cation and electrons, etc., may each influence the thermodynamic stability of the anion in solution.

The measurement of the relative thermodynamic stability of the alkali anions has been attempted in spite of the many pitfalls, by using mixed metal alloys. The metals were always in at least a twofold excess to C222. The products of these reactions are given in Table 22. Tetrahydrofuran has been utilized because it tends not to support $\bar{\mathbf{e}}_{S}$, and yet provides good solubility for the alkali metals in the presence of C222.

Table 22. The products of some alkali metal solution preparations.

Sample	Conc.	Identification by NMR
NaK alloy (xS) C222 in EtNH ₂	≃0.05 M	Na at 2 ppm no NaC
NaK alloy (xS) C222 in EtNH ₂	≃0.07 M	Na at 2 ppm no NaC
NaK alloy (xS) C222 in THF	≃0.07 M	Na at 4 ppm no NaC
NaK alloy (xS) C222 in MeNH ₂	≃0.05 M	KC222 ⁺ at -7 ppm no K ⁻ , very broad
K metal (xS) C222 in THF	≃0.04 M	nothing observed
K, C222 in THF	≃0.12 M	K ⁺ C222 at ≃-20 ppm very broad, no K ⁻
Cs, C222 in EtNH ₂	0.05 M	CsC ⁺ at ≃-433 ppm no Cs ⁻
Cs, C222 in MeNH ₂	0.06 M	CsC ⁺ at -598 ppm, temp. dep. no Cs ⁻ , decomp. at -430
Cs, C222 in THF	0.08 M	CsC^{+} at -584 and Cs^{-} at -43 ppm
NaCs alloy C222 in EtNH ₂	0.06 M	CsC at -418 ppm, no Cs or Na
NaCs alloy C222 in THF		alloying effect to be discussed later
KCs alloy C222 in THF	0.06 M	Cs at -47 ppm, no CsC222
CsRb alloy C222 in THF	0.06 M	Cs at -46 ppm, no CsC222
RbNa alloy C222 in THF	0.05 M	Na at ~3 ppm, no NaC222
Na metal 15-C-5, MeNH ₂		decomp., nothing observed
Na 18-C-6 THF		very slow dissolution

Table 22 (cont'd.)

Sample	Conc.	Identification by NMR
Na 18-C-6 MeNH ₂		NaC ⁺ at -70 ppm, Na ⁻ at +1 ppm EPR gives temp. dep. elec- tron signal; g = 2.0024, linewidth = 0.2 gauss
Na 18-C-6 EtNH ₂		dissolution or solubility problems; powder (metal + crown) observed
Na C221 EtNH ₂		very slow dissolution, Na at 3 ppm, no NaC +
Na C221 THF		very slow dissolution, nothing observed
NaCs C221 THF		Na at 2 ppm, CsC at -564 ppm; Cs at -43 ppm. Very slow dissolution of Nametal.
Cs in EA		nothing in NMR
Cs in THF		nothing in NMR
Cs 18-C-6 in THF	0.11 M ?	CsC ⁺ at -322 ppm very broad at -100, disap- pears at higher temps.
Na C222 +• Na solid		Na metal observed
Na metal film, Disti	lled over :	metalgave a blue solid.
Cs ⁺ C322•Cs ⁻ in THF		Cs ⁺ C322 at -439 ppm, Cs ⁻ at -50

An equimolar alloy of Na and K metals with C222 in THF gives complete conversion to Na-, but no Na+ is observed in the Na 23 NMR spectrum of this solution. The K 39 NMR spectrum has been taken of the sample in MA, which gives only one broad resonance, at -6.5 ± 0.5 ppm (referenced to sat. KNO $_2$ in H $_2$ O), corresponding to K $^+$ C222. These findings suggest that the major product of the reaction is K $^+$ C222·Na-. Optical spectra of films from solutions prepared in the same manner support this conclusion (23). Rb-Na alloys give a similar product, Rb $^+$ C222·Na-. These two findings are entirely expected, since both K $^+$ and Rb $^+$ have a greater affinity for C222 than does Na+(81). Also, Na- has been shown to be more thermodynamically stable than the other anions, since Na+ is converted to Na- in the presence of K $^-$, Rb $^-$, Cs $^-$, or $\overline{\epsilon}_8$ (79).

The products of Cs-K and Cs-Rb alloys with C222 in THF yield the production of Cs as evidenced by their Cs¹³³ NMR spectra, but the NMR signal of Cs is never observed in these solutions. This fact leads to the conclusion that the major products are K C222 · Cs and Rb C222 · Cs respectively, again in line with expectation. The NMR spectra of K³⁹ and both isotopes of Rb are difficult to obtain due to broad lines and low sensitivity. Thus, the measurement of their relative stability is not possible by this technique.

An unusual dilemma is presented in the solutions from the alloys of Na and Cs, C222 in THF (Table 23). The composition of the alloy tends to have a pronounced effect on

Table 23. The products of the reaction of Na and Cs metals and C222 in THF.

Sample in THF	Products	
NaCs (excess metal)	CsC ⁺ , 20% Cs ⁻ , 80% Na ⁻	
NaCs (excess metal)	CsC ⁺ , 20% Cs ⁻ , 80% Na ⁻	
over Na metal first, then over Cs metal	CsC + Cs , slight Na	
over Cs metal first, then over Na metal	CsC ⁺ •Na ⁻ only	
over Na metal (gold powder), then over Cs metal	CsC ⁺ •Cs ⁻ , slight Na ⁻	
NaC+•Na powder over Cs metal	NaC ⁺ •Na ⁻ , slight Cs ⁺ C	

whether the major anion produced is Cs or Na. This occurs because Cs and Na metals form a nonideal alloy, with the production of the compound, Na2Cs (80). The solution in THF is further complicated by the fact that the dissolution of Na is very slow, although it is enhanced by the presence of Cs. Several attempts have been made to overcome this alloying effect, including the formation of Cs C222 Cs over Cs metal first and then taken over Na metal, and the use of Na C222 Na powder dissolved in THF and taken over Cs metal. The former experiment gives Cs C222 Na and the latter, mostly Na C222 Na, although some Cs C222 is also produced. When these solutions are made up over the alloy, which is in great excess to C222, the products of the process usually are Cs C222 and a mixture of Cs (10-20%) and Na (80-90%). The equilibria which control this process are:

$$2 M_{(S)} \stackrel{K}{=} M^{+} + M^{-}$$
 (50)

$$Cs^{-} + Na^{+} \xrightarrow{K_{2}} Na^{-} + Cs^{+}$$
 (51)

$$M^{+} + C = \frac{K_{3}}{M^{+}C}$$
 (52)

The constant, K_1 , is not known because of the alloying effect and K_2 is the one of interest, since it is determined by the anion's relative stability. It appears that the equilibrium is not shifted too far to the right, but definite conclusions are difficult because of the slow dissolution of Na in THF and by the alloying effect.

Another very unusual consequence of this process is that the equilibrium constant, K₃ (which is also influenced greatly by K₁), tends almost exclusively toward the formation of Cs⁺C222 rather than the Na⁺ complex. This is highly irregular because in water, the formation constant of C222 with Na⁺ is more than 100 times greater than that of Cs⁺(81). This may be entirely a function of the alloying effect or possibly even a kinetic phenomenon. The formation constants of the complexes have not been measured in THF or the amines but that of Na⁺ would still be expected to be much greater than that of Cs⁺. This competitive complexation should be explored in more detail in THF. The trend of thermodynamic stability relative to the solid metals from these NMR data indicate Na⁻Cs⁻>K⁻,Rb⁻.

III) IDENTIFICATION OF NEW SPECIES

Attempts to observe K⁻ by NMR. The potassium anion has never been observed by NMR for two reasons, low sensitivity of the potassium nucleus and considerable affinity to dissociate to and interact with \bar{e}_{S} . Even a slight interaction with electrons in solution tends to broaden the signal out of existence (see Historical section). Four attempts have been made to observe K⁻, three in THF with excess metal at concentrations varying from 0.01 M to 0.1 M. The samples were prepared at or near room temperature. Very dark films were observed, but the NMR spectra showed only the complexed cation at about -20 ppm from saturated KNO₂ in water, the line being 300 to 600 Hz broad, depending on the temperature.

The final attempt to obtain a K signal in the NMR utilized IPA as solvent with ligand concentration at about 0.02 M. The sample was again made up at -10 to 0°C with no apparent decomposition. A black powder precipitate was observed which seemed to be somewhat crystalline (black needles), as previously reported by Dye and co-workers (76). The NMR spectrum showed no peaks, an indication of either low solubility or the presence of solvated electrons which broaden both cation and anion peaks. Otherwise, the concentrations should have been high enough to permit observation of the NMR spectra.

Cs, C222 in EA and MA. When Cs is dissolved in EA or MA in the presence of C222, only the complexed cation is

observed in the NMR spectrum at -418 to -433 ppm (depending on sample conditions and temperature) and -591 ppm respectively. The chemical shifts indicate that the complex in EA is an exclusive complex, whereas that in MA is inclusive. Both solutions are somewhat unstable, and decomposition peaks, presumably corresponding to Cs⁺ complexed by the decomposed ligand, occur at -384 and -414 ppm in EA and MA.

The linewidth of the complexed cation is somewhat peculiar in both solvents, since it broadens as the temperature is raised in MA, while the opposite is observed in EA. Figure 52 shows this temperature dependence in MA. The chemical shift of this species is rather temperature invariant in MA, but in EA the line shifts slightly downfield with decreasing temperature. When the ethylamine solution is frozen, the complexed cation resonance shifts to -580 ± 30 ppm, corresponding to an inclusive complex (Table 24).

Table 24. The temperature dependence of the chemical shift of Cs+C222 in EA.

Temperature (°C)	δppm [†]	Δν _{1/2} *
	-580	≃1000 Hz
- 69	-433	108
- 62	-432	83
- 52	- 428	34
- 38	-427	16

 $^{^{\}dagger}$ ± 4 ppm.

^{*} Full width at half height.

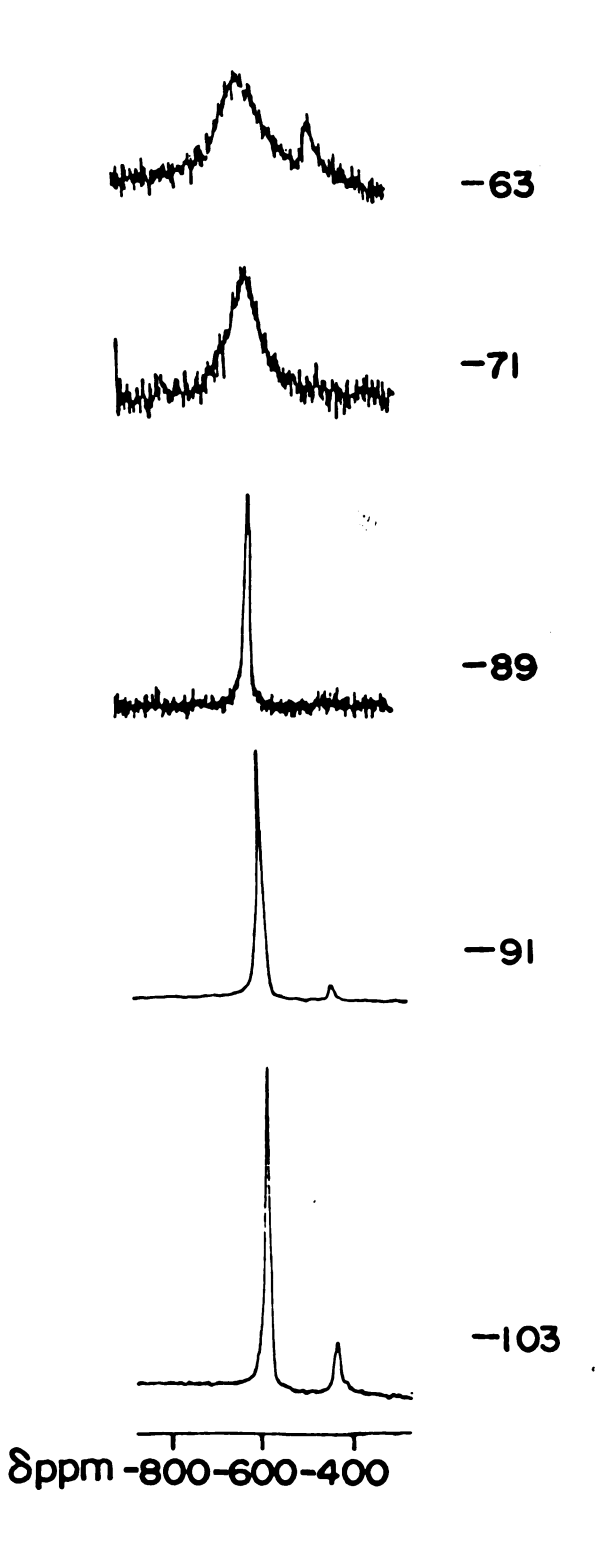


Figure 52. The temperature dependence of the NMR spectrum of Cs+C222.Cs in MA.

The EPR spectrum of a sample prepared in a similar way in EA gives a single, narrow, intense line with g = 2.0024 ± 0.0002 between a temperature range of -32 to -70°C. This spectrum indicates that electrons are present, but that they do not interact to a large extent with the Cs nucleus.

The electronic spectra of films from solutions in MA prepared in a similar way $^{(23)}$, show nearly complete conversion to Cs with only slight presence of $\bar{\mathbf{e}}_{S}$. The concentration of these samples was much lower than those for NMR analysis, however.

All indications suggest that Cs should be observed in the NMR spectrum in MA and EA, but it is possible that exchange between a paramagnetic species in minute concentrations could account for its disappearance. This paramagnetic species could also be the source of the instability of these solutions.

The strange Cs⁺C222 broadening with temperature is probably due to the rapid exchange between inclusive and exclusive complexes, the former being preferred at lower temperatures. In EA the exclusive crown-type complex is favored, whereas in MA the opposite is true. The spectra in EA are especially supportive of this conclusion, because as the temperature is lowered, the Cs⁺C222 line broadens and shifts downfield. When the sample is frozen, the chemical shift of the complexed Cs⁺ is nearly identical to that of the inclusive complex. In methylamine, the equilibrium

seems to highly favor the inclusive complex, but above -90°C the exclusive complex is present in high enough concentration to cause considerable exchange broadening of the Cs⁺C line.

An interesting sidelight to these observations concerns the dissolution of Na metal and C222 in EA which gives Na⁺C222·Na⁻. However, the solution prepared from the alloy of Na and Cs metals in EA with C222 gives a Cs⁺C222 signal at about -418 ppm, but no anion or Na⁺ species is observed. Cs metal is soluble in EA to 10⁻³ or 10⁻⁴ M⁽⁷⁶⁾, and gives rise to solvated Cs monomers. Since these species are paramagnetic, they would cause tremendous broadening and shifting the resonances of those ions with which they exchange or interact strongly. Only minute levels of these species would be necessary to induce the Cs⁻ disappearance, because their chemical shifts are normally tens of thousands of ppm downfield.

Cs and C222 in THF. Samples of Cs metal and C222 in THF seem to be much more stable than in MA and EA. An estimated half-life for decomposition in THF is approximately 12 hours. The NMR spectrum of these samples shows both Cs⁺C222 at -583 to -587 ppm and Cs⁻ at -46 to -41 ppm. The Cs⁻C222 line is about 100 Hz broad at -110°C, and broadens greatly as the temperature is raised (Figure 53). Meanwhile, the Cs⁻ line remains very narrow (<10 Hz), and indicates no exchange broadening, except at -41°C, where slight broadening occurs. These spectra are reproducible upon raising and

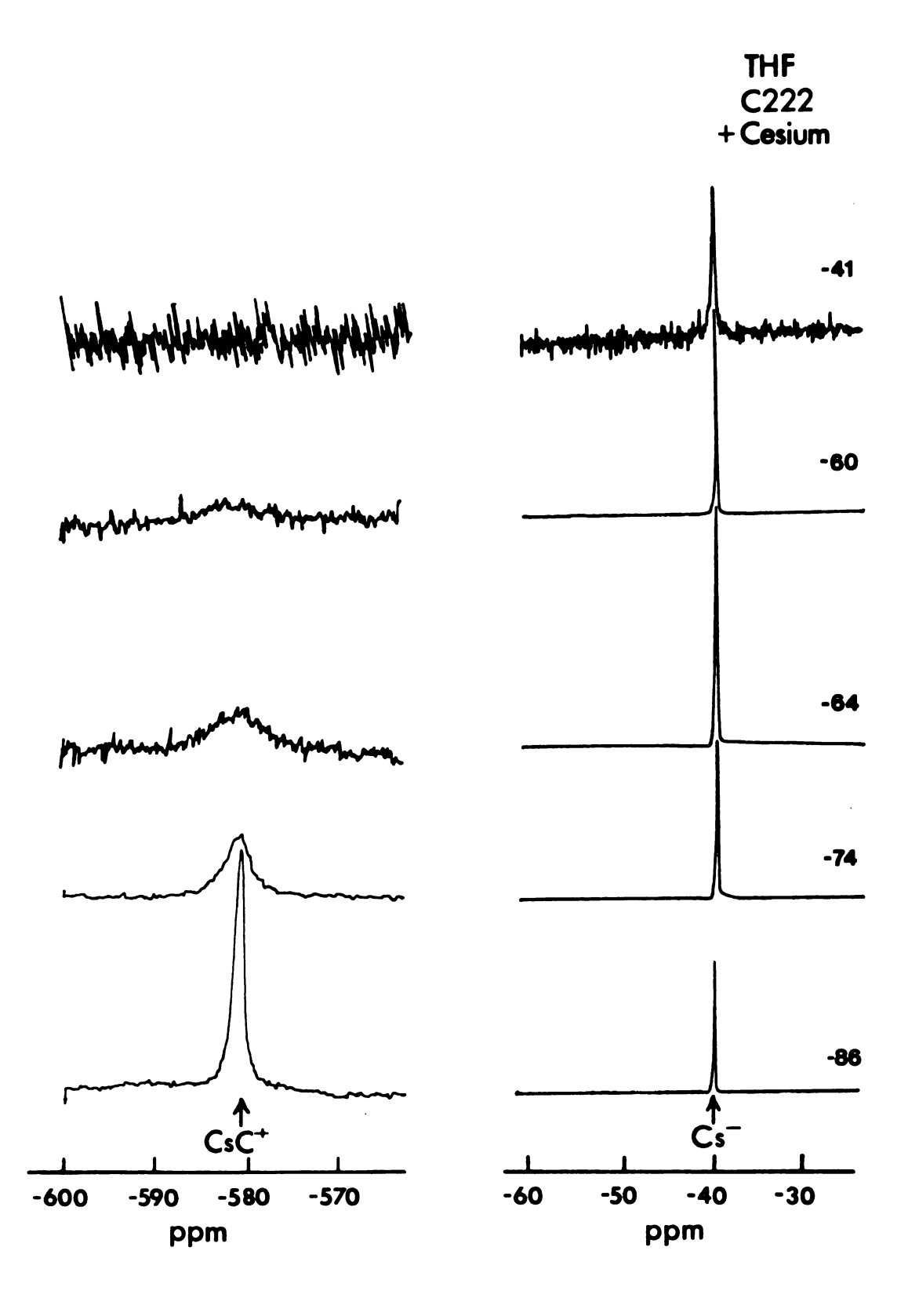


Figure 53. The temperature dependence of the NMR spectrum of Cs⁺C222·Cs⁻ in THF.

lowering the temperature, and are not symptons of decomposition. Above -41°C, however, decomposition occurs rapidly.

This exchange phenomenon is peculiar for two reasons. First, the chemical shift of the complexed Cs⁺ does not change appreciably throughout the temperature range. Secondly, the exchange does not significantly involve the Cs⁻ because it would be expected to broaden by exchange to the same extent as the cation resonance.

The chemical shift of the Cs⁺C222 resonance demonstrates that it is an inclusive complex, and its temperature characteristics are similar to those of its counterpart in MA, which is also an inclusive complex. By inference from the exchange in MA, the line broadening of the Cs⁺C222 resonance in THF might be assigned to the rapid interconversion of inclusive and exclusive complexes with the latter present at lower concentrations which increase with increasing temperature. Above -41°C, the Cs⁺C222 resonance is very broad indicating that the exclusive complex is appreciable. Since this complex allows more efficient interaction between Cs⁺ and Cs⁻, the anion peak also begins to show evidence of the exchange phenomenon.

In order to verify that the exchange process involving the complexed cation was the result of two rapidly interconverting conformations of the ligand, rather than an electron transfer reaction or related process, the temperature characteristics of a simple salt, cesium octanoate, were studied. (Most cesium salts are insoluble in THF, and only cesium

octanoate has been found to be soluble enough for Cs¹³³

NMR analyses.) The chemical shift of the cesium cation in solution of cesium octanoate, C222 in THF comes at -403 to -433 ppm, and indicates no complex formation. This observation further demonstrates that complexation of Cs by C222 in THF is easily perturbed by solvent, temperature, and anion.

Another possible explanation for the exchange broadening of the $\mathrm{Cs}^+\mathrm{C222}$ line would involve its interaction with $\overline{\mathrm{e}}_{\mathrm{S}}$ or cesium monomers, both of which are paramagnetic. Exchanges of this sort would also be expected to involve Cs as in MA and EA, and since this is not observed, interactions of this kind are doubtful.

Na and 18-C-6 in MA. Andrews, Ceraso, and Dye⁽³⁴⁾ described a peculiar two electron exchange process between Na⁺ complexed by 18-crown-6(18-C-6) and Na⁻ in MA. The exchange was followed by line broadening in the NMR, as shown in Figure 54. This process did not seem to originate from a simple two-site exchange, but a more complex reaction was indicated. In order to ascertain whether a paramagnetic species could give rise to a third site, an EPR analysis has been performed. A sample prepared from 0.08 M C222 in MA taken over excess Na metal showed a single narrow line with g = 2.0024. The intensity of the line was very temperature dependent (Table 25), indicating a process:

$$Na \longrightarrow Na^{+} + 2\bar{e}_{S}$$
 or $\bar{e}_{2} \longrightarrow 2\bar{e}$ (53)

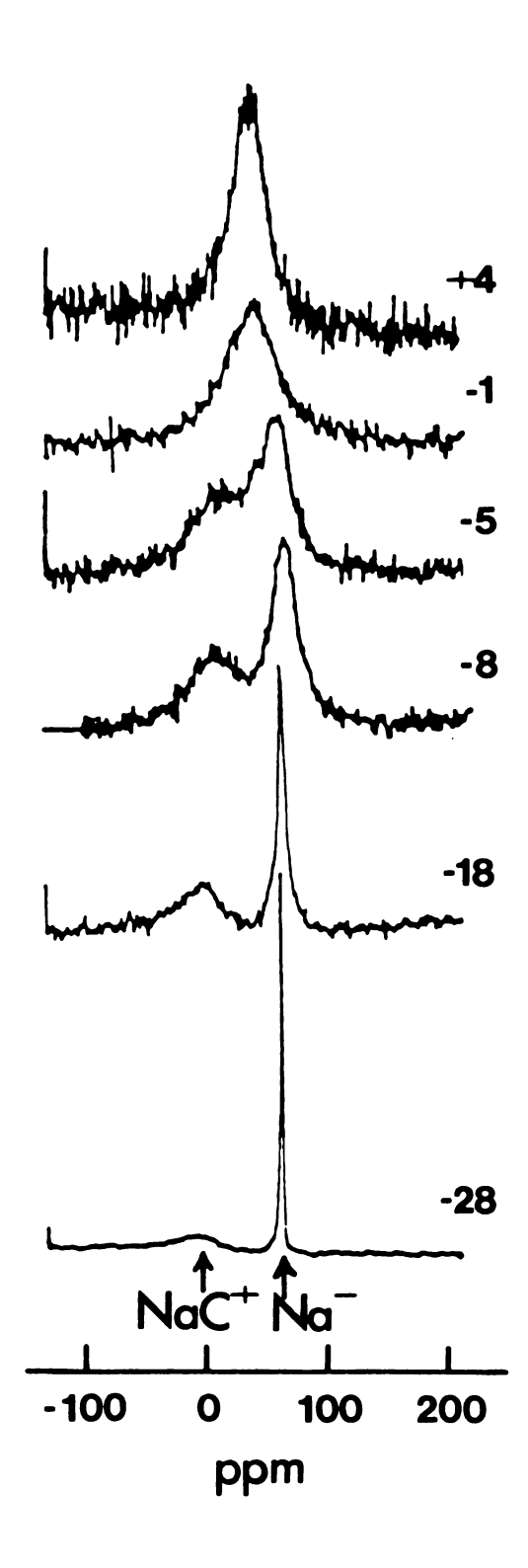


Figure 54. The temperature dependence of the NMR spectrum of Na $^+$ 18-C-6 \cdot Na $^-$ in MA.

Table 25. The temperature dependence of the EPR signal of a 0.08 M solution of Na 18-C-6•Na in MA.

Temp, °K	Intensity	
269	18.1	
259	16.2	
246	10.5	
237	5.1	
227	≤ 0.2	

In either case, the presence of $\overline{\mathbf{e}}_{S}$ could greatly perturb the NMR spectra.

The synthesis of crystals of Cs⁺C222·Cs⁻. Gold colored crystals, very similar in appearance to those of Na⁺C222·Na⁻ were synthesized from a =0.1 M solution of C222 in IPA, taken over excess metal at 0. to -20°C. As the solution was cooled to -78°C, the small crystals precipitated, and seemed to be quite stable if kept at -78°C. The solution phase was less stable, and turned from deep blue to clear upon decomposition, but the crystals remained gold for several days at dry ice temperature. The crystals were never isolated from the solution phase because decomposition occurred too rapidly.

Attempts to grow crystals of other alkali metals and ligands were also made, but without success. They include Cs with 18-C-6 in MA and $K^+C222\cdot\bar{e}$ (1:1 stoichiometry of C222 and metal) from MA, with the addition of DEE. A black

powder precipitated from the latter when the MA was removed and DEE was added.

Complexes With Cryptands Other Than C222. C221 has also been utilized to dissolve Na metal in EA and THF as well as Na-Cs alloy in EA. The rate of dissolution of Na metal by C221 is extremely slow in EA and THF and therefore, the products of these reactions may be greatly dependent on the kinetics of dissolution. The products of the reaction of Na-Cs alloy and C221 in EA are reflective of the slow dissolution of the Na metal since mostly Cs⁺C221 and Cs⁻ are formed. The resonance assigned to the Cs⁺C221 complex at -564 ppm was very broad and may not have been real.

A sample has also been prepared by distilling C221 over a fresh film of Na metal. Upon contact with the metal, the C221 forms a dark blue crust which lasts for weeks at -78°C.

The NMR spectrum of a solution from Cs metal and C322 in THF showed two resonances, one at -439 ppm (1000 Hz broad) and the other at -50 ppm corresponding to Cs⁺C322 and Cs⁻ respectively. The chemical shift of the cation is normal since it is in the range of inclusive complexes of simple salts of Cs⁺ with C322⁽⁸⁵⁾.

APPENDIX

THE THEORY OF CHEMICAL EXCHANGE IN NMR

APPENDIX

The equations which describe the NMR lineshape of a system undergoing chemical exchange of the sort:

$$A + L \stackrel{k_{f}}{\longleftrightarrow} AL \tag{A1}$$

are those of Bloch, modified by McConnell to include chemical exchange. These equations describe the X and Y components of the magnetization in the rotating frame of reference as follows:

$$\frac{dG_{A}}{dt} + \alpha_{A}G_{A} = -i\gamma H_{1}M_{OA} + \tau_{B}^{-1}G_{B} - \tau_{A}^{-1}G_{B}$$
 (A2)

$$\frac{dG_{B}}{dt} + \alpha_{B}G_{B} = -i\gamma H_{1}M_{OB} + \tau_{A}^{-1}G_{A} - \tau_{B}^{-1}G_{B}$$
 (A3)

These equations are solved using the slow passage condition in which:

$$\frac{dG_A}{dt} = \frac{dG_B}{dt} = 0 \tag{A4}$$

thus:

$$-(\alpha_{A} - \tau_{A}^{-1})G_{A} + \tau_{B}^{-1}G_{B} = i\gamma H_{1}M_{OA}$$
 (A5)

$$-(\alpha_{b} - \tau_{b}^{-1})G_{b} + \tau_{a}^{-1}G_{a} = -i\gamma H_{1}M_{ob}$$
 (A6)

The expressions are further simplified by:

$$M_{OA} = p_A M_O \tag{A7}$$

$$M_{OB} = p_B M_O \tag{A8}$$

and by arranging in a matrix form:

$$a_{11}G_A + a_{12}G_B = C_{DA}$$
 (A9)

$$a_{21}G_A + a_{22}G_B = C_{pB}$$
 (A10)

Using Cramer's rule (see any matrix algebra text):

$$G_{A} = \frac{C}{D} \begin{vmatrix} p_{A} & a_{12} \\ p_{B} & a_{22} \end{vmatrix} = \frac{C}{D} [p_{A} a_{22} - p_{B} a_{12}]$$
 (All)

$$G_{B} = \frac{C}{D} \begin{vmatrix} a_{11} & p_{A} \\ a_{21} & p_{B} \end{vmatrix} = \frac{C}{D} [p_{B} a_{11} - p_{A} a_{21}]$$
 (A12)

$$D = \begin{vmatrix} a_{11} & a_{12} \\ a_{21} & a_{22} \end{vmatrix}$$
 (A13)

The total complex moment, G, is the sum of the two:

$$G = G_A + G_B = \frac{C}{D} [p_A(a_{22} - a_{21}) + p_B(a_{11} - a_{12})] (A14)$$

The absorbtion lineshape function is given by the imaginary portion of G, but for lines which are imperfectly phased:

$$g(v) = (real G) sin\theta + (imaginary G) cos\theta$$
 (A15)

where θ is the angle of zero order phase correction.

These equations may be easily expanded to include three or more sites and are equivalent in both P-FT and CW modes (70,71,83) in most cases. They may be used to simulate or fit NMR lineshapes using KINFIT. (The structure of the input deck, subroutine EQN, may be obtained from my first notebook on pages 184 and 185, the entry dated August 25, 1977.)

The mean lifetimes at sites A and B, τ_A and τ_B , are defined in the following way:

the rate of removal of a nucleus from
$$1/\tau_{i} = \frac{\text{site i by exchange}}{\text{the total number of nuclei in site i}}$$
(A16)

and is related to the rate constant of reaction Al in the following way:

$$1/\tau_{A} = k_{f}[A][L] \tag{A17}$$

$$1/\tau_{B} = k_{b}[AL] \tag{A18}$$

 $\tau_{_{A}}$ and $\tau_{_{\mathbf{R}}}$ are not unique, but are coupled by the expression:

$$\tau = \frac{\tau_A \tau_B}{\tau_{A} + \tau_B} \tag{A19}$$

and since:

$$P_{A} = \frac{\tau_{A}}{\tau_{A} + \tau_{B}} \tag{A20}$$

we have:

$$\tau = P_A \tau_B = P_B \tau_A \tag{A21}$$

and only τ is unique.

The temperature dependence of the rate constant, k, may then be utilized to calculate an activation energy for the process, using the Arrhenius equation:

$$k = Ae^{-Ea/RT}$$
 (A22)

 $\Delta H^{\frac{1}{7}}$ is related to the activation energy for reactions in solution by:

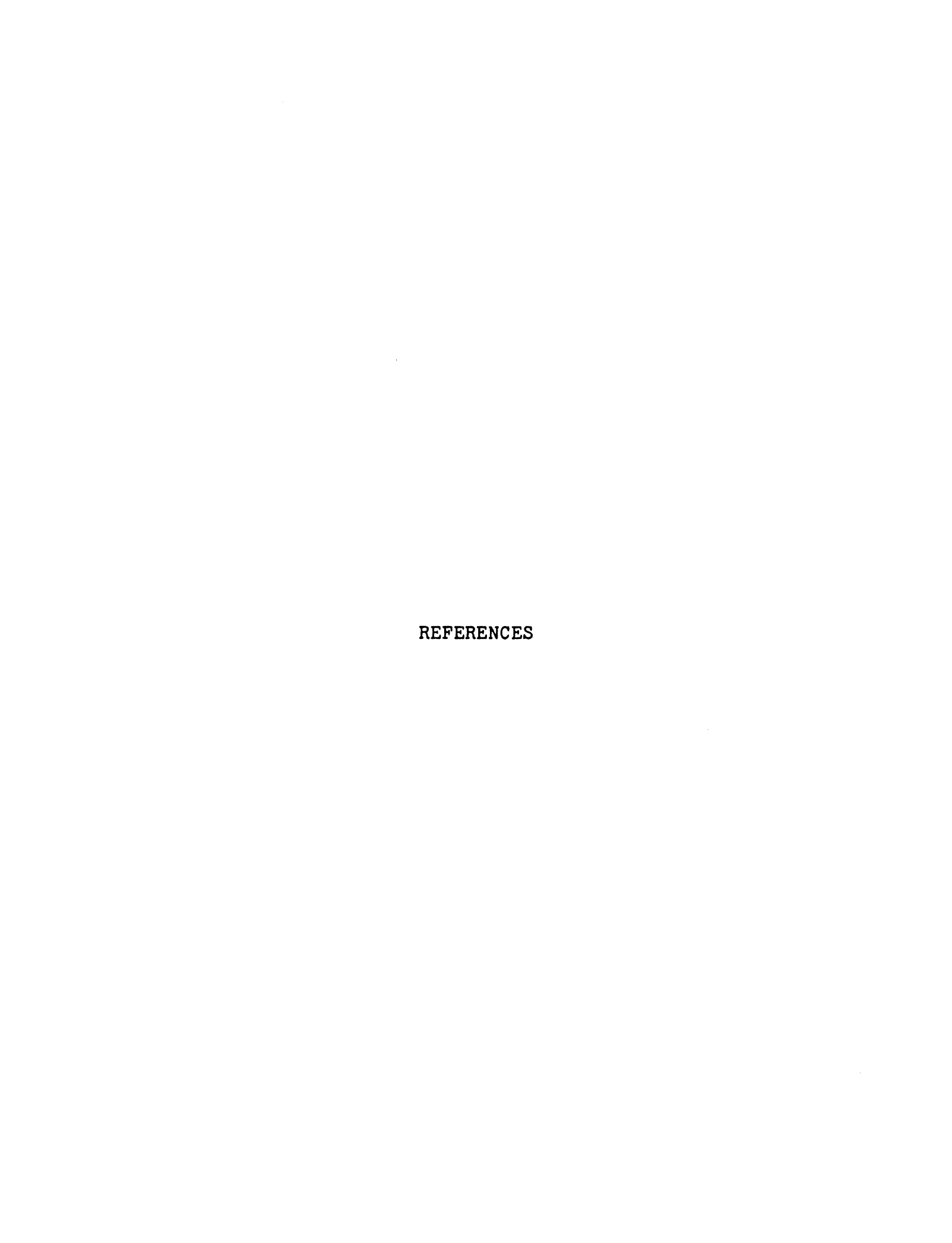
$$\Delta H^{\dagger} = Ea - RT$$
 (A23)

The Eyring equation may be utilized to calculate ΔG^{\dagger} and ΔS^{\dagger} :

$$k = \kappa \left[\frac{kT}{h} \right] e^{-\Delta G^{\frac{1}{4}}/RT}$$
 (A24)

where κ is assumed equal to 1.0, and :

$$\Delta S^{\frac{1}{4}} = \frac{\Delta H^{\frac{1}{4}} - \Delta G^{\frac{1}{4}}}{T}$$
 (A25)



REFERENCES

- 1) D. H. Haynes, B. C. Pressman and A. Kowalski, Biochem-istry, 10, 852 (1971).
- 2) F. A. Cotton and G. Wilkinson, "Advanced Inorganic Chemistry," Interscience Publishers, New York, 1966; R. Winkler, Structure and Bonding, 10, 1 (1972).
- 3) R. M. Izatt, J. D. Lamb, G. E. Maas, R. E. Asay, J. S. Bradshaw and J. J. Christenson, J. Amer. Chem. Soc., 99, 2365 (1977).
- 4) C. J. Pedersen, J. Amer. Chem. Soc., 89, 7017 (1967).
- 5) J. M. Lehn, Acc. Chem. Res., 11, 49 (1978).
- 6) E. V. Dehmlow, Angew. Chem., Int. Ed. Engl., 16, 493 (1977).
- 7) M. Newcomb and D. J. Cram, J. Amer. Chem. Soc., 97, 1251 (1975).
- 8) E. Blasius and P. G. Maurer, Makromol. Chem., 178, 649 (1977).
- 9) E. Blasius, W. Adrian, K. P. Janzen and G. Klautke, J. Chromatog., 96, 89 (1974).
- 10) S. Kopolow, T. E. Hogen Esch and J. Smid, Macromole-cules, 6, 133 (1973).
- 11) W. D. Curtis, D. A. Laidler, J. F. Stoddart and G. H. Jones, J. Chem. Soc. Chem. Comm., 833 (1975).
- 12) D. J. Cram and J. M. Cram, Science, 183, 803 (1974).
- 13) E. V. Kyba, R. C. Hegleson, K. Madan, G. W. Gokel, T. L. Tarkowski, S. S. Moore and D. J. Cram, J. Amer. Chem. Soc., 99, 2564 (1977).
- 14) G. A. Rechnitz and E. Eyal, Anal. Chem., 44, 370 (1972).
- 15) J. W. Mitchell and D. L. Shanks, Anal. Chem., 47, 642 (1975).

- 16) G. Czerwenka and E. Schenbeck, Z. Anal. Chem., 276, 37 (1975).
- 17) B. Kaempf, S. Raynal, A. Collet, F. Schue, S. Boileau and J. M. Lehn, Angew. Chem. Int. Ed. Engl., 13, 611 (1974).
- 18) C. J. Redersen and H. K. Frensdorff, Angew. Chem. Int. Ed. Engl., 11, 16 (1972).
- 19) R. M. Costes, G. Folcher, P. Plurien and P. Rigny, Inorg. Nucl. Chem. Lett., 12, 491 (1976).
- 20) J. M. Ceraso and J. L. Dye, J. Chem. Phys., 61, 1585 (1974).
- 21) J. L. Dye, Scientific American, 237, 92, (1977).
- 22) F. J. Tehan, B. L. Barnett and J. L. Dye, J. Amer. Chem. Soc., 96, 7203 (1974).
- 23) J. L. Dye, M. R. Yemen, M. G. DaGue and J. M. Lehn, J. Chem. Phys., 68, 1665 (1978).
- 24) J. M. Lehn and J. Cheney, private communication.
- 25) B. G. Cox and H. Schneider, J. Amer. Chem. Soc., 99, 2809 (1977).
- 26) J. Cheney, J. P. Kintzinger and J. M. Lehn, to be published.
- 27) J. Cheney and J. M. Lehn, J. Chem. Soc. Chem. Comm., 487 (1972).
- 28) N. F. Ramsey, Phys. Rev., 78, 699 (1950). Ibid, 86, 243 (1952). Ibid, 91, 303 (1953).
- 29) D. Shaw, "Fourier Transform N.M.R. Spectroscopy," Elsevier Scientific Publishing Co., New York, 1976.
- 30) D. J. Farnum, Advances in Physical Organic Chemistry, 11, 129 (1975).
- 31) J. A. Pople, W. G. Schneider and H. G. Bernstein, "High Resolution Nuclear Magnetic Resonance," McGraw-Hill, New York, 1959.
- 32) T. C. Farrar and E. D. Becker, "Pulse and Fourier Transform NMR," Academic Press, New York, 1971.
- 33) A. Abragam, "The Principles of Nuclear Magnetism," Oxford Univ. Press, New York, 1961.

- 34) J. L. Dye, C. W. Andrews and J. M. Ceraso, J. Phys. Chem., 79, 3076 (1975).
- 35) P. Debye, "Polar Molecules," Dover Publications, New York, 1945.
- 36) E. H. Mei, Ph. D. Thesis, Michigan State University (1977).
- 37) D. D. Traficante and J. A. Simms, J. Mag. Res., 15, 484 (1974).
- 38) J. M. Ceraso, Ph. D. Thesis, Michigan State University (1975).
- 39) B. K. J. Leong, T. O. T. Ts'o and M. B. Chenoweth, Toxicol. Appl. Pharmacol., 27, 342 (1974).
- 40) J. M. Lehn, J. P. Sauvage and B. Dietrich, J. Amer. Chem. Soc., 92, 2916 (1970).
- 41) B. Dietrich, J. M. Lehn and J. P. Sauvage, Tetrahedron, 29, 1647 (1973). B. Dietrich, J. M. Lehn, J. P. Sauvage and J. Blanzat, Ibid, p. 1629.
- 42) C. H. Park and H. E. Simmons, J. Amer. Chem. Soc., 94, 7184 (1972).
- 43) H. E. Simmons and C. H. Park, J. Amer. Chem. Soc, 90, 2428 (1968). C. H. Park and H. E. Simmons, Ibid., 70, p. 2429.
- 44) A. C. Coxon and J. F. Stoddart, J. Chem. Soc., Perkin I, 767 (1977).
- 45) B. Metz, D. Moras and R. Weiss, Chem. Comm., 444 (1971).
- 46) M. T. Lok, Ph. D. Thesis, Michigan State University (1973).
- 47) V. M. Loyola, R. Pizer and R. G. Wilkins, J. Amer. Chem. Soc., 99, 7185 (1977).
- 48) R. Pizer, J. Amer. Chem. Soc., 100, 4239 (1978).
- 49) E. Schori, J. Jagur-Grodzinski and M. Shporer, J. Amer. Chem. Soc., 95, 3842 (1973).
- 50) J. M. Ceraso, P. B. Smith, J. S. Landers and J. L. Dye, J. Phys. Chem., 81, 760 (1977).
- 51) Y. M. Cahen, J. L. Dye and A. I. Popov, J. Phys. Chem., 79, 1292 (1975).

- 52) E. Schori, J. Jagur-Grodzinski, Z. Luz and M. Shporer, J. Amer. Chem. Soc., 93, 7133 (1971).
- 53) E. Kauffmann, J. M. Lehn and J. P. Sauvage, Helv. Chim. Acta, 59, 1099 (1976).
- 54) E. Mei, A. I. Popov and J. L. Dye, J. Amer. Chem. Soc., 99, 6532 (1977).
- 55) P. B. Smith and J. L. Dye, unpublished results.
- 56) F. Mathieu, B. Metz, D. Moras and R. Weiss, J. Amer. Chem. Soc., 100, 4412 (1978).
- 57) R. W. Taft and L. S. Levitt, J. Org. Chem, 42, 916 (1977). ✓
- 58) J. F. Wolf, R. H. Staley, I. Koppel, M. Taagepera, R. T. McIver, Jr., J. L. Beauchamp and R. W. Taft, J. Amer. Chem. Soc., 99, 5417 (1977).
- 59) F. Bloch, Phys. Rev., 70, 460 (1946).
- 60) H. M. McConnell, J. Chem. Phys., 28, 430 (1958). see also J. A. Pople, W. G. Schneider and H. J. Bernstein, "High-Resolution Nuclear Magnetic Resonance," McGraw-Hill Book Company, New York, 1959, Chapter 10. Equation (10-25) of the previous reference is in error.
- 61) G. J. Karabatsos and C. E. Orzech, Jr., J. Amer. Chem. Soc., 86, 3574 (1964).
- 62) see the Historical section.
- 63) G. Binsch, J. B. Lambert, B. W. Roberts and J. D. Roberts, J. Amer. Chem. Soc., 86, 5564 (1964).
- 64) G. A. Olah and D. H. Obrien, J. Amer. Chem. Soc., 89, 1725 (1967).
- 65) M. Eigen, Discussions of the Faraday Society, 39, 1965, pp. 7-11.
- 66) A. Albert and E. P. Serjeaut, "Ionization Constants of Acids and Bases," Butler and Tanner Ltd., London, 1962, p. 124.
- 67) P. K. Glasoe and F. A. Long, J. Phys. Chem., 64, 188 (1960).
- 68) W. J. Moore, "Physical Chemistry," Prentice-Hall, Inc., Englewood Cliffs, New Jersey, 1972, p. 383f.

- 69) C. P. Schlicter, "Principles of Magnetic Resonance," Harper and Row Publishers, New York, 1963.
- 70) R. K. Gupta, T. P. Pitner and R. Wasylishen, J. Mag. Res., 13, 383 (1974).
- 71) D. E. Woessner, J. Chem. Phys., 35, 41 (1961).
- 72) V. A. Nicely and J. L. Dye, J. Chem. Edu., 48, 443 (1971).
- 73) see Appendix for details of the calculations.
- 74) W. Weyl, Ann. Physik., 121, 601 (1863).
- 75) J. L. Dye, Pure and Appl. Chem., 49, 3 (1977) and references therein.
- 76) J. L. Dye, submitted as a chapter for a Wiley-Interscience book on "Multidentate Macrocyclic Molecules," J. J. Christensen and R. M. Izatt, editors.
- 77) B. Kaempf, S. Raynal, A. Collet, F. Schue, S. Boileau and J. M. Lehn, Angew. Chem. internat. edit., 13, 611 (1974).
- 78) J. L. Dye, J. Chem. Ed., 54, 332 (1977) and references therein.
- 79) J. L. Dye, C. W. Andrews and S. E. Mathews, J. Phys. Chem., 79, 3065 (1975).
- 80) M. Hansen, "Constitution of Binary Alloys," 578, 1958.
- 81) J. M. Lehn and J. P. Sauvage, Chem. Comm., 440 (1971).
- 82) E. Mei, A. I. Popov and J. L. Dye, J. Amer. Chem. Soc., 99, 6532 (1977).
- 83) D. Shaw, "Fourier Transform NMR Spectroscopy," Elsevier Scientific Publishing Company, New York, 1976, pp. 85-87.
- 84) J. A. Pople and D. L. Beveridge, "Approximate Molecular Orbital Theory," McGraw-Hill Book Company, New York, 1970.
- 85) E. Kauffmann, J. L. Dye, A. I. Popov and J. M. Lehn, unpublished results.
- 86) J. H. Busch and J. R. de la Vega, J. Amer. Chem. Soc., 99, 2397 (1977).

D. F. Shriver, "The Manipulation of Air-sensitive Compounds," McGraw-Hill Book Company, New York, 1969, pp. 146-154.